

244/6/20

MICHIGAN STATE UNIVERSITY LIBRARIES



This is to certify that the

thesis entitled

STRESS ANALYSIS IN CROSS-PLY LAMINATES DAMAGED BY TRANSVERSE MATRIX CRACKS

presented by Jung Ki Lee

has been accepted towards fulfillment of the requirements for

M. S. degree in MECHANICAL ENGINEERING

Major professor

Date August 10, 1989.

**O**-7639

MSU is an Affirmative Action/Equal Opportunity Institution

PLACE IN RETURN BOX to remove this checkout from your record. TO AVOID FINES return on or before date due.

DATE DUE	DATE DUE	DATE DUE

MSU Is An Affirmative Action/Equal Opportunity Institution

# STRESS ANALYSIS IN CROSS-PLY LAMINATES DAMAGED BY TRANSVERSE MATRIX CRACKS

By

Jung Ki Lee

## A THESIS

Submitted to
Michigan State University
in partial fulfillment of the requirements
for the degree of

**MASTER OF SCIENCE** 

Department of Mechanical Engineering

## **ABSTRACT**

# STRESS ANALYSIS IN CROSS-PLY LAMINATES DAMAGED BY TRANSVERSE MATRIX CRACKS

By

## Jung Ki Lee

Damage in composite materials has been a subject of great interest to both engineers in industry and subsequently numerous researchers since the early 1970s when this class of advanced materials began to assume greater utility in the defence, aerospace, automotive and sporting goods industries, for example. Damage mechanisms in cracked composite laminates have been investigated by using micromechanics modelling (ply discount scheme, shear lag analysis, self-consistent scheme, etc.) and internal variable characterization. Stress analysis techniques are crucial for modelling of damage mechanisms in cracked composite laminates, however, due to phenomenological complexities of the field, there are no exact solutions for the stress distributions of cracked composite laminates. In this work, a finite element model for the damage mechanisms of cracked composite laminates is proposed by reducing this class of three-dimensional phenomenological problems to two-dimensional plane-strain problems. In particular, stress distributions in cross-ply laminates damaged by transverse matrix cracks are investigated by employing the ANSYS finite element computer program. Four types of problems for glass/epoxy and graphite/epoxy laminates are considered: (1)  $[0^{\circ}/90^{\circ}]_{s}$  laminate with an isolated crack; (2)  $[0^{\circ}/90^{\circ}]_{s}$  laminate with interacting cracks; (3)  $[0^{\circ}/90^{\circ}_{3}]_{s}$  laminate with an isolated crack; (4)  $[0^{\circ}/90^{\circ}_{3}]_{s}$  laminate nate with interacting cracks. Furthermore, the finite element analysis results for

[0°/90°]<sub>s</sub> glass/epoxy composite laminate with interacting cracks and [0°/90°]<sub>s</sub> glass/epoxy composite laminate with an isolated crack, were compared with the variational calculus results based on the minimum complementary energy theorem. These variational calculus results were obtained by employing a more generalized test function than that used by Hashin. Reasonable agreement is obtained between the finite element analysis results and the variational calculus results. Important aspects of damaged composite laminates are investigated and discussed by utilizing the finite element formulation developed herein.

To my family

### **ACKNOWLEDGMENTS**

I would like to thank my adviser Dr. Mukesh V. Gandhi for his significant contributions to this research, technical guidance, and editorial advice.

I would like to thank Dr. Nicholas J. Altiero and Dr. Brian S. Thompson who served on members of the thesis committee for the time and effort they devoted to helping me on developing and proofreading this thesis.

Numerous people contributed the efforts to complete this thesis. In particular, I would like to thank Mr. Mohammad Usman and Mr. Devang Desai for providing their assistance and proofreading this thesis. Also, I would like to thank numerous Korean students for helping and encouraging me during this research.

Finally, I would like to thank my parents, brother and sisters, my wife and my friends for their concern and everlasting support.

# **TABLE OF CONTENTS**

List of Tabl	esvii		
List of Figu	resviii		
Chapter 1	Introduction 1		
1.1.	Concepts of damage in composite materials 1		
1.2.	Overview 6		
1.3.	Objective		
Chapter 2	Description of the problem and approach 12		
2.1.	Description of present investigation		
2.2.	Methodologies		
Chapter 3	Results and discussion on finite element analysis		
Chapter 4	Comparison of the finite element analysis results with the		
	analytical results		
4.1.	Analysis of a cracked symmetric cross-ply laminate under		
	uniform tension		
4.2.	Analytical results and comparison with the finite element		
	analysis results		
Chapter 5	Concluding remarks		
List of refer	rences 75		

# LIST OF TABLES

Table 2.1	Stress concentration factor for homogeneous material near the		
	crack tip (Type 1)	. 15	
Table 2.2	Material properties for the composite laminates	. 16	
Table 4.1	Ratio $\sigma_1/\sigma_2$ and $\sigma_1/\sigma$ by the classical lamination theory	. 55	
Table 4.2	Complementary energy (U <sub>c</sub> '2) variation with		
	various power n in equations (4.13 d,e,f)	. 56	

# LIST OF FIGURES

Figure 1.1	Schematic representation of the damage accumulation process	
	in composite laminates	,
Figure 1.2	Typical saturation crack patterns observed in [0°/90°] <sub>s</sub>	
	laminate	,
Figure 1.3	Edge replica from a [0°/90°2] <sub>s</sub> laminate at the Characterization	
	Damage State (CDS)	ļ
Figure 1.4	Typical stiffness reduction for a [0°/90° <sub>2</sub> ] <sub>s</sub> laminate	ļ
Figure 1.5	Schematic "flow diagram" of damaged mechanics for	
	composite materials	,
Figure 1.6	A typical one-dimensional model in formulation of	
	shear lag analysis	}
Figure 2.1	Cross-ply laminate damaged by transverse matrix cracks 1	.2
Figure 2.2	Representative volume element	.2
Figure 2.3	[0°/90°] <sub>s</sub> laminate with an isolated crack	.3
Figure 2.4	[0°/90°] <sub>s</sub> laminate with interacting cracks	:3
Figure 2.5	[0°/90° <sub>3</sub> ] <sub>s</sub> laminate with an isolated crack	4
Figure 2.6	[0°/90° <sub>3</sub> ] <sub>s</sub> laminate with interacting cracks	.4
Figure 2.7	Finite element modelling of type 1 composite laminate	
	(Number of elements = 1518, number of nodes = 1598)	.7
Figure 2.8	Finite element modelling of type 1 composite laminate	

		(Enlargement at crack)
Figure 2.	.9	Finite element modelling of type 2 composite laminate
		(Number of elements = 3450, number of nodes = 3595)
Figure 2.	.10	Finite element modelling of type 3 composite laminate
		(Number of elements = 3036, number of nodes = 3162)
Figure 2.	.11	Finite element modelling of type 4 composite laminate
		(Number of elements = 3675, number of nodes = 3833)
Figure 3.	.1	Stress component $\sigma_y$ at the crack plane in 0° ply
		[0°/90°] <sub>s</sub> glass/epoxy composite laminate (Type 1)
Figure 3.	.2	Stress component $\sigma_y$ at the crack plane in $0^\circ$ ply
		[0°/90°] <sub>s</sub> graphite/epoxy composite laminate (Type 1)
Figure 3.	.3	Stress component $\sigma_y$ at the interface in 0° ply
		[0°/90°] <sub>s</sub> glass/epoxy composite laminate (Type 1)
Figure 3.	.4	Stress component $\sigma_y$ at the interface in 0° ply
		[0°/90°] <sub>s</sub> graphite/epoxy composite laminate (Type 1)
Figure 3.	.5	Stress component $\sigma_y$ at the interface in $0^\circ$ ply
		[0°/90°] <sub>s</sub> glass/epoxy composite laminate (Type 2)
Figure 3.	.6	Stress component $\sigma_y$ at the interface in 0° ply
		[0°/90°] <sub>s</sub> graphite/epoxy composite laminate (Type 2)
Figure 3.	.7	Stress component $\sigma_y$ at the interface in $0^\circ$ ply
		[0°/90° <sub>3</sub> ] <sub>s</sub> glass/epoxy composite laminate (Type 3)
Figure 3.	.8	Stress component $\sigma_y$ at the interface in 0° ply
		[0°/90° <sub>3</sub> ] <sub>s</sub> graphite/epoxy composite laminate (Type 3)

Figure 3.9	Stress component $\sigma_y$ at the interface in 0° ply
	[0°/90° <sub>3</sub> ] <sub>s</sub> glass/epoxy composite laminate (Type 4)
Figure 3.10	Stress component $\sigma_y$ at the interface in 0° ply
	[0°/90° <sub>3</sub> ] <sub>s</sub> graphite/epoxy composite laminate (Type 4) 29
Figure 3.11	Stress component $\sigma_x$ and $\sigma_{xy}$ at the interface in $0^\circ$ ply
	[0°/90°] <sub>s</sub> glass/epoxy composite laminate (Type 1) 30
Figure 3.12	Stress component $\sigma_x$ and $\sigma_{xy}$ at the interface in 0° ply
	[0°/90°] <sub>s</sub> graphite/epoxy composite laminate (Type 1)30
Figure 3.13	Stress component $\sigma_x$ and $\sigma_{xy}$ at the interface in 0° ply
	[0°/90°] <sub>s</sub> glass/epoxy composite laminate (Type 2) 31
Figure 3.14	Stress component $\sigma_x$ and $\sigma_{xy}$ at the interface in 0° ply
	[0°/90°] <sub>s</sub> graphite/epoxy composite laminate (Type 2)
Figure 3.15	Stress component $\sigma_x$ and $\sigma_{xy}$ at the interface in 0° ply
	[0°/90° <sub>3</sub> ] <sub>s</sub> glass/epoxy composite laminate (Type 3)
Figure 3.16	Stress component $\sigma_x$ and $\sigma_{xy}$ at the interface in 0° ply
	[0°/90° <sub>3</sub> ] <sub>s</sub> graphite/epoxy composite laminate (Type 3) 32
Figure 3.17	Stress component $\sigma_x$ and $\sigma_{xy}$ at the interface in 0° ply
	[0°/90° <sub>3</sub> ] <sub>s</sub> glass/epoxy composite laminate (Type 4)
Figure 3.18	Stress component $\sigma_x$ and $\sigma_{xy}$ at the interface in $0^\circ$ ply
	[0°/90° <sub>3</sub> ] <sub>s</sub> graphite/epoxy composite laminate (Type 4) 33
Figure 3.19	Stress component $\sigma_y$ at the interface in 90° ply
	[0°/90°] <sub>s</sub> glass/epoxy composite laminate (Type 1)

Figure 3.20	Stress component $\sigma_y$ at the interface in 90° ply
	[0°/90°] <sub>s</sub> graphite/epoxy composite laminate (Type 1)
Figure 3.21	Stress component $\sigma_y$ at the interface in 90° ply
	[0°/90°] <sub>s</sub> glass/epoxy composite laminate (Type 2)
Figure 3.22	Stress component $\sigma_y$ at the interface in 90° ply
	[0°/90°] <sub>s</sub> graphite/epoxy composite laminate (Type 2)
Figure 3.23	Stress component $\sigma_y$ at the interface in 90° ply
	[0°/90° <sub>3</sub> ] <sub>s</sub> glass/epoxy composite laminate (Type 3)
Figure 3.24	Stress component $\sigma_y$ at the interface in 90° ply
	[0°/90° <sub>3</sub> ] <sub>s</sub> graphite/epoxy composite laminate (Type 3) 36
Figure 3.25	Stress component $\sigma_y$ at the interface in 90° ply
	[0°/90° <sub>3</sub> ] <sub>s</sub> glass/epoxy composite laminate (Type 4)
Figure 3.26	Stress component $\sigma_y$ at the interface in 90° ply
	[0°/90° <sub>3</sub> ] <sub>s</sub> graphite/epoxy composite laminate (Type 4) 37
Figure 3.27	Stress component $\sigma_x$ at the midplane in 90° ply
	[0°/90°] <sub>s</sub> glass/epoxy composite laminate (Type 1)
Figure 3.28	Stress component $\sigma_x$ at the midplane in 90° ply
	[0°/90°] <sub>s</sub> graphite/epoxy composite laminate (Type 1)
Figure 3.29	Stress component $\sigma_x$ at the midplane in 90° ply
	[0°/90°] <sub>s</sub> glass/epoxy composite laminate (Type 2)
Figure 3.30	Stress component $\sigma_x$ at the midplane in 90° ply
	[0°/90°] <sub>s</sub> graphite/epoxy composite laminate (Type 2)

Figure 3.31	Stress component $\sigma_x$ at the midplane in 90° ply
	[0°/90° <sub>3</sub> ] <sub>s</sub> glass/epoxy composite laminate (Type 3)
Figure 3.32	Stress component $\sigma_x$ at the midplane in 90° ply
	[0°/90° <sub>3</sub> ] <sub>s</sub> graphite/epoxy composite laminate (Type 3)
Figure 3.33	Stress component $\sigma_x$ at the midplane in 90° ply
	[0°/90° <sub>3</sub> ] <sub>s</sub> glass/epoxy composite laminate (Type 4) 41
Figure 3.34	Stress component $\sigma_x$ at the midplane in 90° ply
	[0°/90° <sub>3</sub> ] <sub>s</sub> graphite/epoxy composite laminate (Type 4)
Figure 3.35	Stress component $\sigma_x$ at the crack location in 90° ply
	[0°/90° <sub>3</sub> ] <sub>s</sub> glass/epoxy composite laminate (Type 4)
Figure 3.36	Stress component $\sigma_x$ at the crack location in 90° ply
	[0°/90° <sub>3</sub> ] <sub>s</sub> graphite/epoxy composite laminate (Type 4)
Figure 4.1	[0°/90° <sub>n</sub> ] <sub>s</sub> laminate between two cracks
Figure 4.2	[0°/90° <sub>n</sub> ] <sub>s</sub> laminate with an isolated crack
Figure 4.3	Stress component $\sigma_y$ at the interface in $0^{\circ}$ ply
	[0°/90°] <sub>s</sub> glass/epoxy composite laminate (Type 2)
Figure 4.4	Stress component $\sigma_{xy}$ at the interface in $0^{\circ}$ ply
	[0°/90°] <sub>s</sub> glass/epoxy composite laminate (Type 2) 62
Figure 4.5	Stress component $\sigma_x$ at the interface in 0° ply
	[0°/90°] <sub>s</sub> glass/epoxy composite laminate (Type 2)
Figure 4.6	Stress component $\sigma_y$ at the interface in 90° ply
	[0°/90°] <sub>s</sub> glass/epoxy composite laminate (Type 2)

Figure 4.7	Stress component $\sigma_y$ at the midplane in 90° ply
	[0°/90°] <sub>s</sub> glass/epoxy composite laminate (Type 2) 65
Figure 4.8	Stress component $\sigma_{\mathbf{x}}$ at the midplane in 90° ply
	[0°/90°] <sub>s</sub> glass/epoxy composite laminate (Type 2) 66
Figure 4.9	Stress component $\sigma_y$ at the interface in 0° ply
	[0°/90°] <sub>s</sub> glass/epoxy composite laminate (Type 1) 67
Figure 4.10	Stress component $\sigma_{xy}$ at the interface in $0^{\circ}$ ply
	[0°/90°] <sub>s</sub> glass/epoxy composite laminate (Type 1)
Figure 4.11	Stress component $\sigma_x$ at the interface in 0° ply
	[0°/90°] <sub>s</sub> glass/epoxy composite laminate (Type 1) 69
Figure 4.12	Stress component $\sigma_y$ at the interface in 90° ply
	[0°/90°] <sub>s</sub> glass/epoxy composite laminate (Type 1) 70
Figure 4.13	Stress component $\sigma_y$ at the midplane in 90° ply
	[0°/90°] <sub>s</sub> glass/epoxy composite laminate (Type 1)
Figure 4.14	Stress component $\sigma_x$ at the midplane in 90° ply
	[0°/90°] <sub>s</sub> glass/epoxy composite laminate (Type 1)

# CHAPTER 1 INTRODUCTION

## 1.1 Concepts of damage in composite materials

Damage can be loosely defined as the effect of micro-failure events on material behavior, or, as a collection of permanent (irreversible) microstructural changes brought about in the material by a physical process, resulting from the application of loads. The identification of damage in composite materials consists of a number of damage modes, such as matrix cracking, fiber breaks, fiber/matrix debonds, delamination cracking and interlaminar cracking.

One of the major differences between the mechanical response of fiber reinforced composite laminates and that of more conventional structural materials, such as aluminum and steel, is that the damage that develops in such composites is generally much more complex. Metals usually fail by crack initiation and its growth; in a manner which is predictable through fracture mechanics analysis. Whereas composites exhibit several modes of damage including matrix crazing, fiber failure, void growth, matrix cracking, delamination and composite cracking. A particular structure may exhibit any or all of these damage modes, a priori, it is not known which mode will dominate and cause failure.

In the succeeding part of this section, it would be useful to discuss the physical aspects of damage in composite materials. In advanced composites, e.g. graphite/epoxy, the microstructural changes are in the form of cracks of various geometries and orientations, as mentioned earlier. The development of the micromechanical changes is conveniently observed in fatigue, since the rate of change is small

compared to that in, for instance, quasi-static fracture and impact failure. Based on fatigue damage studies of advanced composite laminates, certain patterns that seem to be valid for a large class of composite materials can be investigated. A schematic representation of damage development under fatigue is shown in Figure 1.1<sup>[1],[2]</sup>. Also, a typical stiffness reduction under fatigue is shown in Figure 1.4<sup>[3]</sup>.

Damage development consists of three stages (namely, initiation, growth, and localization) leading to ultimate failure. The initial stage consists of primary transverse matrix cracking along fibers in off-axis plies. The parallel cracks appear in the cracking ply. According to the stresses in the ply and the constraints to cracking given by the neighboring plies, the crack number density increases. The cracking process may continue until cracks in each ply have attained equilibrium or saturation spacing. The saturation spacing is a property of the laminate and is independent of the loading history. The state of damage given by the saturated and stable matrix cracking pattern in a laminate has been termed the Characterization Damage State (CDS), a well-established condition of saturated ply cracks (Figures 1.2 and 1.3)[3],[4]. It appears to indicate the termination of the first stage of matrix cracking having an insignificant interaction between cracks. Also, it is noted that after sufficient loading the off-axis plies in a laminate reach a saturation state, where the distance between consecutive cracks in a particular ply is nearly uniform throughout the specimen. This fact can be attributed to the fact that transverse cracking reduces the load-carrying capacity of those plies only in a local region adjacent to the cracks. The material between adjacent cracks outside of these relaxed zones is capable of carrying some load and hence contributing to the laminate stiffness. This mechanism causes the fiber breaks to occur in a more localized configuration, in regions of stress concentration created by the primary cracks.

The primary cracks also initiate longitudinal cracks. The longitudinal cracks are generally perpendicular to the primary cracks. The longitudinal cracks are caused by

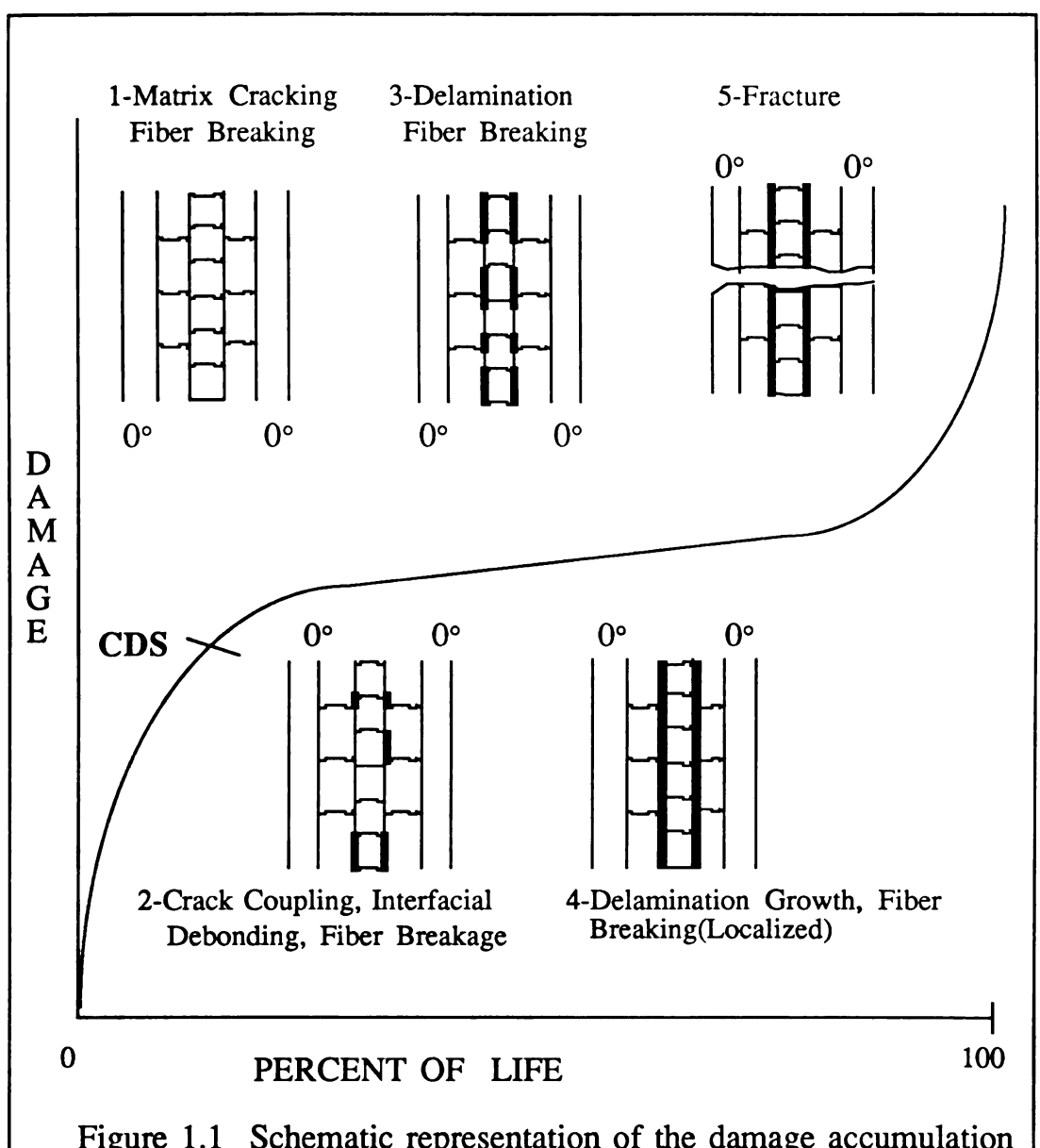


Figure 1.1 Schematic representation of the damage accumulation process in composite laminates<sup>[1],[2]</sup>.

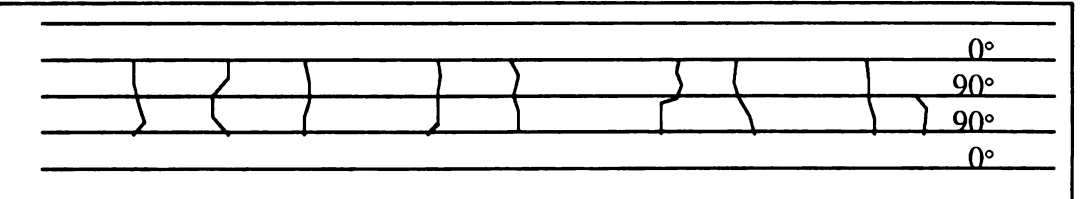
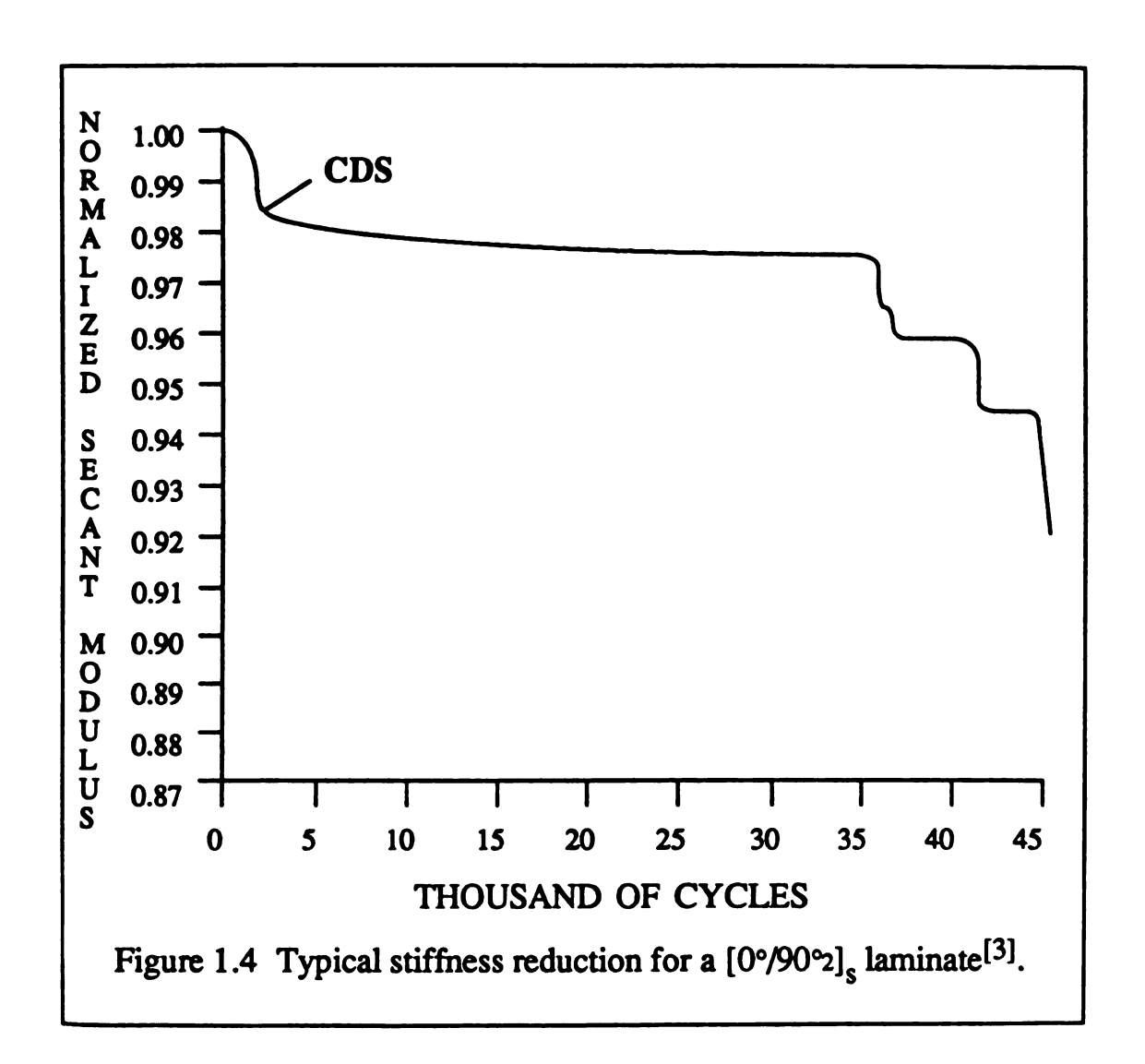


Figure 1.2 Typical saturation crack patterns observed in  $[0^{\circ}/90^{\circ}]_{s}$  laminate<sup>[4]</sup>.



Figure 1.3 Edge replica from a [0°/90°2]<sub>s</sub> laminate at the Characterization Damage State (CDS)<sup>[3]</sup>.



the tensile stress along the crack axis ahead of the primary cracks. The material in the 0° ply adjacent to the crack tip is subjected to the tensile stress in its lowest strength direction. So, the transverse crack can be considered a likely site for the nucleation of longitudinal cracks.

Next, delamination takes place in the interior of a laminate. In regions where the primary transverse matrix cracks and the longitudinal cracks intersect; a local out-of-plane tensile stress condition is created by the transverse matrix cracks and the longitudinal cracks. Hence, the centers of incipient delaminations frequently coincide with crack interactions. They are also the points of maximum delamination opening. These delaminations coalesce in regions between longitudinal cracks, isolating small volumes of material in the 0° plies that become longitudinal splits.

Numerous fiber fractures occur during the damage development of transverse matrix cracking, longitudinal cracks, and delamination. However, these fractures do not occur in randomly distributed array but instead have a distinct, consistent pattern. It suggests the involvement of the adjacent transverse cracks whose tips are a fiber fracture initiator in the 0° ply. In addition, the fiber fractures that occur are segregated into zones that are bounded by fiber fracture-free zones. Delamination appears to isolate the 0° plies from the transverse cracks and thereby prevents related fiber breaks. The formation of broken fibers in this way produces numerous weakened net sections in the load-bearing ply. Such a crack structure, if repeated across the width of a laminate, has serious implications for laminate failure. So, the effect of this ordering of fiber fractures cannot be ignored.

Many of these damage modes occur long before the ultimate failure, hence, there can be many types of subcritical failures. These phenomena, in turn, contribute to the final fracture which seems to be either controlled from rapid fiber failures or from severe interactions of cracks leading to loss of material integrity.

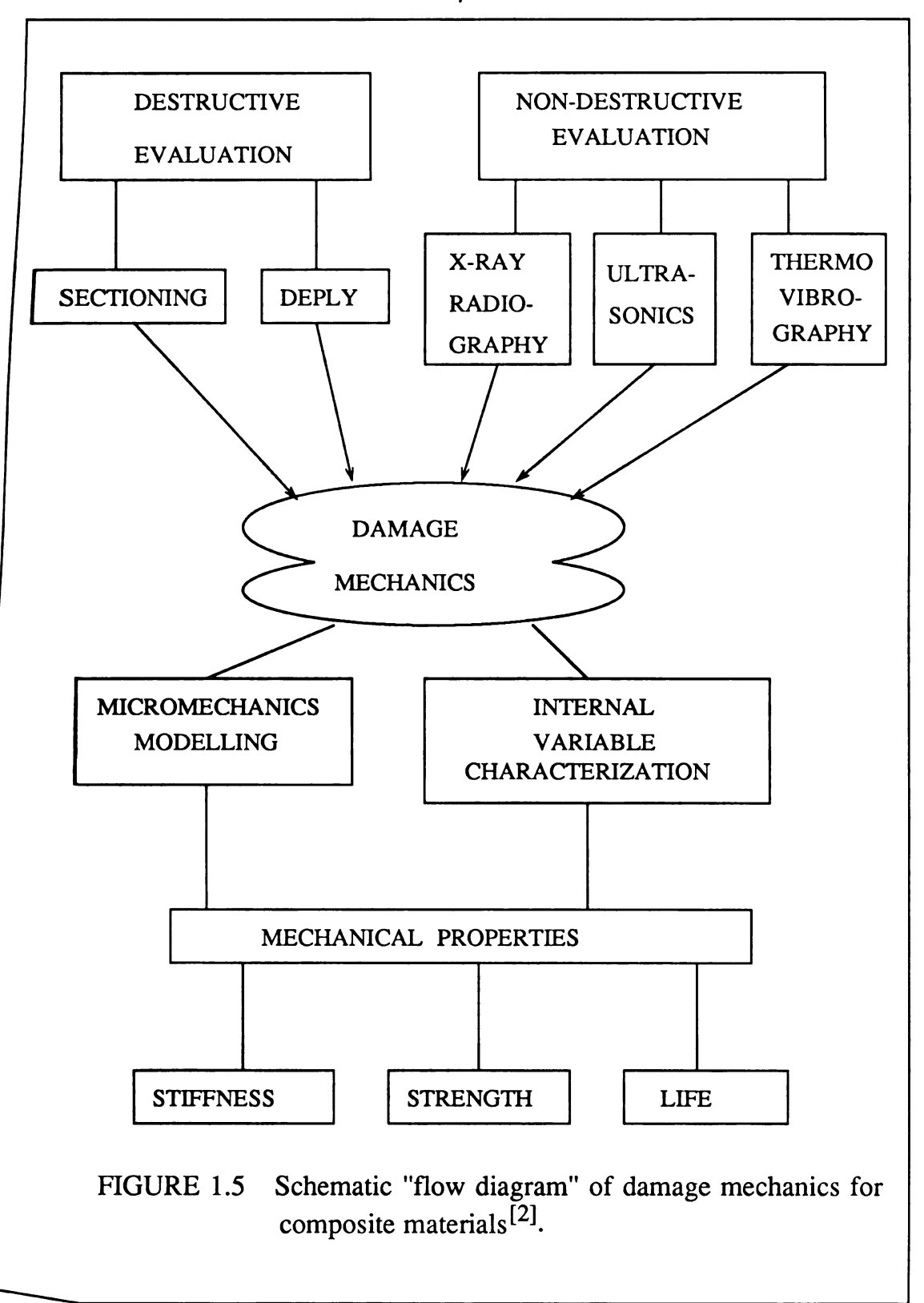
In addition, numerous numerical and experimental investigations have

demonstrated the free edge effect in composite laminates subjected to remote tension. It has been suggested that high interlaminar stresses in the boundary layer play a dominant role in the delamination failure mode of the composite laminates. At the free edges of a laminate (sides of a laminate or holes), the interlaminar shearing stress is very high (perhaps even singular) and would therefore cause the debonding that has been observed in such regions.

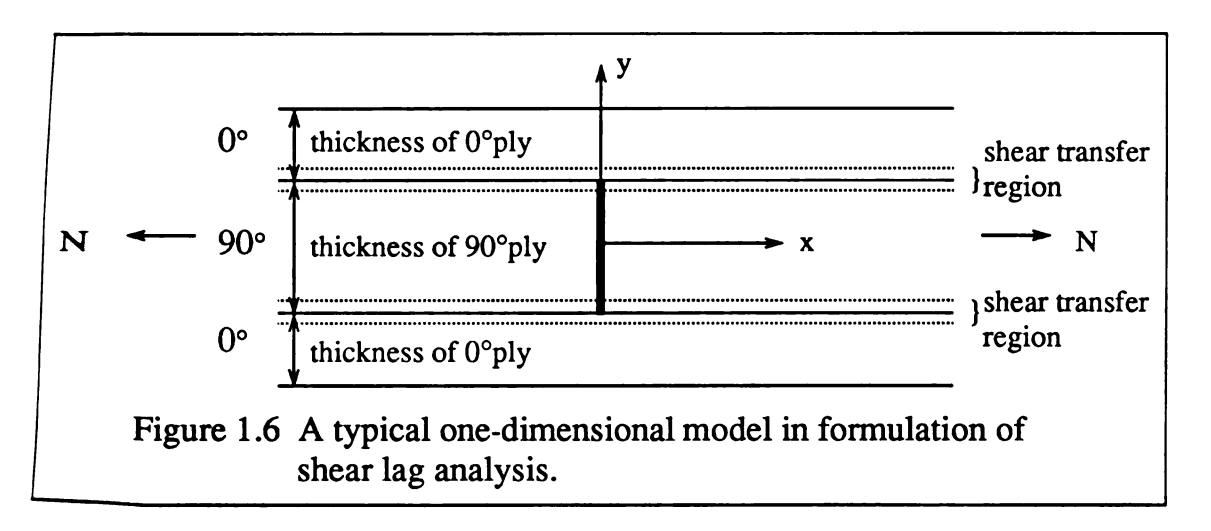
### 1.2 Overview

For more than two decades, considerable effort has been expended in understanding the phenomena of damage in composite materials, and new theories of the mechanisms still continue to emerge. The literature contains an important record of information on the subject of damage, both experimental and theoretical. Particularly, the transverse ply cracking in composite materials and the development of a satisfactory theory for cross-ply laminates damaged by transverse matrix cracking under monotonic loading have been a subject of extensive research. A schematic "flow-rule" of damage mechanics related to composite materials is shown in Figure 1.5<sup>[2]</sup>. A large body of information has been collected utilizing various non-destructive techniques including edge replication, light and electron microscopy, X-ray radiography, ultrasonic C-scan and also destructive techniques, e.g. specimen sectioning and de-ply for microscopy observations. The above are used to generate knowledge that constitutes a damage mechanics analysis. Therefore they may be utilized, broadly speaking, in one of the two common approaches to performing a damage mechanics analysis. One is micromechanics modelling approach, and the other is internal variable characterization approach.

As a method of micromechanics modelling analysis for cross-ply laminates damaged by transverse matrix cracking, the formation of a shear lag model appears to have been first proposed in a series of papers by Bailey and his co-workers<sup>[5]-[7]</sup>.



Subsequent contributions to the theory have been given by numerous researchers. Especially, Reifsnider and co-authors<sup>[4]</sup> evaluated stiffness reduction in terms of shear lag analysis. Figure 1.6 shows a typical one-dimensional model in formulation of shear lag analysis.



The shear lag analysis is based on the following assumptions: (a) The normal stress in external load direction is constant over ply thickness; (b) Shear deformations in any given ply are restricted to a thin region in the vicinity of interfaces of that ply with adjacent plies. Further, this region tends to be resin-rich, and thus is less stiff in response to shear loads than the central portion of the lamina. This thin region is assumed to be a shear transfer region. However, the thickness of the boundary layer must be assumed in somewhat arbitrary fashion and the transverse normal stresses cannot be estimated.

An another method of micromechanics modelling analysis, the self-consistent scheme was first devised by Hershey<sup>[9]</sup> and Kröner<sup>[10]</sup> as a means to model the behavior of polycrystalline materials. Such materials are just one phase media. The extension of the self-consistent scheme to multiphase media was given by Hill<sup>[11]</sup> and Budianski<sup>[12]</sup>. As discussed by

Budianski<sup>[12]</sup>, the method has a very simple geometric interpretation. Specially, each phase of the composite is alternatively viewed as being lumped as a single ellipsoidal inclusion in an infinite matrix of the unknown effective properties of the problem. The application of uniform stress or strain conditions at infinity allows the determination of the average conditions in the inclusion. After this operation is performed for all phases, the average conditions are known in all phases, in terms of the individual phase properties and the effective properties. Thence, average conditions in the entire composite are known and the effective moduli can be calculated from the averages.

The method of estimating the effective elastic properties of a cracked solid have been adopted by Budianski and O'Connell<sup>[13]</sup>. The model predicts the elastic properties for a material consisting of a homogeneous isotropic matrix in which flat elliptical cracks are dispersed. And, analytical solutions for effective moduli of elastic bodies with distributed cracks have been obtained by Laws and Dvorak<sup>[14]-[17]</sup>. The cracks are aligned and the total crack surface area has a first order effect on the stiffness. These theoretical results apply only to elastic bodies with cracks of homogeneous and predetermined dimensions.

In an important series of papers, Talreja<sup>[18]-[23]</sup> has presented a different approach for characterizing damage in composite materials. Talreja utilized vector fields for characterization of damage in fatigue, or any other loading mode. Constitutive equations are derived for isothermal small-deformation behavior following attainment of a damage state. Talreja used a continuum model for damage characterization that will predict the thermomechanical constitution of elastic composites. Damage is characterized by a set of second order tensor valued internal state variables representing locally averaged measures of specific damage states. However, in the formulation of stiffness reduction, the phenomenological constants must be evaluated by conducting a suitable set of experiments.

### 1.3 Objective

Historically, stress analysis has been closely related to the analysis on the loss of stiffness in cracked composite laminates. Stress analysis techniques are crucial for modelling of damage mechanisms in cracked cross-ply laminates with transverse matrix cracking. Chen and Sih<sup>[24]</sup> analyzed stress distributions for a three-layered plate with a crack in the center layer. They modeled the laminated composite as a multilayered plate each layer being made of a different material. They assumed that the stresses could vary in all three space coordinate directions in cracked composite laminates and the problem would be as a three-dimensional one. They applied the minimum complementary energy theorem in variational calculus such that the qualitative three-dimensional character of the crack edge stresses was retained while approximations were made in a quantitative sense on the stress intensity factor. But, in this analysis, they assumed that each layer was made of isotropic and homogeneous materials. So, the middle layer was assumed to be made of the material with elastic properties (E<sub>1</sub>, v<sub>1</sub>) while the two outer layers possessed the same material properties  $(E_2, v_2)$ . (Note:  $E_1, E_2$  are Young's modulus, and  $v_1, v_2$  are Poisson's ratios.) Therefore, the results from Chen and Sih<sup>[24]</sup> are not sufficiently accurate for cracked composite laminates.

Laws and Dvorak<sup>[14]-[17]</sup> analyzed stress distributions by employing the self-consistent scheme, as an additional work on the loss of stiffness for cross-ply laminates which have been damaged by transverse matrix cracking under monotonic loading. But, one problem with this analysis is of conceptual nature for their model of a cracked material is infinite in all directions while a cracked ply may be assumed to extend to infinity only in one direction and crack opening is significantly constrained by adjacent plies.

Hashin<sup>[25]-[26]</sup> presented a variational approach to the problems of stress evaluation which incorporates all of the important aspects of the problem and involves only one assumption that normal ply stresses in the load direction are constant over ply thickness. Hashin<sup>[25]-[26]</sup> thus constructed admissible stress fields which satisfy equilibrium and all boundary and interface conditions and determined stresses on the basis of the minimum complementary energy theorem. Hashin<sup>[25]-[26]</sup> has good agreement with experimental data for [0°/90°]<sub>s</sub> ply in predicting the stiffness reduction. However, the primary perturbation stresses in cracked composite laminates are incapable of evaluating the stress concentrations produced by transverse matrix cracks.

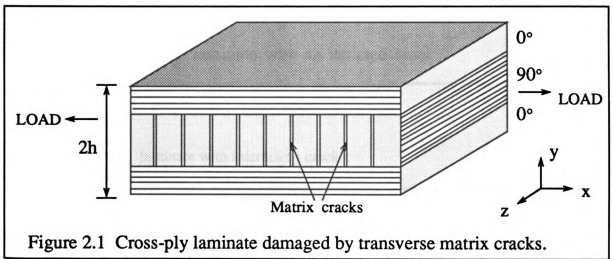
Hence, the objective of present investigation is to develop more generalized variational calculus stress distributions which have stress concentrations at the crack tips in 0° ply than those used by Hashin. In addition, it would be very useful to compare variational stress distributions with stress distributions from numerical simulation (finite element analysis) and to see what the stress distributions in cross-ply laminates damaged by transverse matrix cracks would be physically possible. Therefore, based on the stress distributions in cracked composite laminates, several important physical damage aspects can be obtained and discussed.

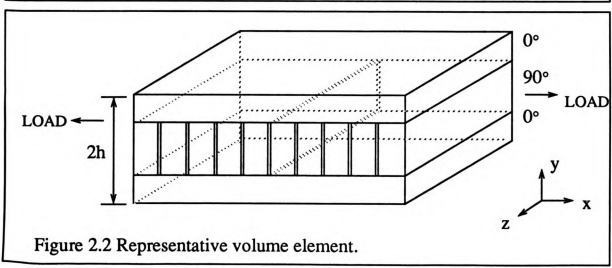
#### **CHAPTER 2**

#### DESCRIPTION OF THE PROBLEM AND APPROACH

#### 2.1 Description of present investigation

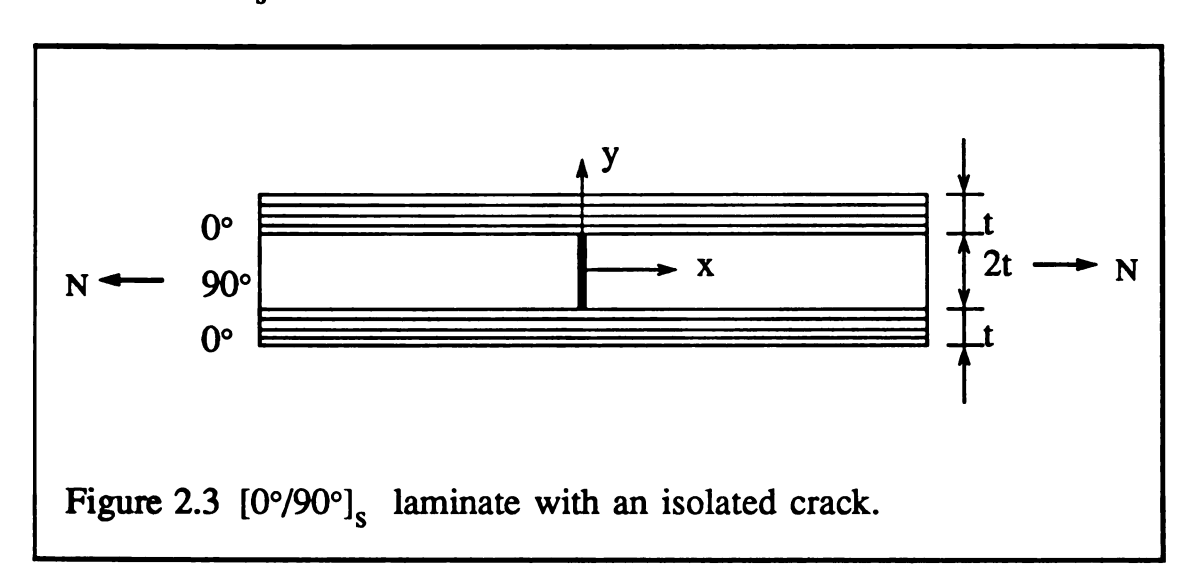
Consider a symmetric cross-ply laminate which is subjected to uniform in-plane tensile loads. It is assumed that the 90° ply has well-established continuous intralaminar cracks in the fiber direction. The cracks extend from edge to edge in z direction. Figures 2.1 and 2.2 describe the problem under investigation.



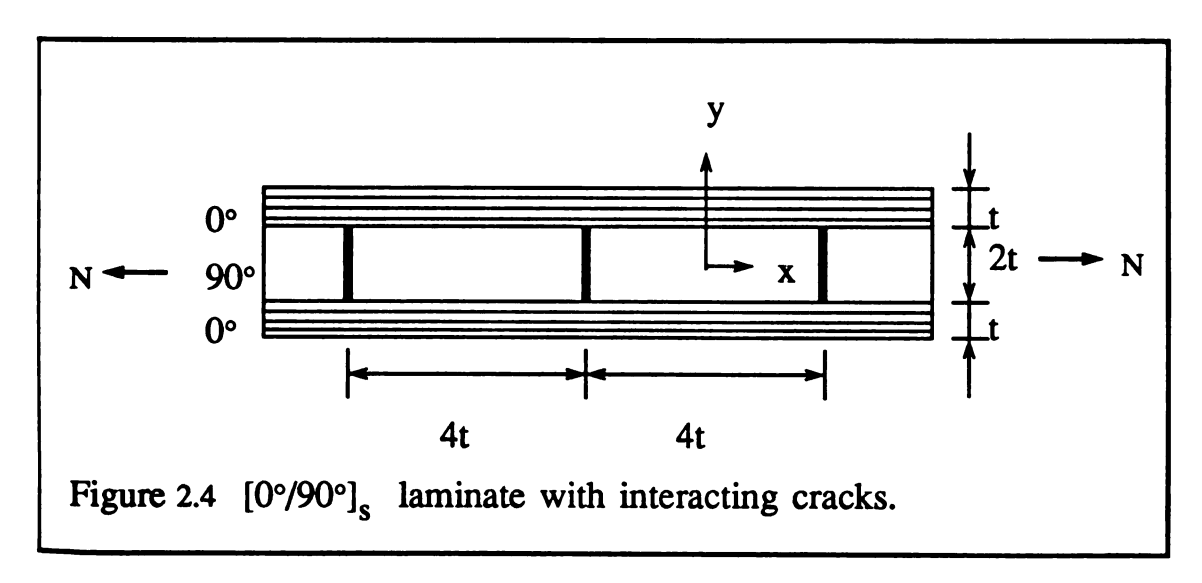


Finite element method has been employed to find stress distributions in crossply laminates damaged by transverse matrix cracks. The following four types of problems are considered:

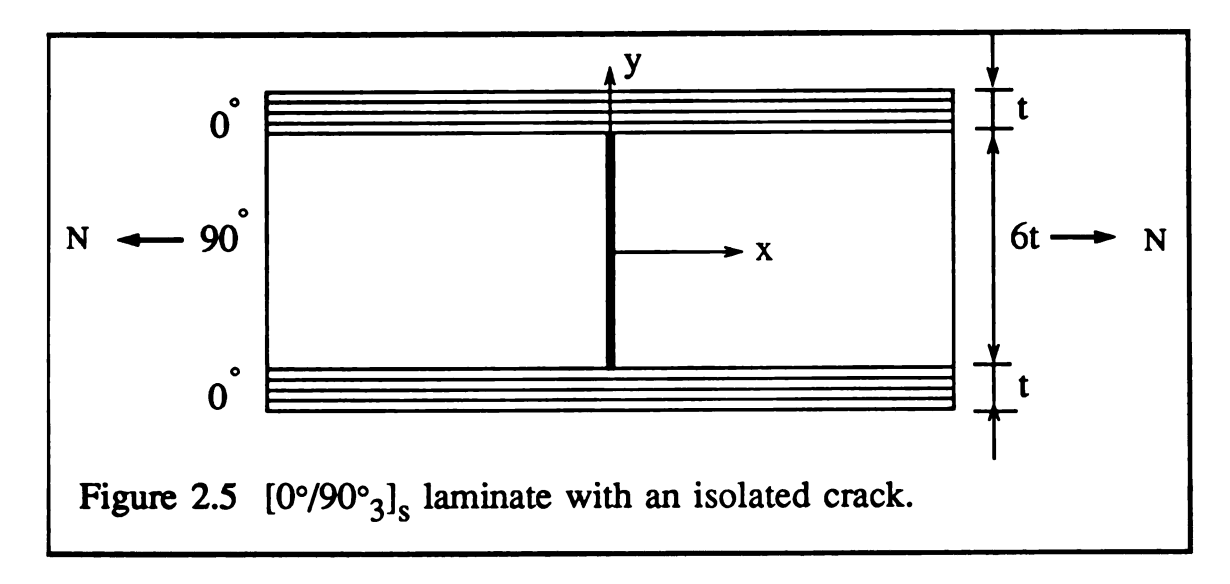
# (1) [0°/90°]<sub>s</sub> laminate with an isolated crack;



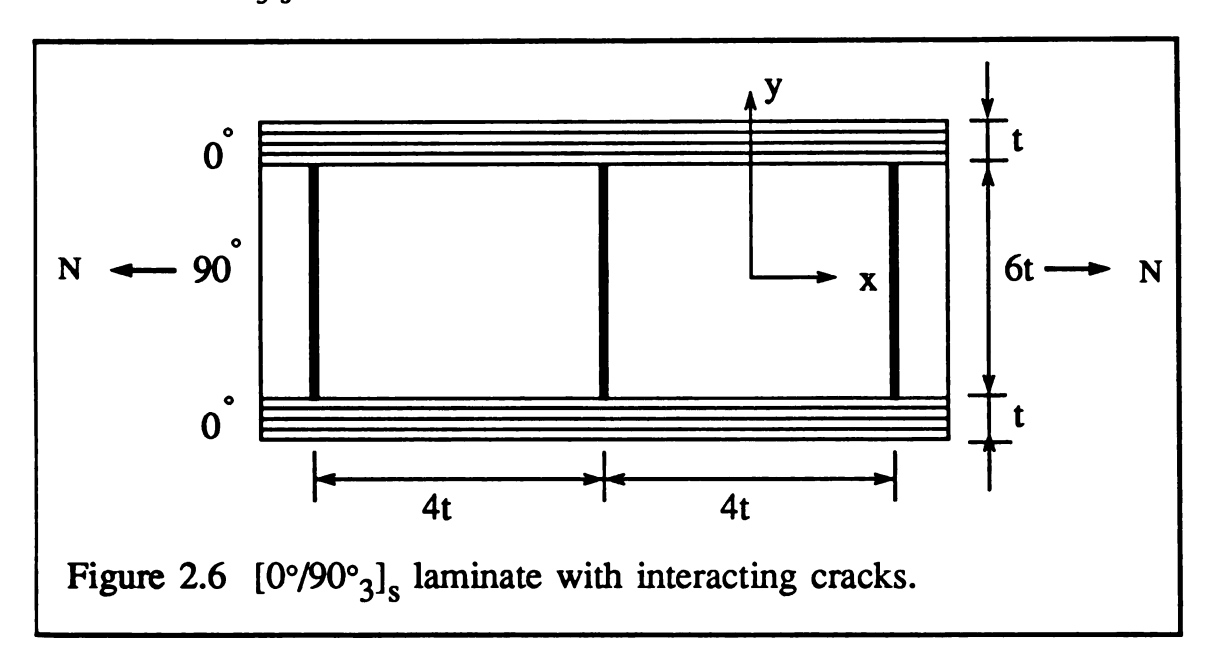
# (2) [0°/90°]<sub>s</sub> laminate with interacting cracks;



# (3) [0°/90°<sub>3</sub>]<sub>s</sub> laminate with an isolated crack; and



# (4) [0°/90°<sub>3</sub>]<sub>s</sub> laminate with interacting cracks.



The above cracked composite laminates are subjected to axisymmetric tensile loading at their ends. One of the main purposes of present analysis is to study the effect of transverse matrix cracks on the stress concentrations near the defective sites of the composite laminates.

## 2.2 Methodologies

Each type of composite laminate is modeled by employing the ANSYS finite element computer program using a 2-Dimensional isoparametric solid element (Element 42)<sup>[27]</sup>. Plane-strain analysis using a linear quadrilateral element is used in all types of composite laminates.

Usually the accuracy of solution in finite element analysis, especially near the crack tip, is sensitive to mesh configuration. Guydish et. al<sup>[28]</sup> stated the following important findings:

- (1) It is necessary that the elements immediately adjacent to the crack tip be very small in proportion to crack length;
- (2) The most efficient mesh results from a smooth progression of node spacing from the minimum space at the crack tips.

To check the validity of using present modelling for the cracked composite laminates, the stress concentration factor for homogeneous, isotropic material with same modelling as the present was compared to that from modelling of different methods.

Table 2.1 shows that the present modelling has good accuracy.

Table 2.1 Stress concentration factor for homogeneous material near the crack tip (Type 1).

Method	Stress concentration factor
Initial Mesh [29]	about 4.0
Subdomain Mesh [29]	about 15.0
Adaptive Mesh [29]	about 23.0
Present Mesh	25.36

Table 2.2 Material properties for the composite laminates.

Property	Glass/epoxy	Graphite/epoxy
Axial Young's modulus in fiber direction E <sub>A</sub> Gpa	41.7	208.3
Transverse Young's modulus  E <sub>T</sub> Gpa	13.0	15.5 (6.5 *)
Axial shear modulus  G <sub>A</sub> Gpa	3.40	1.65
Transverse shear modulus $G_T$ Gpa	4.58	2.30
Associated axial Poison's ratio $v_A$	0.30	0.255
Associated transverse Poisson's ratio $V_T$	0.42	0.413

From Table 2.2, for glass/epoxy the unidirectional properties are chosen as those reported by Highsmith, et al. [4] for scotch-ply specimens. For graphite/epoxy, the properties are chosen as those reported by Hashin for graphite(T300)/epoxy. [25] For computational convenience, the property of transverse Young's modulus,  $E_T$ , will be used as 15.5 Gpa instead of 6.5 Gpa.

For the analysis of type 1, due to symmetry, only one quarter of the composite laminate was considered. The dimensions of the composite laminate were taken as: length=6.0; thickness in 0° ply = 1.0; thickness in 90° ply=1.0. Keeping in view the application of Saint-Venant's principle in composite materials<sup>[30]</sup>, the total length in

finite element modelling was chosen as 10.0. Figures 2.7 and 2.8 show the finite element modelling of type 1 composite laminate.

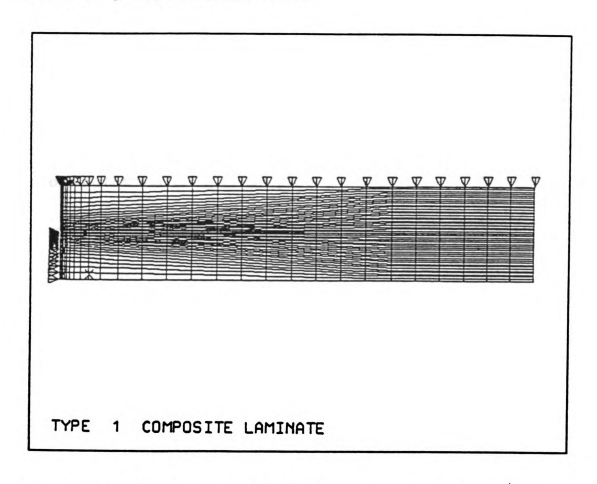


Figure 2.7 Finite element modelling of type 1 composite laminate.
(Number of elements = 1518, number of nodes = 1598)

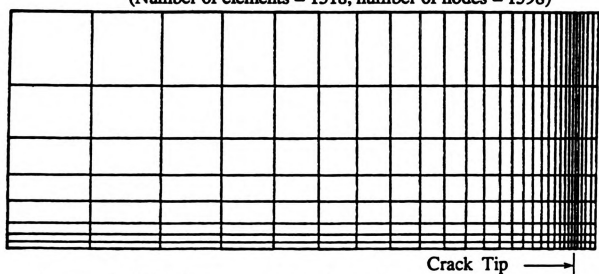


Figure 2.8 Finite element modelling of type 1 composite laminate. (Enlargement at crack)

For the analysis of type 2, one quarter of the composite laminate was considered. The dimensions of the composite laminate were taken as: length between two interacting cracks =4.0; thickness in 0° ply =1.0; thickness in 90° ply =1.0. The total length in finite element modelling was chosen as 10.0. Figure 2.9 shows the finite element modelling of type 2 composite laminate. In Figure 2.9, in order to include the upper crack in the finite element modelling, each node at the crack location was numbered twice so that one number was used in the lower element connectivity, and the second number was used in the upper element connectivity at the crack location.

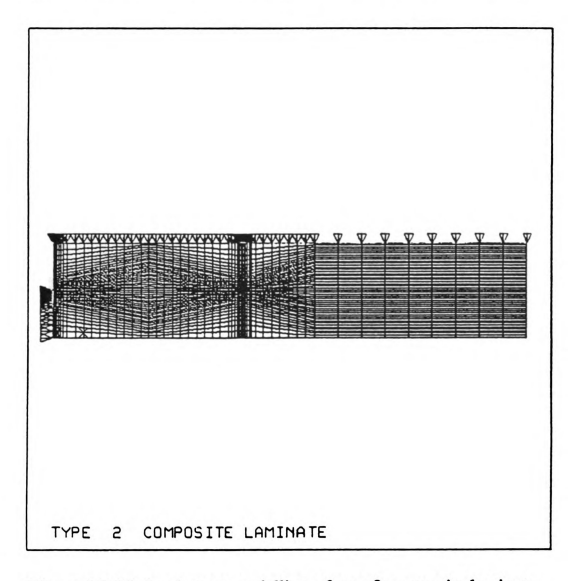


Figure 2.9 Finite element modelling of type 2 composite laminate. (Number of elements = 3450, number of nodes = 3595)

For the analysis of type 3, one quarter of the composite laminate was considered. The dimensions of the composite laminate were taken as: length = 6.0; thickness in  $0^{\circ}$  ply = 1.0; thickness in  $90^{\circ}$  ply = 3.0. The length in finite element modelling was taken as 10.0. Figure 2.10 shows the finite element modelling of type 3 composite laminate.

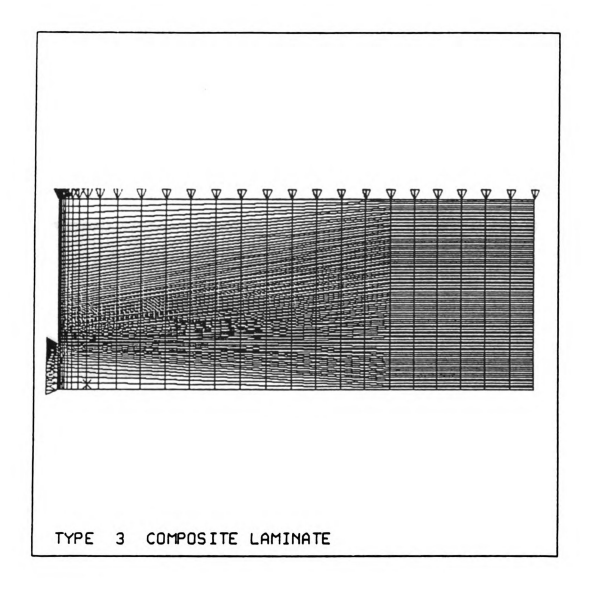


Figure 2.10 Finite element modelling of type 3 composite laminate. (Number of elements = 3036, number of nodes = 3162)

Finally, for the analysis of type 4, one quarter of the composite laminate was considered. The dimensions of the composite laminate were taken as: length between two interacting cracks = 4.0; thickness in  $0^{\circ}$  ply = 1.0; thickness in  $90^{\circ}$  ply = 3.0. The total length in finite element modelling was chosen as 13.0. Figure 2.11 shows the finite element modelling of type 4 composite laminate.

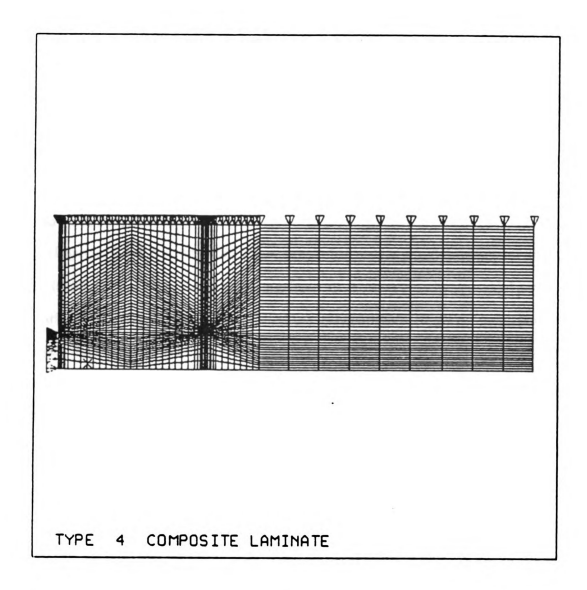


Figure 2.11 Finite element modelling of type 4 composite laminate.
(Number of elements = 3675, number of nodes = 3833)

### **CHAPTER 3**

# RESULTS AND DISCUSSION ON FINITE ELEMENT ANALYSIS

The results of the finite element analysis are presented in this section. Axial, shear, and transverse stress distributions at the interface in 0° ply, and axial stress distributions at the interface and transverse stress distributions at the midplane in 90° ply will be mainly discussed for all four different types of composite laminates (glass/epoxy and graphite/epoxy laminates). (Note: x, y coordinates in the following figures are set up differently from those in Figures 2.1-2.6. The new x, y coordinates are shown in the following figures.)

Figures 3.1-3.2 show the axial stress distribution in x-direction at the crack plane in  $0^{\circ}$  ply for type 1 composite laminate. It is observed that an axial stress concentration occurs at the crack tip. The stress concentration in glass/epoxy laminate is stronger than that in graphite/epoxy laminate. The same phenomenon may be observed for all four different types of composite laminates. The existence of this phenomenon is due to the fact that the ratio  $E_{axial}$  /  $E_{transverse}$  = 41.7/13.0 = 3.21 in glass/epoxy laminate is much lower than  $E_{axial}$  /  $E_{transverse}$  = 208.3 / 15.5 =13.44 in graphite/epoxy laminate.

Figures 3.3-3.10 show the axial stress distribution along y-direction at the interface in 0° ply for four different types of composite laminates (glass/epoxy and graphite/epoxy laminates). It is easily observed that an axial stress concentration occurs at the crack tip. The above result predicts that the transverse matrix crack can be

considered a likely site for the nucleation of longitudinal cracks and/or delamination cracking. It may also be noted that the stress concentrations for type 3 and 4 composite laminates are much stronger than those for type 1 and 2 composite laminates. From the theory of fracture mechanics, it seems very reasonable. But, for type 2 and 4 composite laminates, exactly symmetric axial stress distributions between two interacting cracks are not obtained. For this case, more discrepancies may be found in graphite/epoxy laminates rather than in glass/epoxy laminates. Furthermore, it is observed that as the Poisson's ratio(v) in 90° ply increases, the axial stress concentration becomes stronger for all four different types of composite laminates (glass/epoxy and graphite/epoxy laminates).

Figures 3.11-3.18 show the transverse and shear stress distributions along y-direction at the interface in 0° ply for four different types of composite laminates (glass/epoxy and graphite/epoxy laminates). Initially, type 1 and 3 composite laminates are considered. It is observed that near the crack tip, the transverse stress is tensile, then it drops rapidly to zero, changes to compressive, and tends to zero again. It is also observed that near crack tip, the shear stress is positive, and it drops rapidly to zero, and changes to negative, and stays negative. It may be noted that at almost the same place, in the vicinity of the crack tip, the transverse and shear stresses reach the maximum negative limit. But, it is observed that the magnitude of tensile transverse stress is much larger than that of tensile shear stress.

The above results predict that the possible debonding which might occur due to the tensile transverse stress ( $\sigma_{\mathbf{X}}(1,\mathbf{y})$ ,  $\sigma_{\mathbf{X}}(3,\mathbf{y})$ ) near the crack tip is unlikely to propagate in the fiber direction because of the change of sign of  $\sigma_{\mathbf{X}}(1,\mathbf{y})$ , and  $\sigma_{\mathbf{X}}(3,\mathbf{y})$ . And it is noted that a short crack transversing a few fibers in 0° ply cannot propagate too far in the original crack direction before it turned to propagate along the fiber direction.

Next, type 2 and 4 composite laminates are considered. It is observed that near the lower crack tip, the transverse stress is tensile, and it drops rapidly to zero, changes to compressive, and reaches zero again at the midpoint between two interacting cracks. The transverse stress distribution is almost symmetric about the midpoint between two interacting cracks. It is indicated that near the lower crack tip, the shear stress is tensile, and it drops rapidly to zero, changes to compressive, and reaches zero again at the midpoint between two interacting cracks. After the midpoint, it changes tensile and reaches the maximum tensile, drops to zero, and becomes rapidly compressive. Also, the shear stress distribution is almost anti-symmetric about the midpoint between two interacting cracks. It may also be noted that the magnitudes in transverse and shear stresses for type 3 and 4 composite laminates are larger than those for type 1 and 2 composite laminates.

Figures 3.19-3.26 show the axial stress distribution along y-direction at the interface in 90° ply for four different types of composite laminates (glass/epoxy and graphite/epoxy laminates). For glass/epoxy laminates, an axial stress concentration may be found at the crack tip for all four different types of composite laminates.

The axial stress concentration in 90° ply is not so strong as that in 0° ply. However, the stress concentrations for type 3 and 4 composite laminates are much stronger than those for type 1 and 2 composite laminates. For graphite/epoxy laminates, a strong axial stress concentration may not be seen near the crack tip. It is expected that this is due to the small ratio of  $E_{axial}$  /  $E_{transverse}$  in 90° ply for graphite/epoxy laminates.

Figures 3.27-3.34 show the transverse stress distribution in the midplane for four different types of composite laminates (glass/epoxy and graphite/epoxy laminates). First, glass/epoxy laminates are considered. For type 1 and 3 composite laminates, a kind of compressive stress concentration occurs near the crack location. This is due to a very strong tensile axial stress concentration at the crack tip. So, the compressive transverse stress concentration for type 3 composite laminate is stronger than that for type 1 composite laminate.

It is observed that near the crack location, the transverse stress is maximum compressive, and it goes to zero, changes to tensile, and reaches maximum tensile, in the vicinity of the crack location, and then it goes to zero. However, the maximum tensile transverse stress is not critical. For type 2 composite laminate, it is also observed that near the lower crack location, the transverse stress is maximum compressive, and it goes to zero, changes to tensile, and reaches the maximum tensile within the vicinity of the lower crack location, and continues to the neighborhood of the upper crack location, and goes to zero, and then becomes compressive, and reaches the maximum compressive. The transverse stress distribution is almost symmetric about the midpoint between two interacting cracks. For type 4 composite laminate, it is observed that near the lower crack location, the transverse stress is the maximum compressive, and it goes to zero, changes to tension, and then reaches the maximum tensile at the midpoint between two interacting cracks. This is due to the fact that the maximum compressive transverse stress occurs in the neighborhood of the crack tip, rather than at the midplane, as shown in Figure 3.35. So, the compressive transverse stress concentration for type 4 composite laminate at the midplane is not as strong as that for type 3 composite laminate.

Similar results as for glass/epoxy laminates are obtained for graphite/epoxy laminates. The distinctive difference is that there is hardly any tensile transverse stress region in graphite/epoxy laminates.

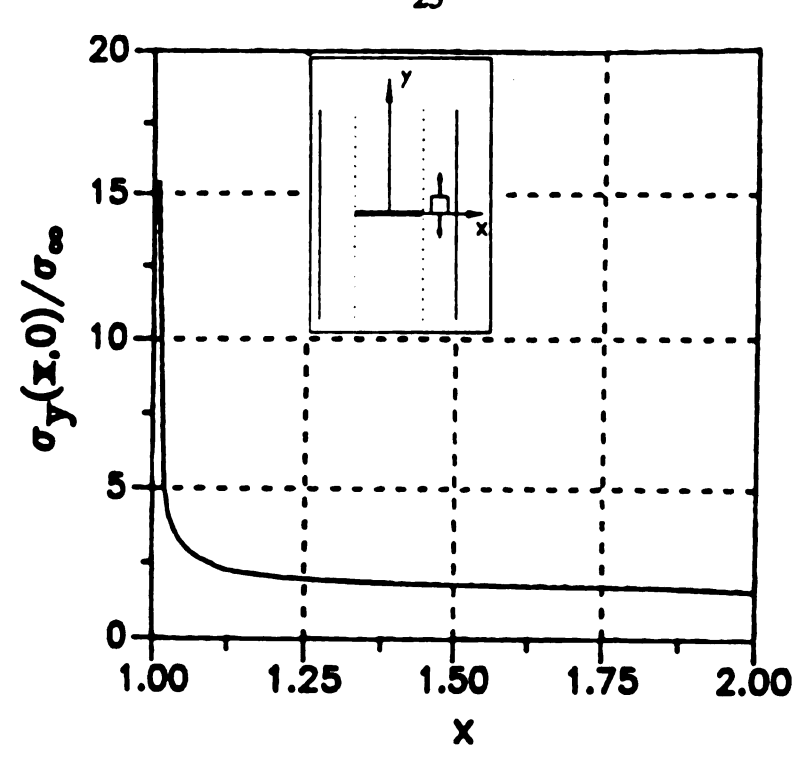


Figure 3.1 Stress component  $\sigma_y$  at the crack plane in 0° ply.  $[0^\circ/90^\circ]_s$  glass/epoxy composite laminate (Type 1).

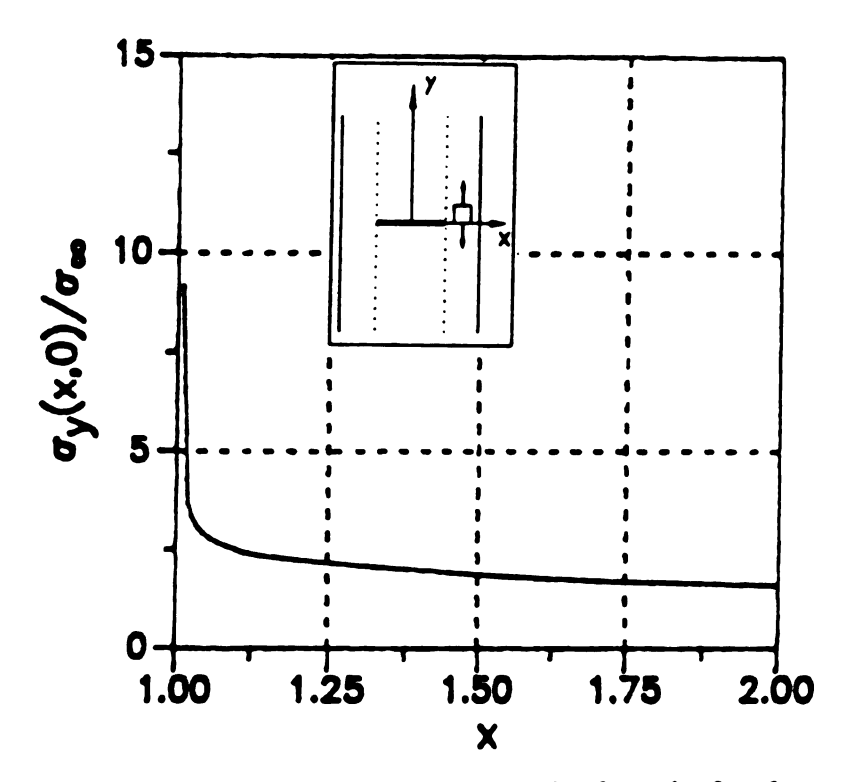


Figure 3.2 Stress component  $\sigma_y$  at the crack plane in 0° ply.  $[0^{\circ}/90^{\circ}]_s$  graphite/epoxy composite laminate (Type 1).



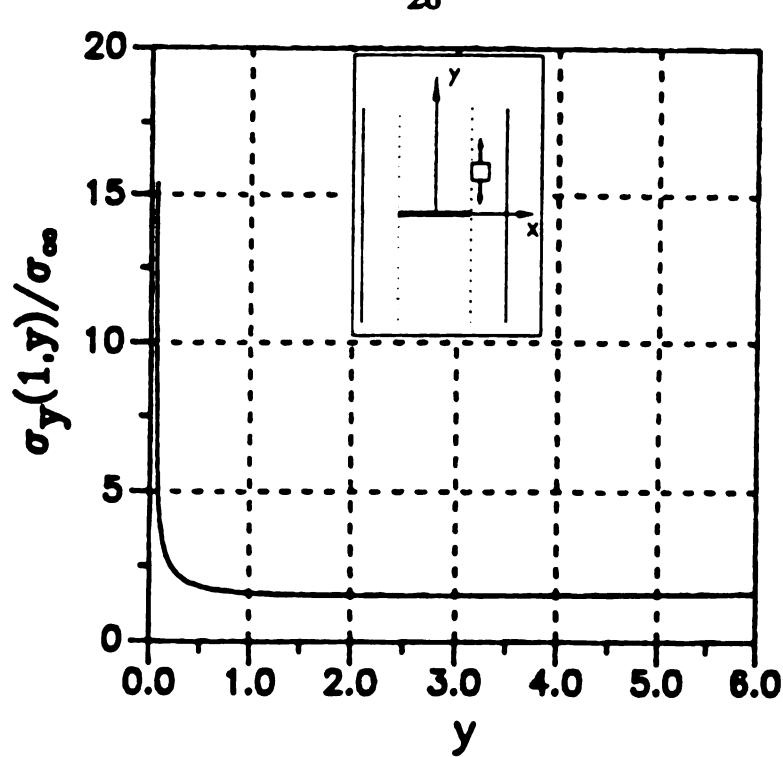


Figure 3.3 Stress component  $\sigma_y$  at the interface in 0° ply.  $[0^{\circ}/90^{\circ}]_s$  glass/epoxy composite laminate (Type 1).

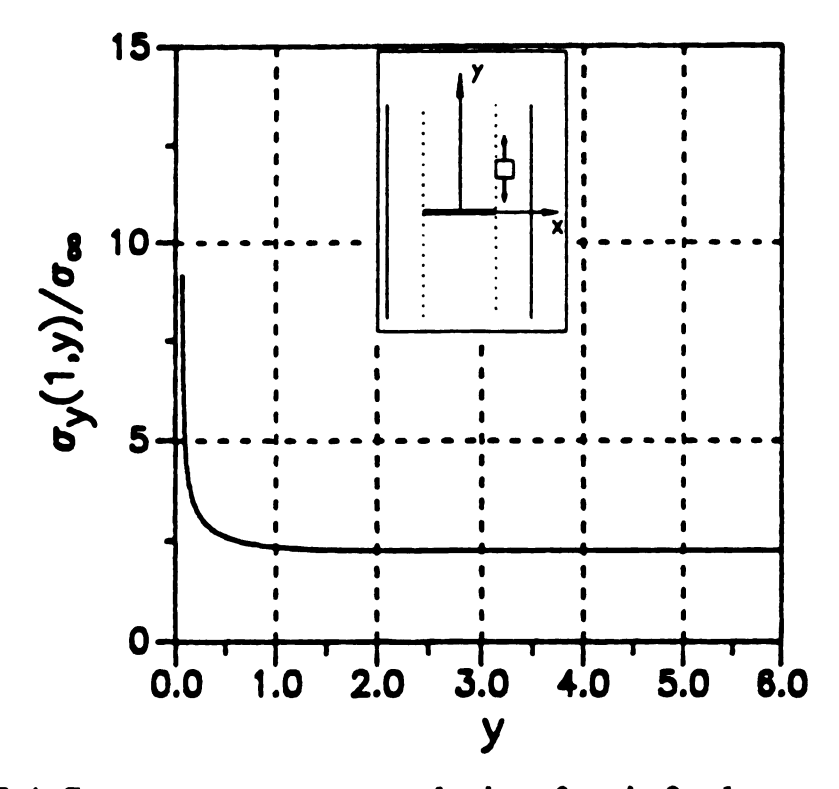


Figure 3.4 Stress component  $\sigma_y$  at the interface in 0° ply.  $[0^{\circ}/90^{\circ}]_s$  graphite/epoxy composite laminate (Type 1).



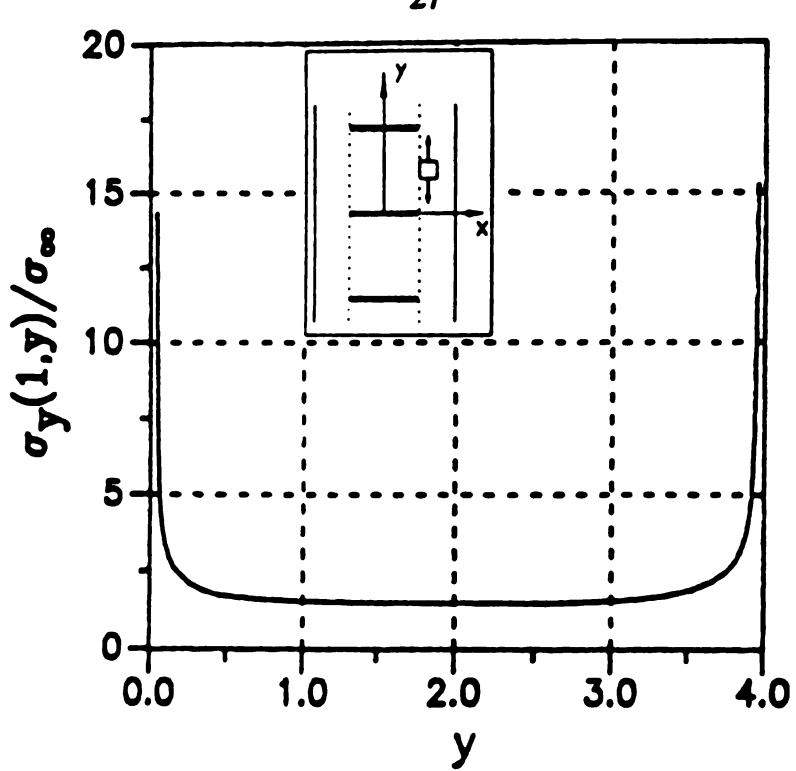


Figure 3.5 Stress component  $\sigma_y$  at the interface in 0° ply.  $[0^\circ/90^\circ]_s$  glass/epoxy composite laminate (Type 2).

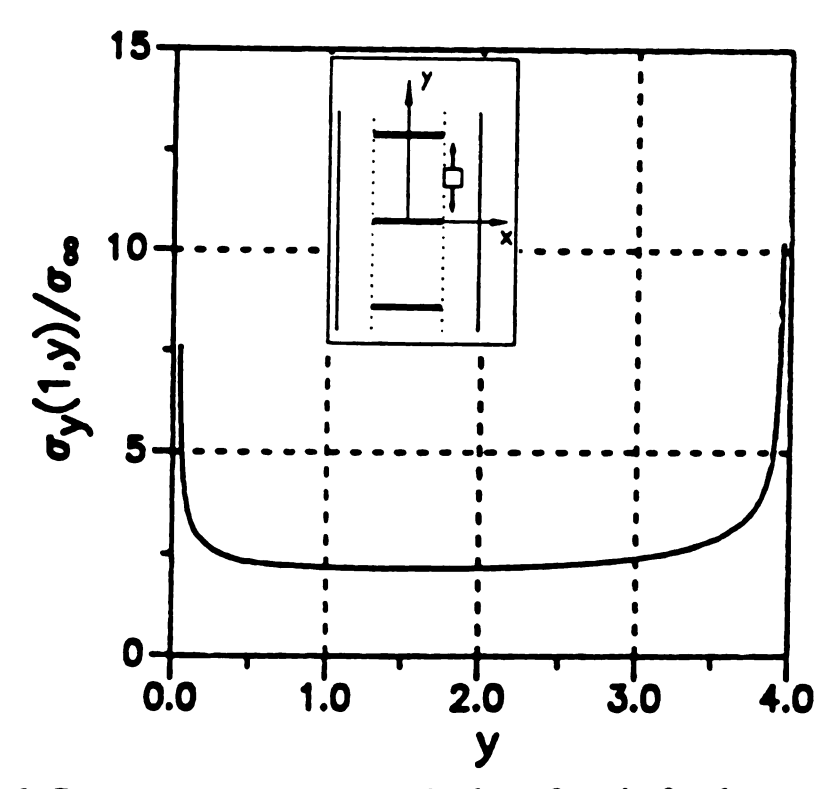


Figure 3.6 Stress component  $\sigma_y$  at the interface in 0° ply.  $[0^\circ/90^\circ]_s$  graphite/epoxy composite laminate (Type 2).



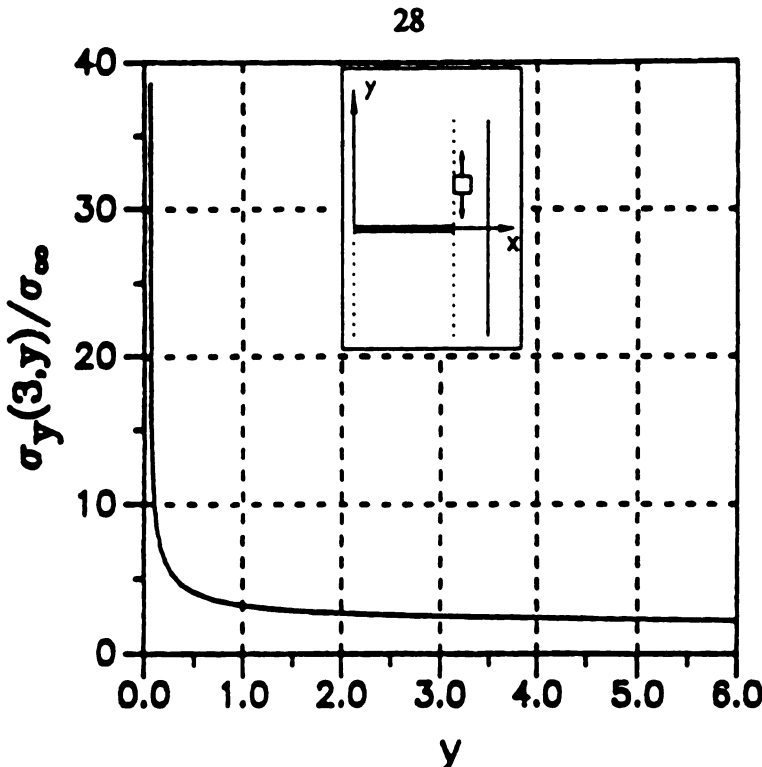


Figure 3.7 Stress component  $\sigma_y$  at the interface in 0° ply. [0°/90°3]<sub>s</sub> glass/epoxy composite laminate (Type 3).

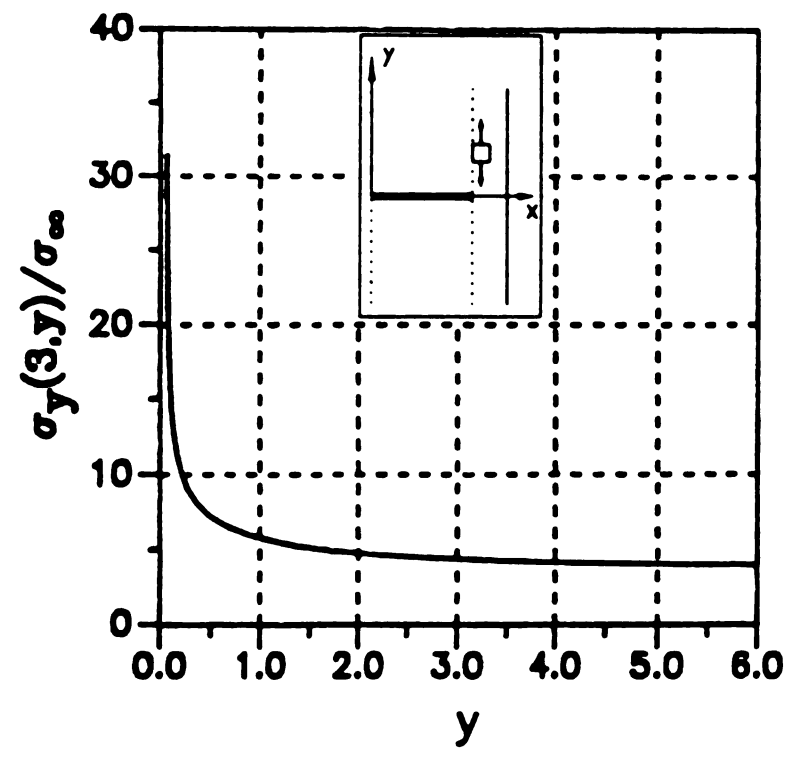


Figure 3.8 Stress component  $\sigma_y$  at the interface in 0° ply. [0°/90°3]<sub>s</sub> graphite/epoxy composite laminate (Type 3).



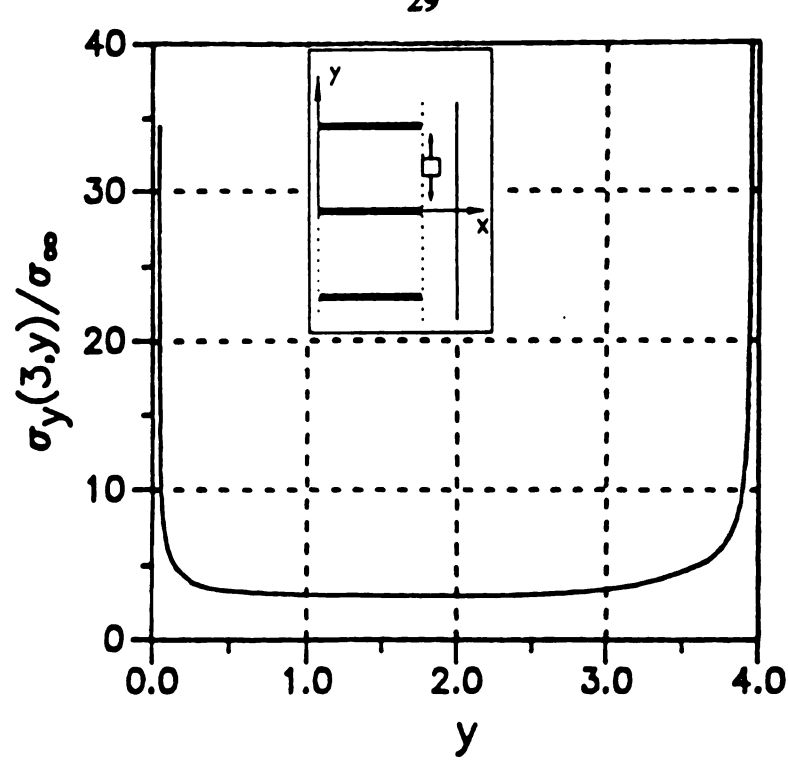


Figure 3.9 Stress component  $\sigma_y$  at the interface in 0° ply.  $[0^{\circ}/90^{\circ}_{3}]_{s}$  glass/epoxy composite laminate (Type 4).

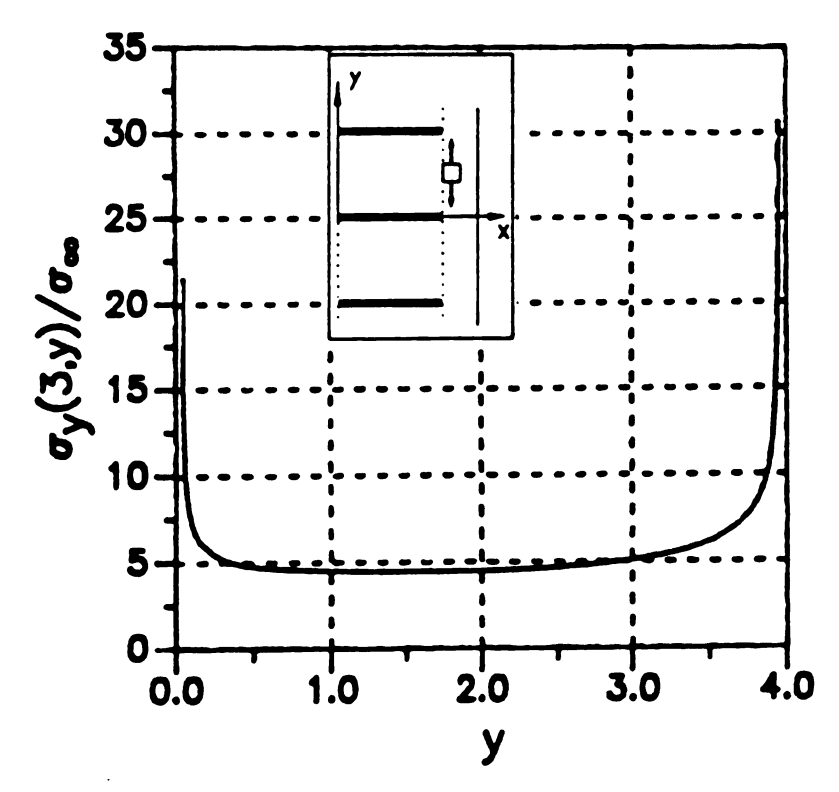


Figure 3.10 Stress component  $\sigma_y$  at the interface in 0° ply.  $[0^\circ/90^\circ_3]_s$  graphite/epoxy composite laminate (Type 4).

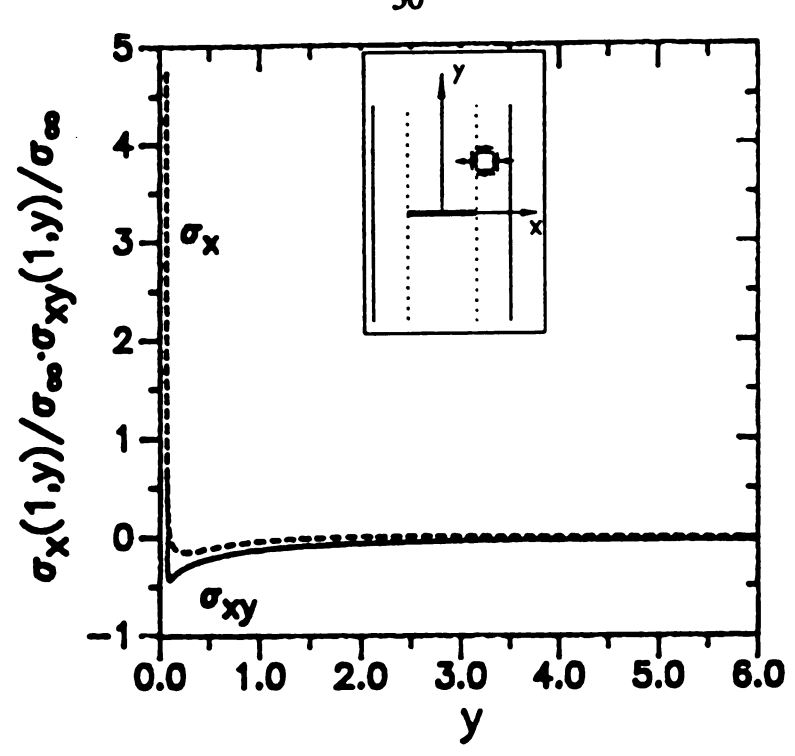


Figure 3.11 Stress components  $\sigma_x$  and  $\sigma_{xy}$  at the interface in 0° ply.  $[0^\circ/90^\circ]_x$  glass/epoxy composite laminate (Type 1).

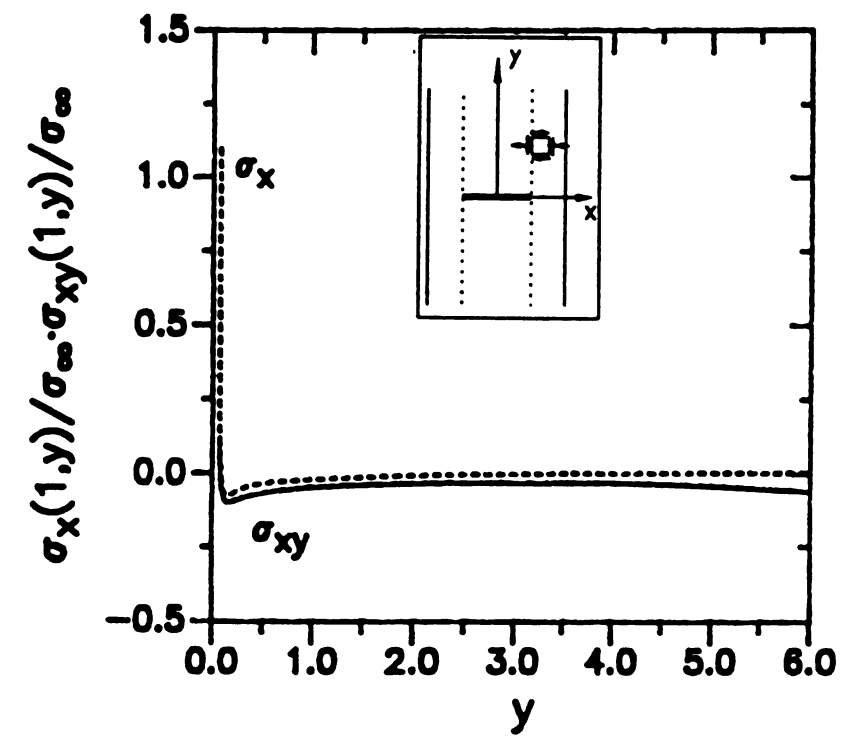


Figure 3.12 Stress components  $\sigma_x$  and  $\sigma_{xy}$  at the interface in 0° ply.  $[0^\circ/90^\circ]_s$  graphite/epoxy composite laminate (Type 1).

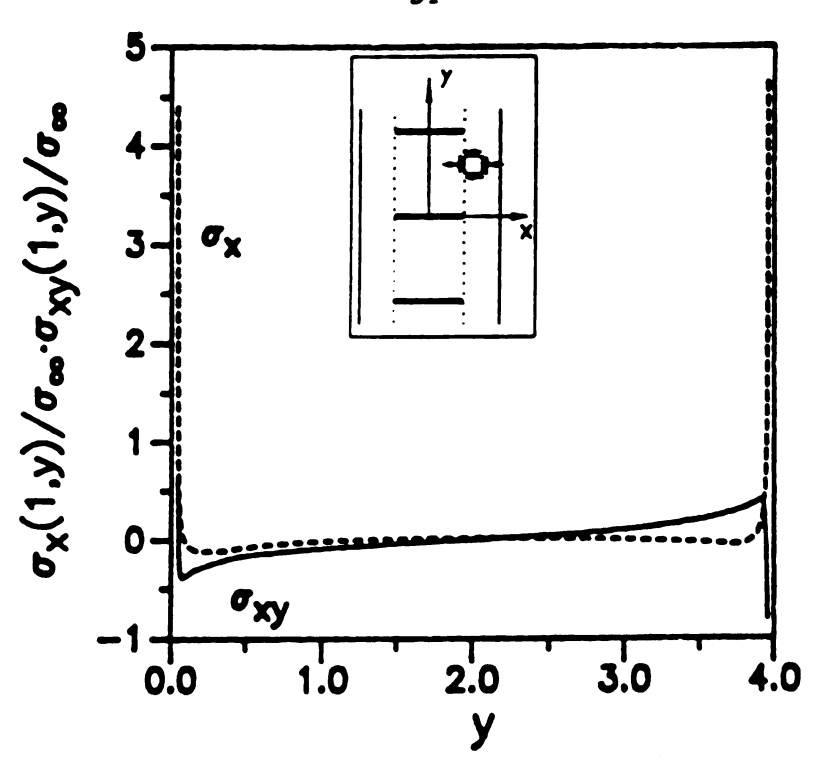


Figure 3.13 Stress components  $\sigma_x$  and  $\sigma_{xy}$  at the interface in 0° ply.  $[0^{\circ}/90^{\circ}]_s$  glass/epoxy composite laminate (Type 2).

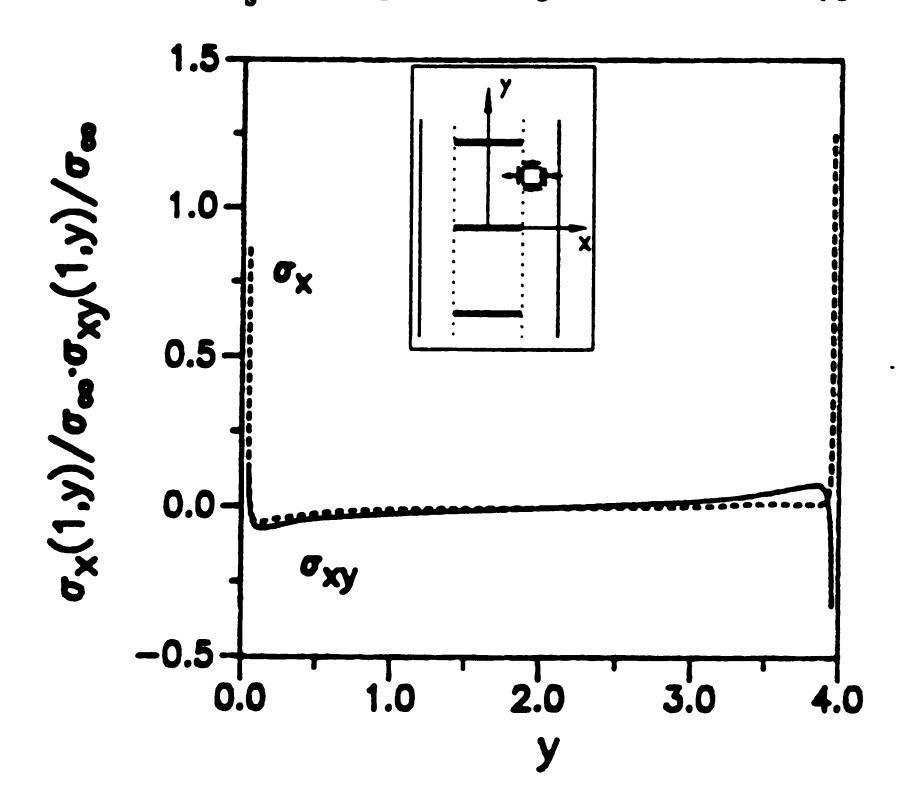


Figure 3.14 Stress components  $\sigma_x$  and  $\sigma_{xy}$  at the interface in 0° ply.  $[0^{\circ}/90^{\circ}]_s$  graphite/epoxy composite laminate (Type 2).

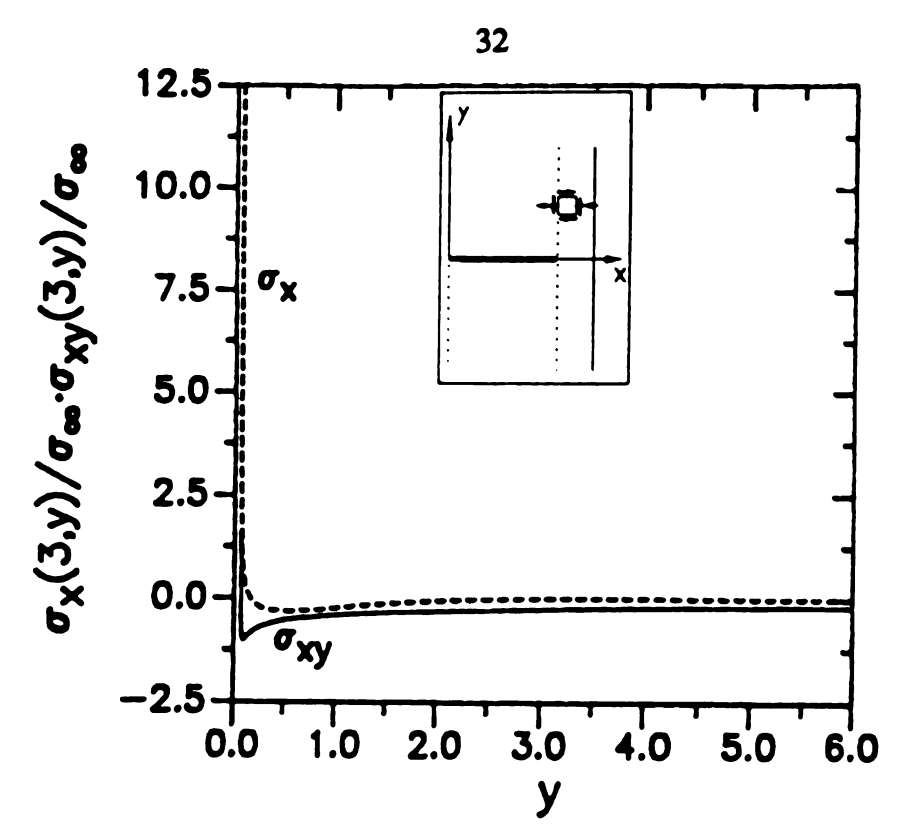


Figure 3.15 Stress components  $\sigma_x$  and  $\sigma_{xy}$  at the interface in 0° ply.  $[0^\circ/90^\circ_3]_s$  glass/epoxy composite laminate (Type 3).

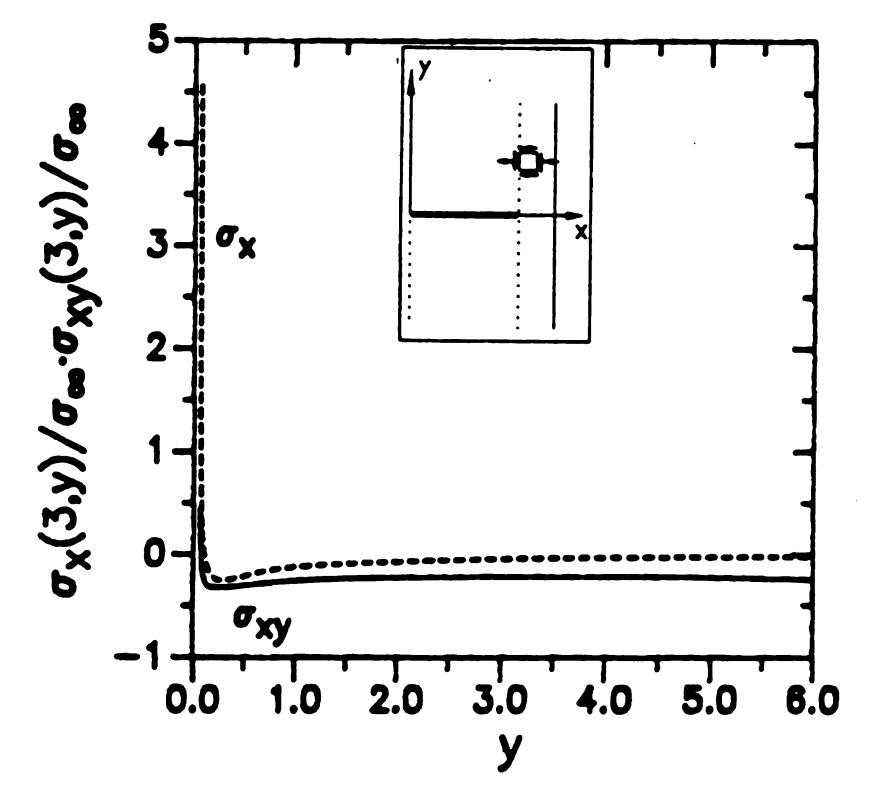


Figure 3.16 Stress components  $\sigma_x$  and  $\sigma_{xy}$  at the interface in 0° ply.  $[0^\circ/90^\circ_3]_s$  graphite/epoxy composite laminate (Type 3).

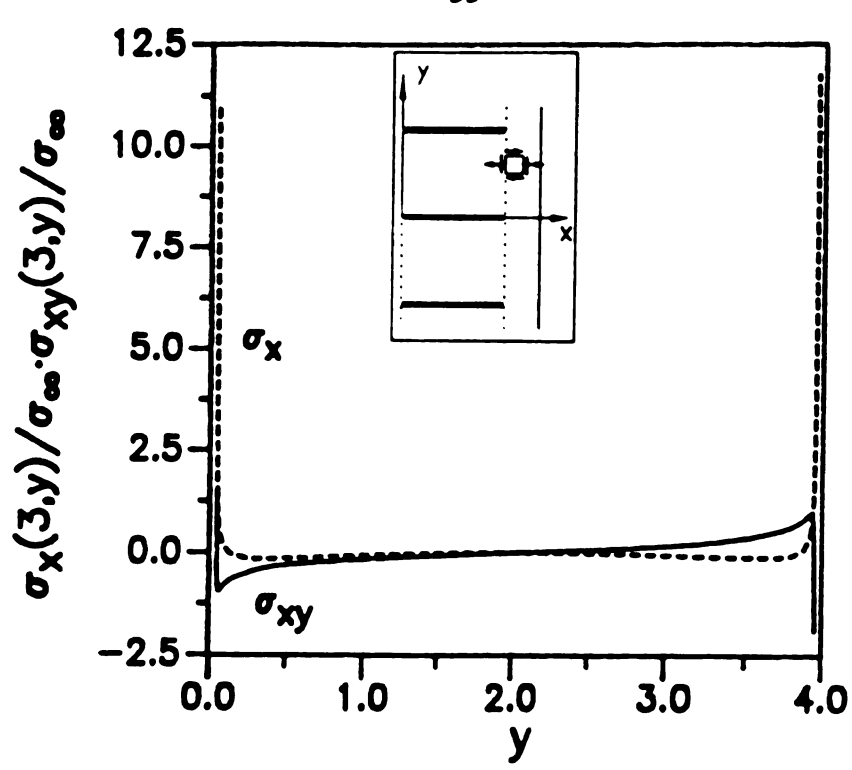


Figure 3.17 Stress components  $\sigma_x$  and  $\sigma_{xy}$  at the interface in 0° ply.  $[0^\circ/90^\circ_3]_s$  glass/epoxy composite laminate (Type 4).

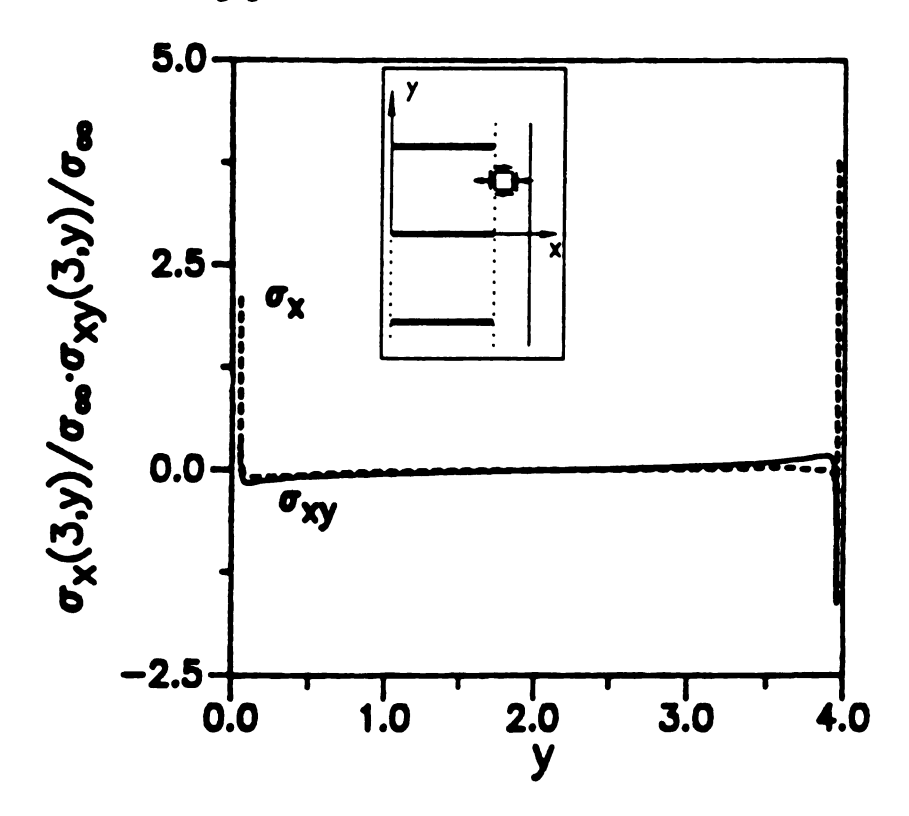


Figure 3.18 Stress components  $\sigma_x$  and  $\sigma_{xy}$  at the interface in 0° ply.  $[0^\circ/90^\circ_3]_s$  graphite/epoxy composite laminate (Type 4).

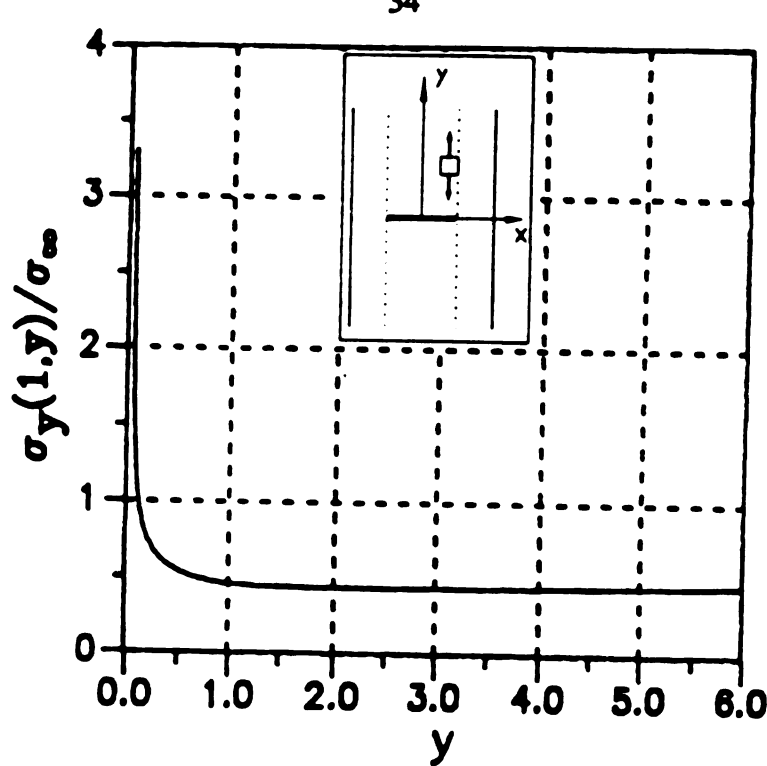


Figure 3.19 Stress component  $\sigma_y$  at the interface in 90° ply.  $[0^{\circ}/90^{\circ}]_s$  glass/epoxy composite laminate (Type 1).

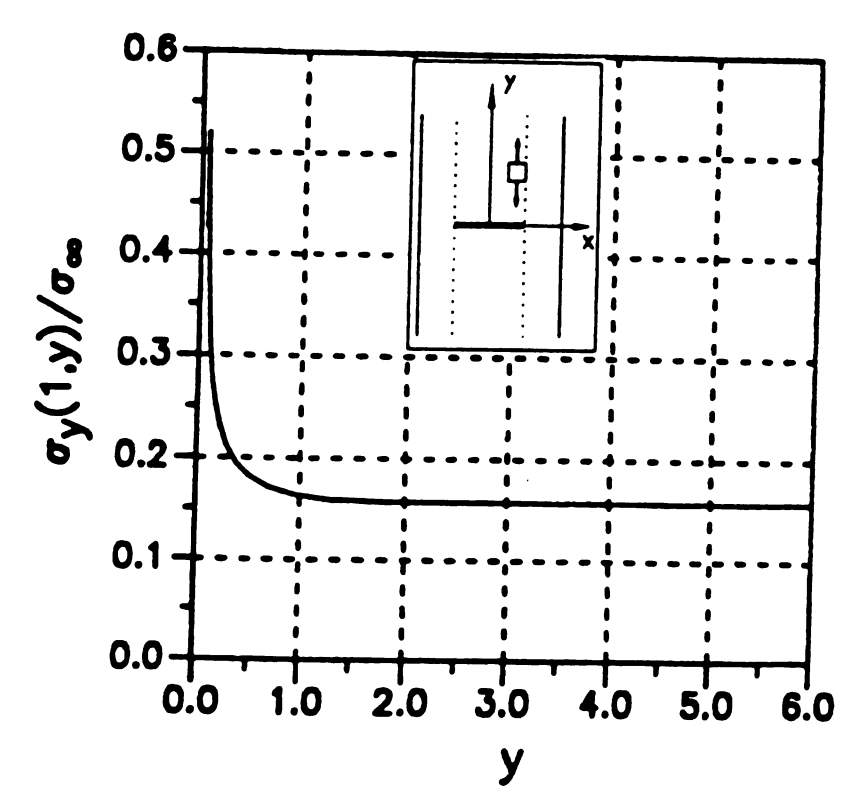


Figure 3.20 Stress component  $\sigma_y$  at the interface in 90° ply.  $[0^{\circ}/90^{\circ}]_s$  graphite/epoxy composite laminate (Type 1).

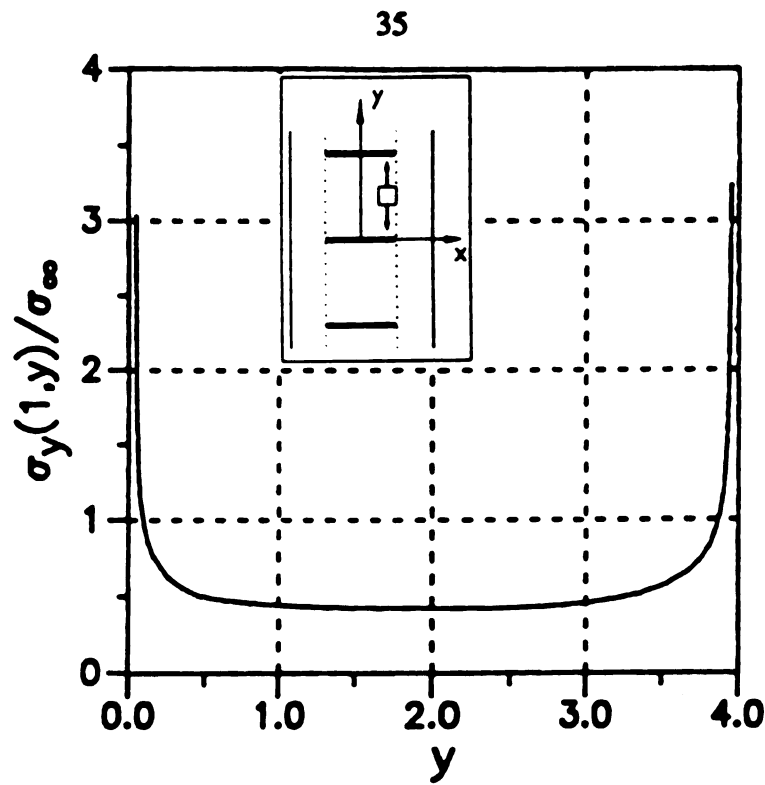


Figure 3.21 Stress component  $\sigma_y$  at the interface in 90° ply. [0°/90°]<sub>s</sub> glass/epoxy composite laminate (Type 2).

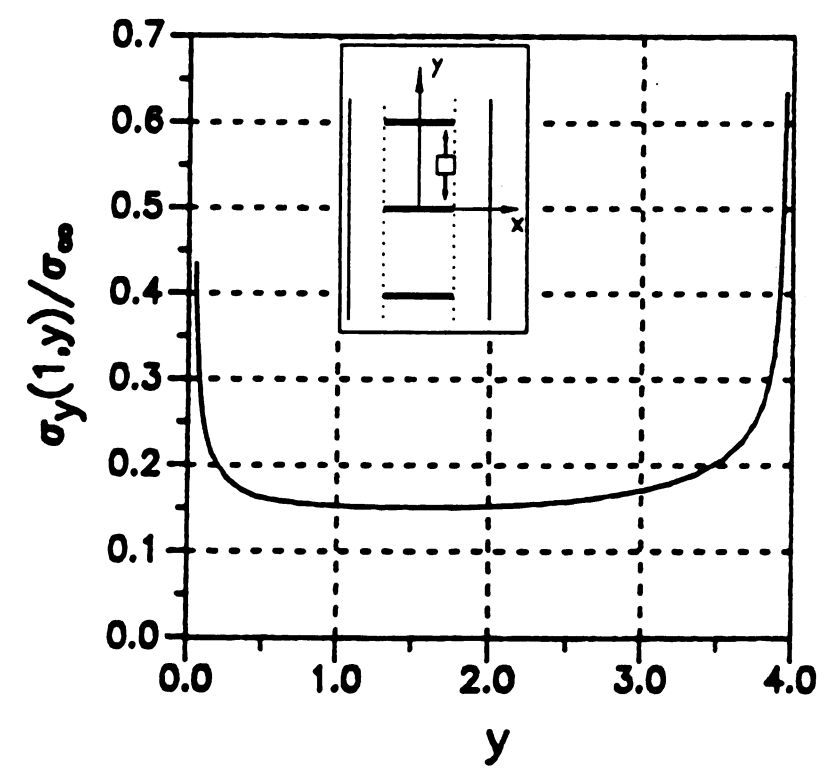


Figure 3.22 Stress component  $\sigma_y$  at the interface in 90° ply. [0°/90°]<sub>s</sub> graphite/epoxy composite laminate (Type 2).



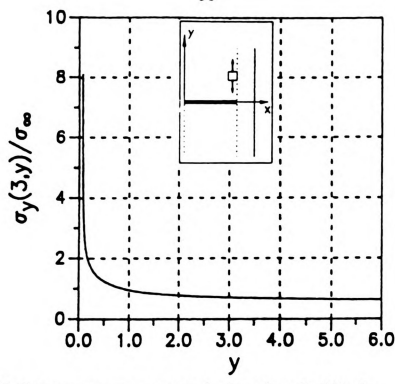


Figure 3.23 Stress component  $\sigma_y$  at the interface in 90° ply. [0°/90°3]<sub>s</sub> glass/epoxy composite laminate (Type 3).

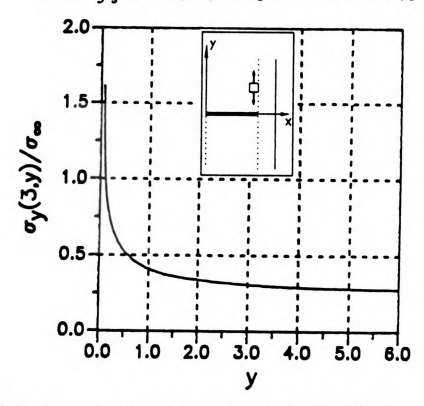


Figure 3.24 Stress component  $\sigma_{\rm v}$  at the interface in 90° ply. [0°/90°<sub>3</sub>]<sub>s</sub> graphite/epoxy composite laminate (Type 3).



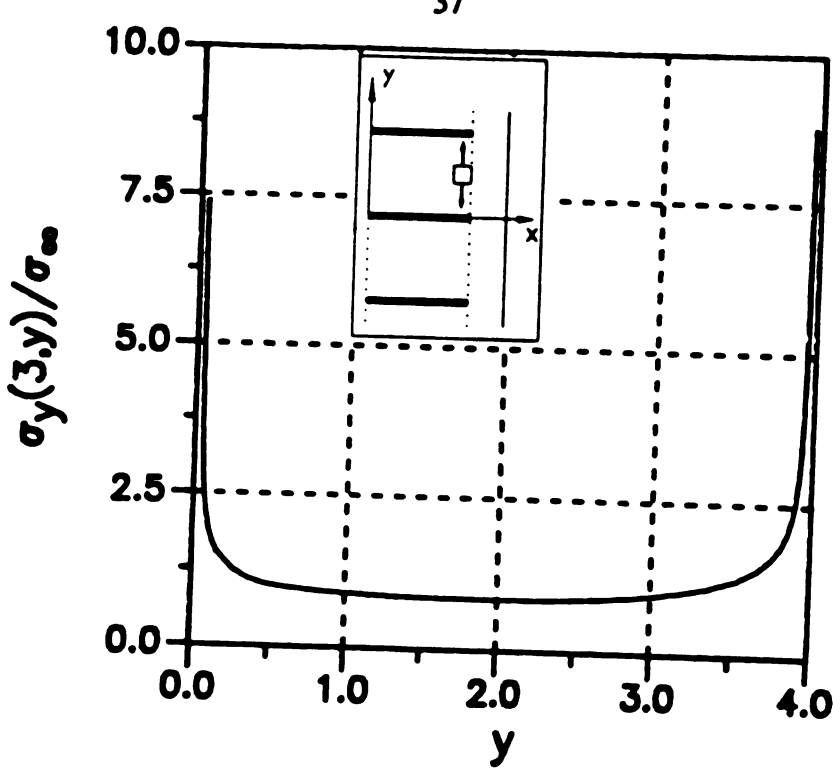


Figure 3.25 Stress component  $\sigma_y$  at the interface in 90° ply.  $[0^{\circ}/90^{\circ}_{3}]_{s}$  glass/epoxy composite laminate (Type 4).

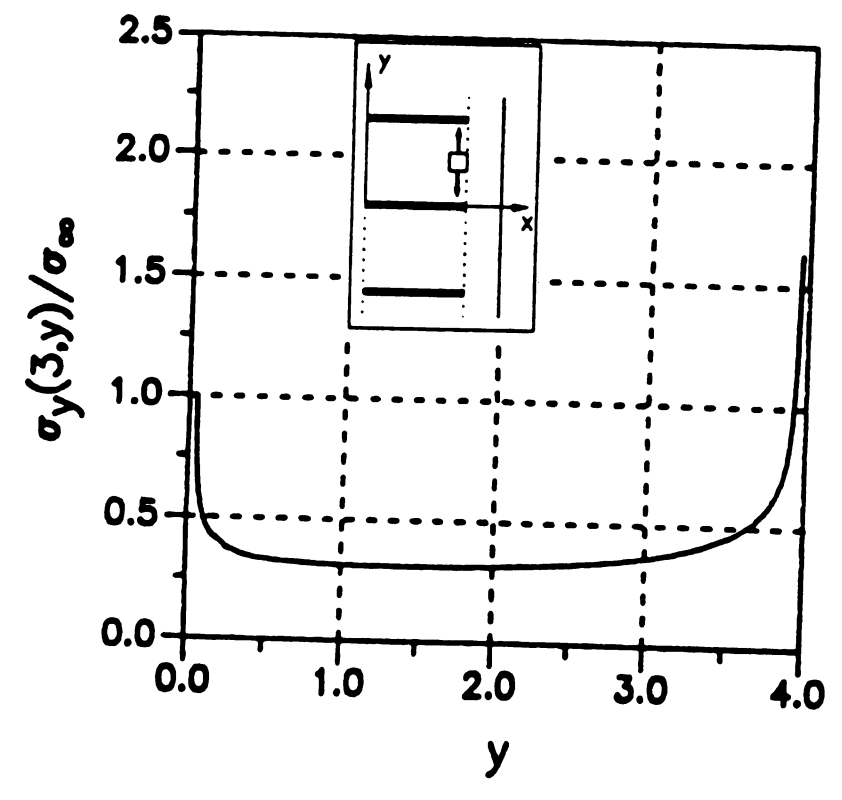


Figure 3.26 Stress component  $\sigma_y$  at the interface in 90° ply.  $[0^\circ/90^\circ_3]_s$  graphite/epoxy composite laminate (Type 4).

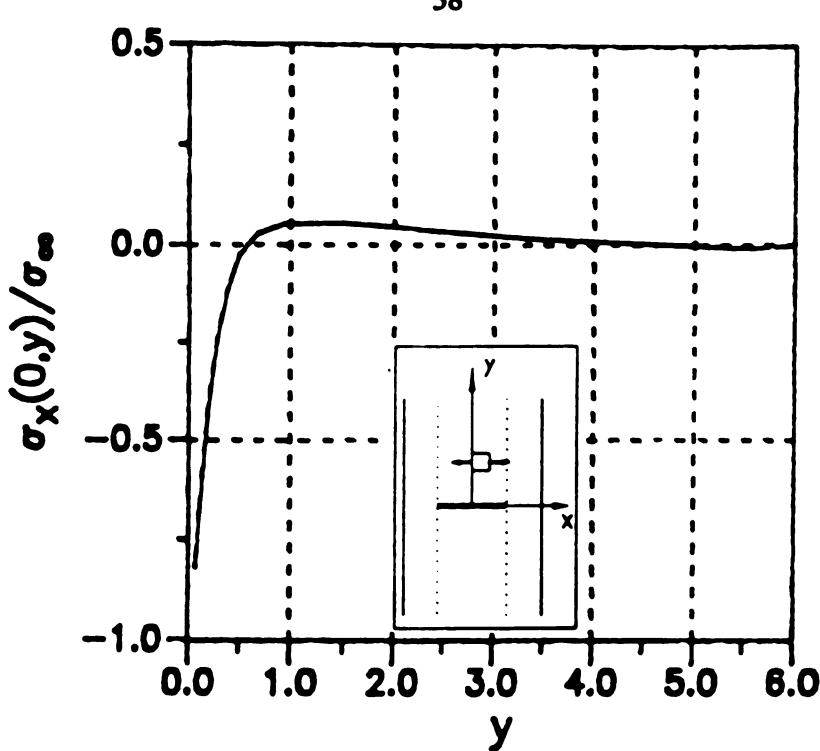


Figure 3.27 Stress component  $\sigma_x$  at the midplane in 90° ply. [0°/90°]<sub>s</sub> glass/epoxy composite laminate (Type 1).

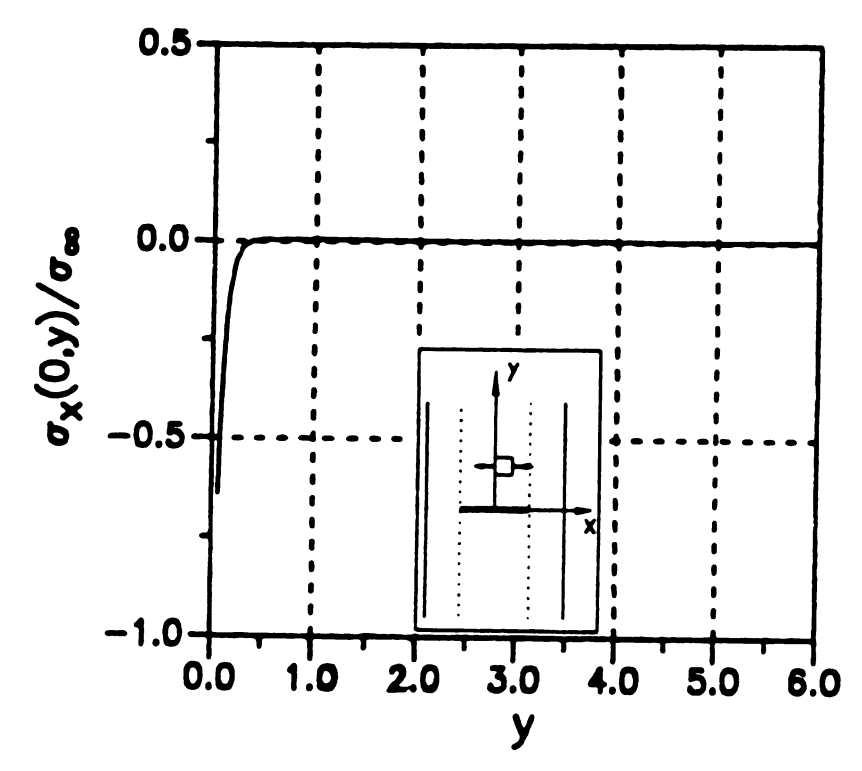


Figure 3.28 Stress component  $\sigma_x$  at the midplane in 90° ply. [0°/90°]<sub>s</sub> graphite/epoxy composite laminate (Type 1).

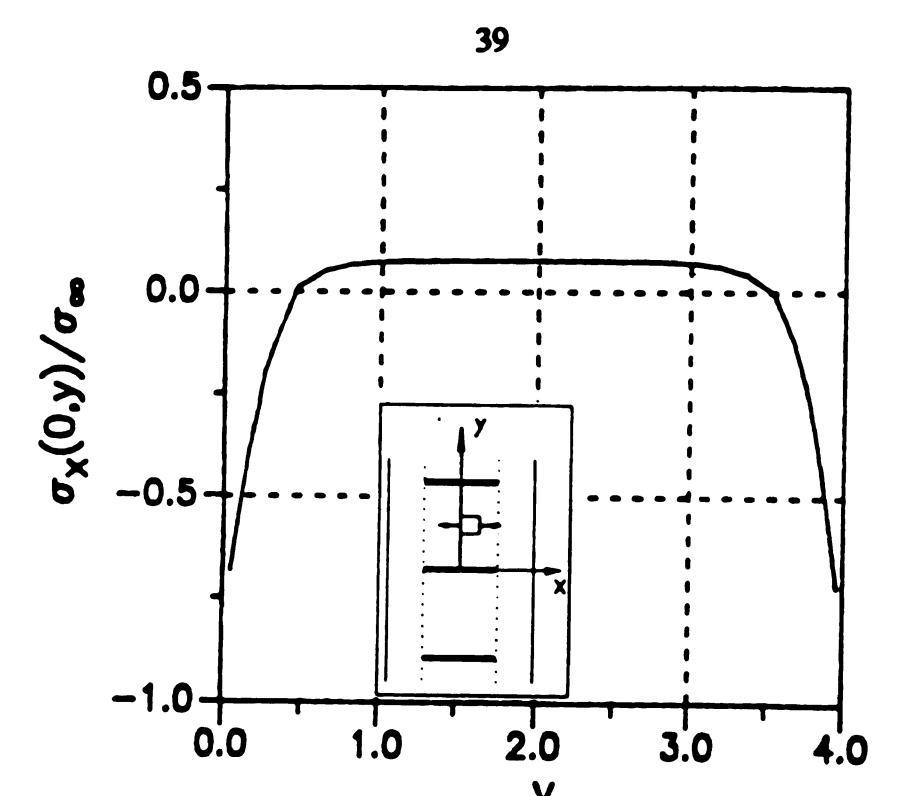


Figure 3.29 Stress component  $\sigma_x$  at the midplane in 90° ply. [0°/90°]<sub>s</sub> glass/epoxy composite laminate (Type 2).

2.0 y

1.0

3.0

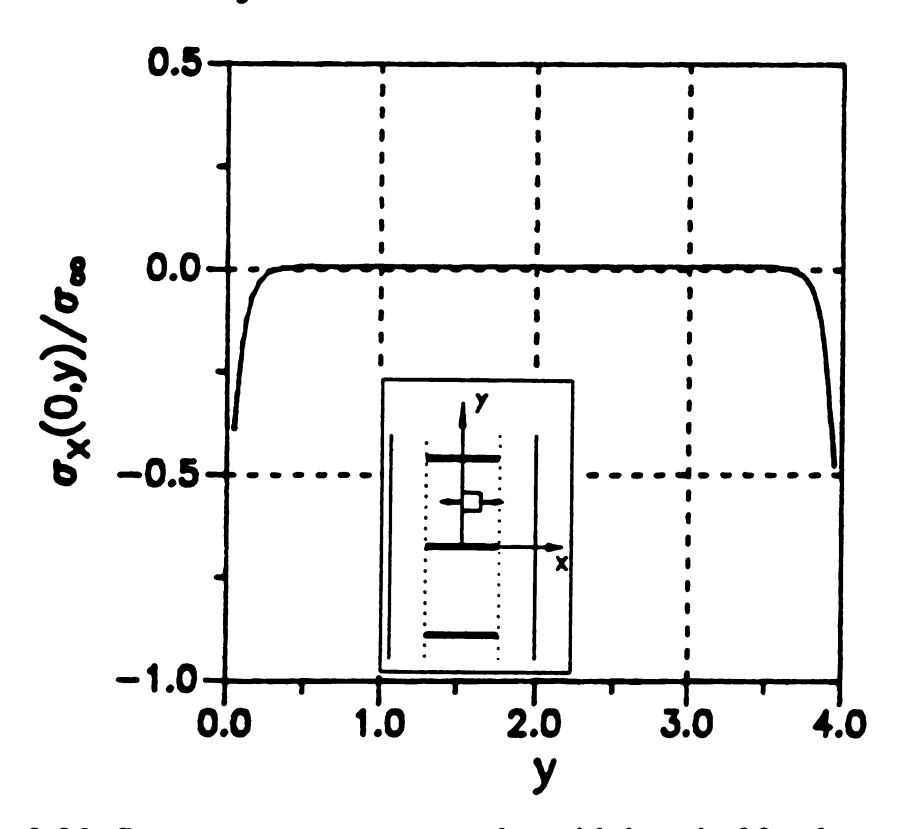


Figure 3.30 Stress component  $\sigma_x$  at the midplane in 90° ply. [0°/90°]<sub>s</sub> graphite/epoxy composite laminate (Type 2).

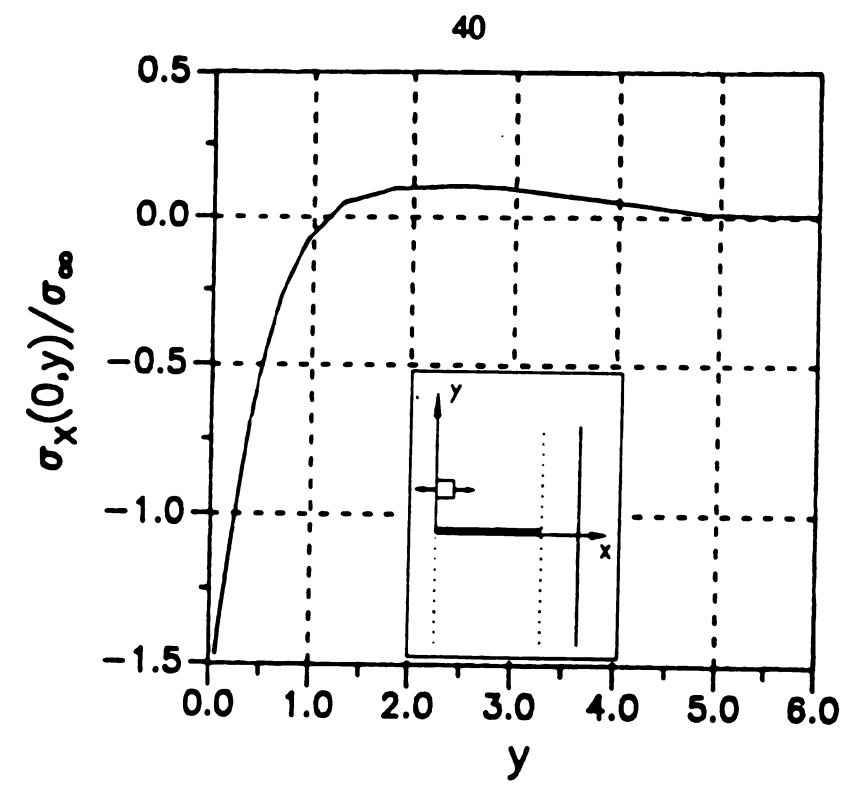


Figure 3.31 Stress component  $\sigma_x$  at the midplane in 90° ply.  $[0^{\circ}/90^{\circ}_{3}]_{s}$  glass/epoxy composite laminate (Type 3).

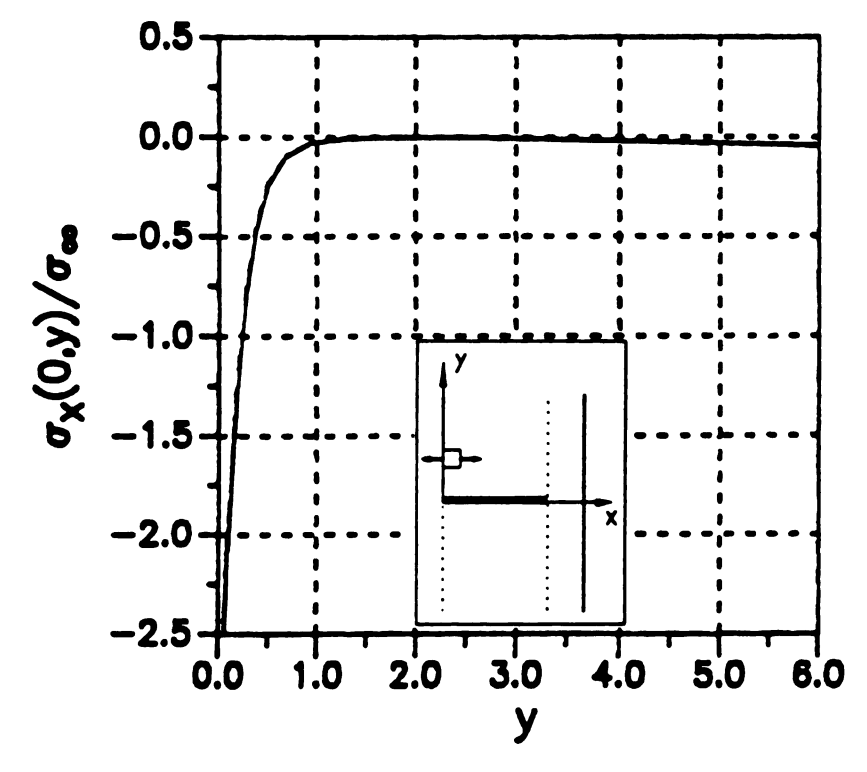


Figure 3.32 Stress component  $\sigma_x$  at the midplane in 90° ply.  $[0^\circ/90^\circ_3]_s$  graphite/epoxy composite laminate (Type 3).



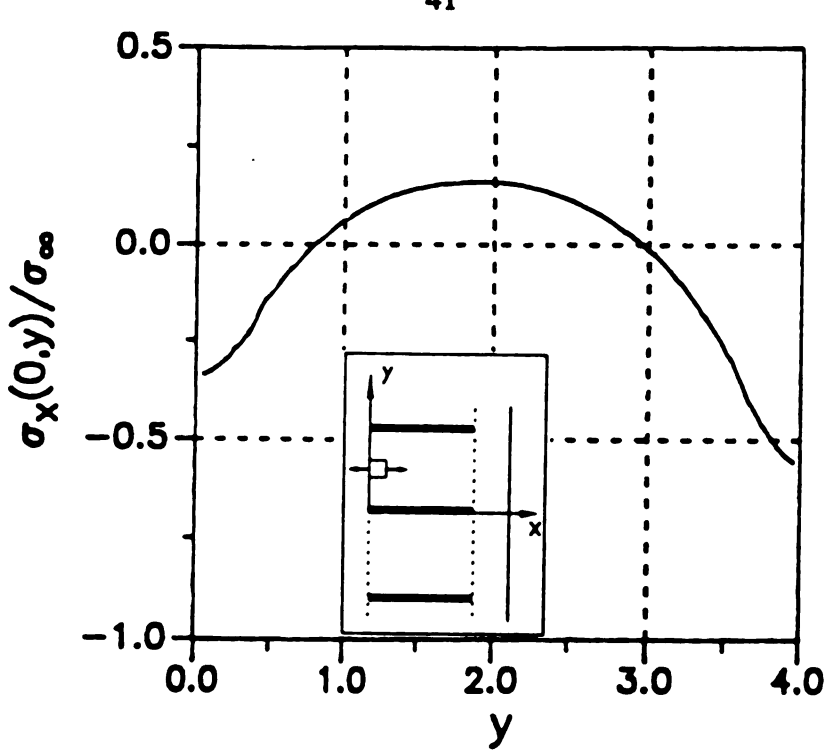


Figure 3.33 Stress component  $\sigma_x$  at the midplane in 90° ply.  $[0^\circ/90^\circ_3]_s$  glass/epoxy composite laminate (Type 4).

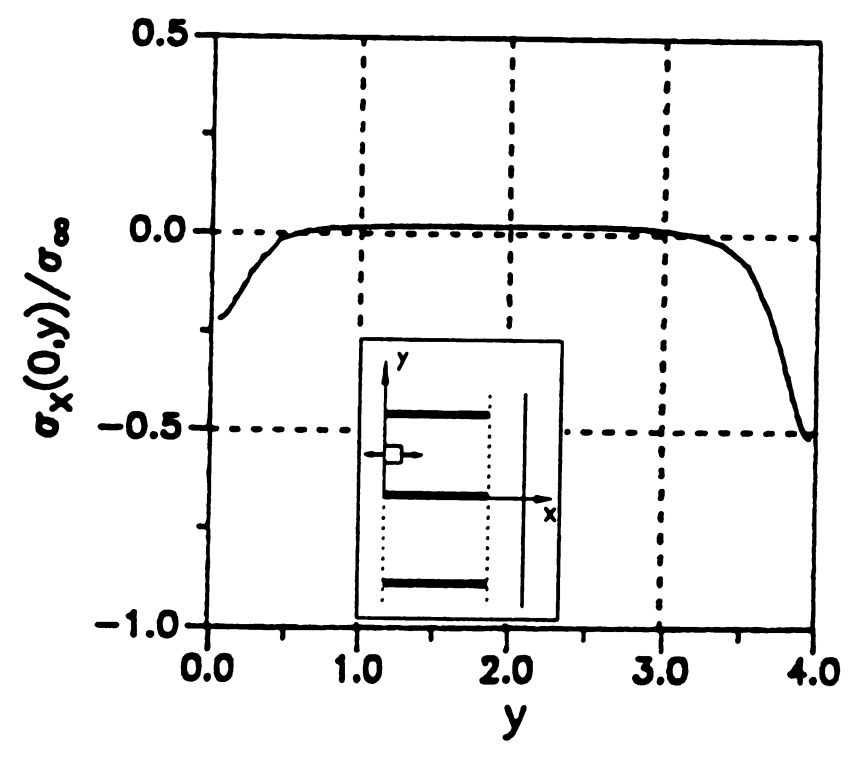


Figure 3.34 Stress component  $\sigma_x$  at the midplane in 90° ply.  $[0^\circ/90^\circ_3]_s$  graphite/epoxy composite laminate (Type 4).

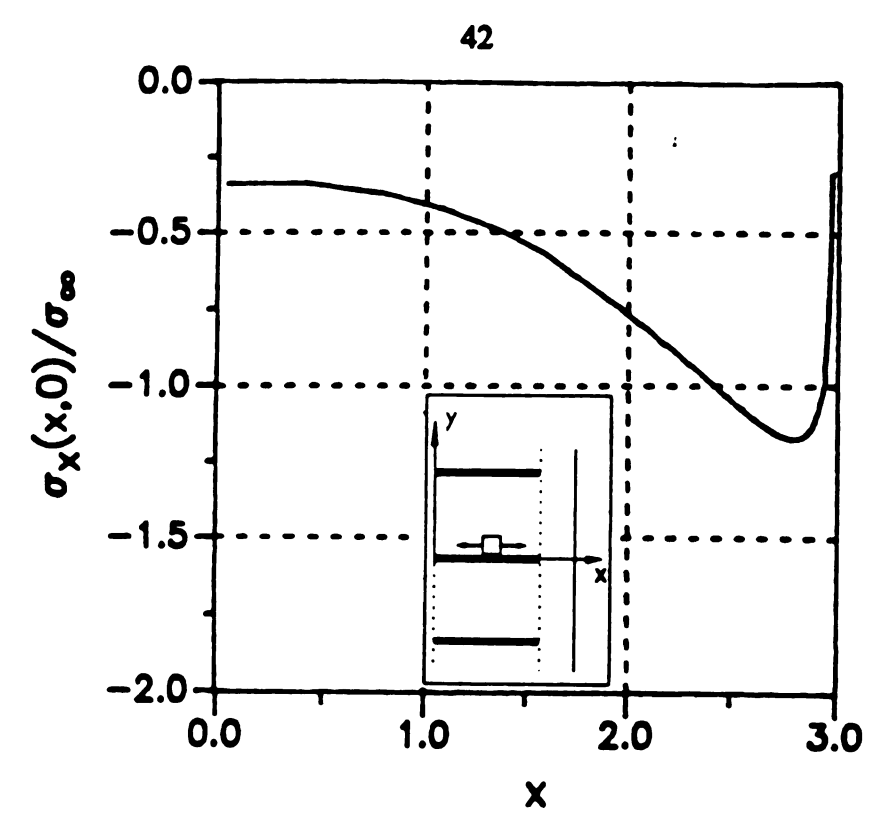


Figure 3.35 Stress component  $\sigma_x$  at the crack location in 90° ply.  $[0^{\circ}/90^{\circ}_{3}]_{s}$  glass/epoxy composite laminate (Type 4).

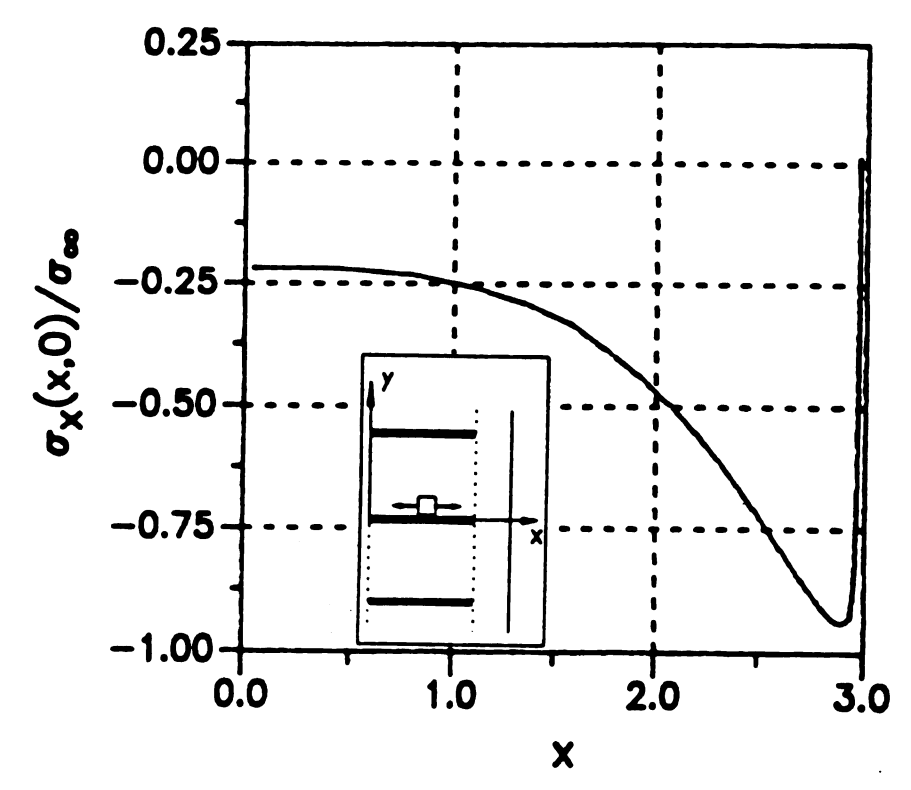


Figure 3.36 Stress component  $\sigma_x$  at the crack location in 90° ply.  $[0^\circ/90^\circ_3]_s$  graphite/epoxy composite laminate (Type 4).

#### **CHAPTER 4**

### COMPARISON OF THE FINITE ELEMENT ANALYSIS RESULTS WITH THE ANALYTICAL RESULTS

### 4.1 Analysis of a cracked symmetric cross-ply laminate under uniform tension

For the analytical work, the variational principle of minimum complementary potential energy is used<sup>[25]</sup>. Consider a symmetric cross-ply laminate which is subjected to uniform in-plane tensile loads, as shown in Figures 2.1 and 2.2. Hashin's primary stress analysis does not include stress concentration effect at the crack tip, especially in the 0° ply. The finite element analysis shows a strong axial stress concentration at the crack tip in the 0° ply. It is also noted that the axial stress concentration at the crack tip in the 90° ply is not so strong as that in the 0° ply. Therefore, based on the finite element analysis, it is necessary to obtain more refined stress distributions including the stress concentration effects at the crack tips in the 0° ply, for cross-ply laminates damaged by transverse matrix cracking.

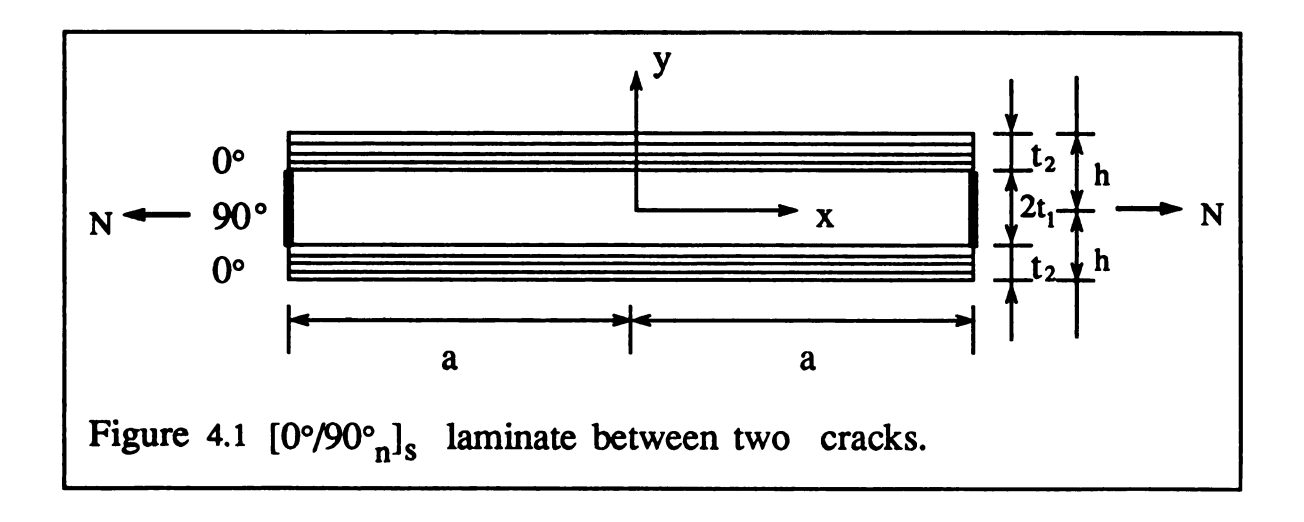


Figure 4.1 shows a representative element between any two consecutive cracks. Let the 90° ply be ply 1 with thickness  $t_1$ , and let the 0° ply be ply 2 with thickness  $t_2$ , as shown in Figure 4.1. For all cases, the thickness of a single lamina is chosen as  $t = 0.203 \text{ mm}^{[4]}$ .

This problem can be solved in two steps: (1) When there are no intralaminar cracks in 90° ply, the ply stresses are determined by the classical lamination theory. The stress component  $\sigma_{\mathbf{x}}^{\mathbf{c}(m)}$  (m = ply index 1,2) in each ply is constant through the respective plies; (2) When there are cracks, the cracks introduce stress perturbations which are denoted by  $\sigma_{ij}^{\mathbf{p}(m)}$ . The superposition of the two solutions will then provide the stress field in the laminate with intralaminar cracks in the 90° ply as given by

$$\sigma_{ij}^{(m)} = \sigma_{ij}^{c(m)} + \sigma_{ij}^{p(m)}, \qquad (4.1)$$

where i, j are restricted to x, y.

Now, the stress component  $\sigma_{\mathbf{x}}^{c(m)}$  (m = ply index 1,2) in each ply may be expressed in the form

$$\sigma_{x}^{c(1)} = \sigma_{1, \text{ and}} \quad \sigma_{x}^{c(2)} = \sigma_{2}.$$
 (4.2a)

Furthermore, in order to simplify the problem, perturbation stress in the 90° ply,  $\sigma_x^{p(1)}$ , is assumed to be constant through the ply thickness. Hence, the stress may be expressed as

$$\sigma_{\mathbf{x}}^{\mathbf{p}(1)} = -\sigma_{1} \,\phi_{1}(\mathbf{x}),\tag{4.2b}$$

where  $\phi_1(x)$  is an unknown function. In order to obtain more refined stress distributions including stress concentration effects in the  $0^{\circ}$  ply, it is necessary that

perturbation stress in the 0° ply,  $\sigma_x^{p(2)}$ , should be functions of x and y. This stress may be chosen as,

$$\sigma_{\mathbf{x}}^{p(2)} = -\sigma_{2}(\mathbf{h} - \mathbf{y})^{n} \phi_{2}(\mathbf{x}),$$
 (4.2c)

where  $h = t_1 + t_2$ , and  $\phi_2(x)$  is an unknown function. The choice of the perturbation stress in the 0° ply,  $\sigma_x^{p(2)}$ , is motivated by the knowledge of the series expansion of the crack tip stresses. The equilibrium equations for the plies are

$$\partial \sigma_{\mathbf{x}}^{\mathbf{p}(\mathbf{m})} / \partial \mathbf{x} + \partial \sigma_{\mathbf{x}\mathbf{y}}^{\mathbf{p}(\mathbf{m})} / \partial \mathbf{y} = 0$$
, and (4.3a)

$$\partial \sigma_{xy}^{p(m)} / \partial x + \partial \sigma_{y}^{p(m)} / \partial y = 0.$$
 (4.3b)

The stresses  $\sigma_{ij}^{c(m)}$  disappear since they are constant through respective plies. The form of the perturbation stress components for each ply of the cracked laminate will be chosen as a product of a function of the transverse variable y multiplied by a function of x and y (in some cases, only x) and are given as

$$\sigma_{x}^{p(m)} = f^{(m)}''(y) Q^{(m)}(x),$$
 (4.4a)

$$\sigma_{xy}^{p(m)} = -f^{(m)}'(y) R^{(m)}(x), \text{ and}$$
 (4.4b)

$$\sigma_{y}^{p(m)} = f^{(m)}(y) S^{(m)}(x),$$
 (4.4c)

where prime designates differentiation with respect to the variable  $y^{[24]}$ . The function  $f^{(m)}(y)$  describes the stress distribution through a given ply of the cracked laminate.

The equilibrium equations (4.3a,b) yield the following equations involving the variable x only:

$$R^{(m)}(x) = \partial Q^{(m)}(x) / \partial x, \text{ and}$$
 (4.5a)

$$S^{(m)}(x) = \partial R^{(m)}(x) / \partial x. \tag{4.5b}$$

The equations (4.2b,c) and (4.4a) yield the relations

$$f^{(1)}''(y) = -\sigma_1,$$
  $f^{(2)}''(y) = -\sigma_2(h-y)^n,$  (4.6a)

$$Q^{(1)}(x) = \phi_1(x)$$
, and  $Q^{(2)}(x) = \phi_2(x)$ . (4.6b)

It is noted that stress variations through the ply thickness depend on the function  $f^{(m)}(y)$ . It is easily seen that this problem is not well-posed, and there is no unique solution to this problem. One of the main purposes of this work is to find out a more physically reasonable solution using the finite element analysis.

Now, the perturbation stresses take the forms

$$\sigma_{xy}^{p(1)} = [\sigma_1 y + a_1(x)] \phi_1'(x),$$
 (4.7a)

$$\sigma_{y}^{p(1)} = -\left[\frac{1}{2}\sigma_{1}y^{2} + a_{1}(x)y + a_{2}(x)\right]\phi_{1}''(x), \tag{4.7b}$$

$$\sigma_{xy}^{p(2)} = \left[\sigma_2 \frac{1}{n+1} (h-y)^{n+1} + a_3(x)\right] \phi_2'(x), \text{ and}$$
 (4.8a)

$$\sigma_{y}^{p(2)} = -\left[\sigma_{2} \frac{1}{n+1} \frac{1}{n+2} (h-y)^{n+2} + a_{3}(x)y + a_{4}(x)\right] \phi_{2}^{"}(x), \tag{4.8b}$$

where  $a_1(x)$ ,  $a_2(x)$ ,  $a_3(x)$  and  $a_4(x)$  are unknown functions.

The applied load per unit specimen width, N, is simply given by

$$N = 2(\sigma_{\mathbf{x}}^{c(1)} t_1 + \sigma_{\mathbf{x}}^{c(2)} t_2)$$

$$= 2(\sigma_1 t_1 + \sigma_2 t_2). \tag{4.9}$$

Therefore, equilibrium condition in x direction for perturbation stresses is obtained as

$$2(\sigma_{\mathbf{x}}^{p(1)} t_{1} + \int_{t_{1}}^{h} \sigma_{\mathbf{x}}^{p(2)} dy)$$

$$= 2(-\sigma_{1}\phi_{1}(\mathbf{x}) t_{1} - \sigma_{2}\phi_{2}(\mathbf{x}) \frac{1}{n+1} t_{2}^{n+1}) = 0. \tag{4.10}$$

From equation (4.10), the following relation between  $\phi_1(x)$  and  $\phi_1(x)$  is given as

$$\phi_2(x) = -(n+1)\frac{\sigma_1}{\sigma_2} \frac{t_1}{t_2^{n+1}} \phi_1(x). \tag{4.11}$$

The origin of the system of coordinates is set up at the center of the distance 2a between any two typical cracks, as shown in Figure 4.1. The perturbation stresses in the region  $|x| \le a$ ,  $|y| \le b$  must satisfy the following interface and boundary conditions:

1. from symmetry condition,

$$\sigma_{xy}^{p(1)}(x,0) = 0,$$
 (4.12a)

2. from continuity condition,

$$\sigma_{xy}^{p(1)}(x,t_1) = \sigma_{xy}^{p(2)}(x,t_1),$$
 (4.12b)

$$\sigma_{\mathbf{y}}^{p(1)}(\mathbf{x}, \mathbf{t}_1) = \sigma_{\mathbf{y}}^{p(2)}(\mathbf{x}, \mathbf{t}_1),$$
 (4.12c)

3. from traction free condition at the free surfaces,

$$\sigma_{xy}^{p(2)}(x,h) = 0,$$
 (4.12d)

$$\sigma_{\mathbf{y}}^{p(2)}(\mathbf{x},\mathbf{h}) = 0,$$
 (4.12e)

4. from traction free condition at the crack surfaces,

$$\sigma_{\mathbf{x}}^{p(1)}(\pm a, y) = -\sigma_{1}, \text{ and } |y| \le t_{1}$$
 (4.12f)

Let  $\phi_1(x)$  be  $\phi(x)$ , then using equations (4.3)-(4.6) and (4.12), the perturbation stresses can be written in the forms

$$\sigma_{\mathbf{x}}^{\mathbf{p}(1)} = -\sigma_{1}\phi(\mathbf{x}),\tag{4.13a}$$

$$\sigma_{xy}^{p(1)} = \sigma_1 y \phi'(x), \qquad (4.13b)$$

$$\sigma_{y}^{p(1)} = \sigma_{1}(-\frac{1}{2}y^{2} + \frac{t_{1}t_{2}}{n+2} + \frac{1}{2}t_{1}^{2})\phi''(x),$$
 (4.13c)

$$\sigma_{\mathbf{X}}^{p(2)} = \sigma_{1}(n+1) \frac{t_{1}}{t_{2}^{n+1}} (h-y)^{n} \phi(\mathbf{x}), \tag{4.13d}$$

$$\sigma_{xy}^{p(2)} = \sigma_1 t_1 \left(\frac{h-y}{t_2}\right)^{n+1} \phi'(x), \text{ and}$$
 (4.13e)

$$\sigma_{y}^{p(2)} = \sigma_{1} t_{1} \frac{1}{n+2} \frac{(h-y)^{n+2}}{t_{2}^{n+1}} \phi''(x).$$
 (4.13f)

From equations (4.13a,b), the crack surface boundary conditions (4.12f,g) assume the form

$$\phi(\pm a) = 1$$
, and  $\phi'(\pm a) = 0$ .  $|y| \le t_1$  (4.14)

From equations (4.13d,e), it is seen that

$$\sigma_{x}^{p(2)}(\pm a,y) = \sigma_{1}(n+1)\frac{t_{1}}{t_{2}^{n+1}}(h-y)^{n}, \text{ and } t_{1} \le |y| \le h$$
 (4.15a)

$$\sigma_{xy}^{p(2)}(\pm a,y) = 0.$$
  $t_1 \le |y| \le h$  (4.15b)

From equations (4.14)-(4.15), it is found that equation (4.14) is valid for the entire thickness of the cracked laminates. Thus,

$$\phi(\pm a) = 1$$
, and  $\phi'(\pm a) = 0$ .  $0 \le |y| \le h$  (4.16)

A consistent approach of developing mathematical theories of plates is to use the principle of variational calculus, furthermore, it is convenient to use the theorem of minimum complementary potential energy<sup>[31]</sup>. Suppose a body B which has volume V and boundary A, is in equilibrium under the action of surface forces  $T_i$  assigned over a part  $A_1$  of the surface A, and on the remaining part  $A_2$  of A the displacements  $u_i$  are assumed to be known.

If the  $\sigma_{\dot{1}\dot{1}}$  are the stress components of the equilibrium state, then

$$\partial \sigma_{ij} / \partial x_j = 0$$
 in B, (4.17a)

$$\sigma_{ij} n_j = T_i$$
 on  $A_1$ , and (4.17b)

$$u_i = f_i$$
 on  $A_2$ . (4.17c)

Now, introduce a set of functions  $\sigma^{'}_{\ ij}$  such that

$$\sigma'_{ij} = \sigma_{ij} + \delta\sigma_{ij}, \tag{4.17d}$$

with the properties

$$\partial \sigma'_{ij} / \partial x_j = 0,$$
 in B, (4.17e)

$$\sigma'_{ij}n_{j} = T_{i}$$
, on  $A_{1}$ , and (4.17f)

$$\sigma'_{ij}$$
 are arbitrary on  $A_2$ . (4.17g)

It follows from these equations that the variations  $\delta\sigma_{ij}$  satisfy the conditions

$$\partial(\delta\sigma_{ij})/\partial x_i = 0,$$
 in B, (4.17h)

$$(\delta \sigma_{ij})$$
n<sub>j</sub> = 0, and on A<sub>1</sub>, and (4.17i)

$$\delta\sigma_{ij}$$
 are arbitrary on  $A_2$ . (4.17j)

It may be observed that the  $\sigma_{ij}$  are associated with the equilibrium state of the body and hence they satisfy the Beltrami-Michell compatibility equations, but we do not assume that  $\delta\sigma_{ij}$  satisfy any such conditions. We define the complementary energy U by the relationship,

$$U_{c} = \int_{V} W \, dV - \int_{A_{2}} T_{i} u_{i} \, dA, \qquad (4.18)$$

where W is the strain energy density function. The theorem of minimum of complementary energy states that the complementary energy  $U_c$  has an absolute minimum

when the stress tensor  $\sigma_{ij}$  is that of the equilibrium state and the varied states of stress fulfill the equations (4.17h,i,j).

Suppose that the body B is an elastic material without cracks, there is another elastic body B' which has same shape A and same volume V with the body B, and both bodies, B and B', have space variable compliances  $S_{ijkl}$  and are subjected to the same external mixed boundary conditions. In the body B, the complementary energy will be

$$U_c^{1} = \frac{1}{2} \int_{V} S_{ijkl} \sigma_{ij}^{c} \sigma_{kl}^{c} dV - \int_{A_2} T_i^{c} u_i dA.$$
 (4.19)

In the cracked body B , if we let  $\sigma_{ij}^{\ \ p}$  be perturbation stresses due to cracks,

$$U_c^2 = \frac{1}{2} \int_V S_{ijkl} \sigma_{ij}^a \sigma_{kl}^a dV - \int_{A_2} T_i^a u_i dA, \qquad (4.20)$$

where

$$\sigma_{ij}^{a} = \sigma_{ij}^{c} + \sigma_{ij}^{p}$$
, and  $T_{i}^{a} = T_{i}^{c} + T_{i}^{p}$ . (4.21)

It is useful to record a theorem due to Hashin<sup>[25]</sup> which is given as

$$U_c^2 = U_c^1 + \frac{1}{2} \int_V S_{ijkl} \sigma_{ij}^p \sigma_{kl}^p dV.$$
 (4.22)

where,

$$U_{c}^{1} = \frac{1}{2} \int_{V} S_{ijkl} \, \sigma_{ij}^{c} \, \sigma_{kl}^{c} \, dV.$$
 (4.23)

Next, we consider the cracked laminate region in Figure 4.1. Because of symmetry, it is sufficient to take the region  $-a \le x \le a$ ,  $0 \le y \le h$  with unit thickness in z direction. Further symmetry consideration shows

$$\phi(\mathbf{x}) = \phi(-\mathbf{x}). \tag{4.24}$$

It is necessary to calculate the strain energy density W of a transversely isotropic composite materials for the calculation of complementary energy,

$$2W = \sigma_{ij} \varepsilon_{ij} = \frac{\sigma_{11}^{2}}{E_{1}} - \frac{v_{21}}{E_{2}} \sigma_{11} \sigma_{22} - \frac{v_{21}}{E_{2}} \sigma_{11} \sigma_{33} + \frac{\sigma_{12}^{2}}{G_{12}} + \frac{\sigma_{13}^{2}}{G_{12}}$$

$$- \frac{v_{21}}{E_{2}} \sigma_{11} \sigma_{22} + \frac{\sigma_{22}^{2}}{E_{2}} - \frac{v_{32}}{E_{3}} \sigma_{22} \sigma_{33} + \frac{\sigma_{23}^{2}}{G_{23}}$$

$$- \frac{v_{21}}{E_{2}} \sigma_{11} \sigma_{33} - \frac{v_{32}}{E_{3}} \sigma_{22} \sigma_{33} + \frac{\sigma_{33}^{2}}{E_{2}}$$

$$= \frac{\sigma_{11}^{2}}{E_{1}} + \frac{\sigma_{22}^{2} + \sigma_{33}^{2}}{E_{2}} - \frac{2\sigma_{11}(\sigma_{22} + \sigma_{33})v_{12}}{E_{1}}$$

$$- \frac{2v_{23}}{E_{2}} \sigma_{22} \sigma_{33} - \frac{\sigma_{23}^{2}}{G_{23}} + \frac{\sigma_{12}^{2} + \sigma_{13}^{2}}{G_{12}}, \qquad (4.25)$$

where 1 is in fiber direction and 2,3 are transverse directions.  $U_c^{\prime 2}$ , the second term in right hand side in equation (4.22) for this region, is given by

$$U_{c}'^{2} = 2 \int_{-a}^{a} \int_{0}^{t_{1}} W_{1} dy dx + 2 \int_{-a}^{a} \int_{t_{1}}^{h} W_{2} dy dx, \qquad (4.26a)$$

where,

$$2W_1 = \frac{\sigma_x^{p(1)}^2}{E_T} - \frac{2\sigma_x^{p(1)}\sigma_y^{p(1)}v_T}{E_T} + \frac{\sigma_y^{p(1)}^2}{E_T} + \frac{\sigma_{xy}^{p(1)}^2}{G_T}, \text{ and } (4.26b)$$

$$2W_2 = \frac{\sigma_x^{p(2)}}{E_A^2} - \frac{2\sigma_x^{p(2)}\sigma_y^{p(2)}v_A}{E_A} + \frac{\sigma_y^{p(2)}}{E_T^2} + \frac{\sigma_{xy}^{p(2)}}{G_A^2}.$$
 (4.26c)

Inserting equation (4.13) into equations (4.26b,c), integration of equation (4.26a) with respect to y and introduction the nondimensional variable

$$\eta = \frac{x}{t_1}, \tag{4.27}$$

yields

$$U_{c}^{'2} = \sigma_{1}^{2} \int_{-\rho}^{\rho} \left[ C_{1} \phi^{2} + C_{2} \phi \left( \frac{d^{2} \phi}{d \eta^{2}} \right) + C_{3} \left( \frac{d^{2} \phi}{d \eta^{2}} \right)^{2} + C_{4} \left( \frac{d^{2} \phi}{d \eta^{2}} \right)^{2} \right] d\eta, \tag{4.28}$$

where

$$\rho = \frac{a}{t_1},\tag{4.29a}$$

$$C_1 = \frac{t_1^2}{E_T} + \frac{1}{E_A} \frac{t_1^3}{t_2} \frac{(n+1)^2}{2n+1}, \qquad (4.29b)$$

$$C_2 = \frac{2v_T t_1}{E_T} \left( \frac{t_1}{3} + \frac{t_2}{n+2} \right) - \frac{2v_A t_1 t_2}{E_A} \left\{ \frac{(n+1)}{(2n+3)(n+2)} \right\}, \quad (4.29c)$$

$$C_3 = \frac{1}{E_T} \left\{ \frac{2}{15} t_1^2 + \frac{2t_1t_2}{3(n+2)} + \left(\frac{t_2}{n+2}\right)^2 \right\}$$

$$+\frac{1}{E_{\rm T}}\frac{{\rm t_2}^3}{{\rm t_1}} \left\{ \frac{1}{(2{\rm n}+5)({\rm n}+2)^2} \right\}$$
, and (4.29d)

$$C_4 = \frac{t_1^2}{3G_T} + \frac{1}{G_A} \left(\frac{t_1 t_2}{2n+3}\right).$$
 (4.29e)

Equation (4.28) yields the Euler equation which minimizes equation (4.28) as

$$\left\{2 C_{1} \phi + C_{2} \left(\frac{d^{2} \phi}{d \eta^{2}}\right)\right\} - \frac{d}{d \eta} \left(2 C_{4} \frac{d \phi}{d \eta}\right) + \frac{d^{2}}{d \eta^{2}} \left\{C_{2} \phi + 2 C_{3} \left(\frac{d^{2} \phi}{d \eta^{2}}\right)\right\}$$

$$= 2 \left[ \frac{d^{4} \phi}{d \eta^{4}} + \left( \frac{C_{2} - C_{4}}{C_{3}} \right) \frac{d^{2} \phi}{d \eta^{2}} + \left( \frac{C_{1}}{C_{3}} \right) \phi \right] = 0,$$

thus,

$$\frac{d^{4}\phi}{d\eta^{4}} + \left(\frac{C_{2} - C_{4}}{C_{3}}\right) \frac{d^{2}\phi}{d\eta^{2}} + \left(\frac{C_{1}}{C_{3}}\right) \phi = 0. \tag{4.30}$$

The solutions to equation (4.30) are of the form

$$\phi = e^{\pm \alpha \eta} \cos \beta \eta, e^{\pm \alpha \eta} \sin \beta \eta, \tag{4.31}$$

where

$$\alpha = \left(\frac{C_1}{C_3}\right)^{\frac{1}{4}} \cos \frac{1}{2} \theta, \quad \beta = \left(\frac{C_1}{C_3}\right)^{\frac{1}{4}} \sin \frac{1}{2} \theta, \text{ and}$$
 (4.32a)

$$\tan\theta = \sqrt{4\left(\frac{C_1}{C_3}\right)/\left(\frac{C_2-C_4}{C_3}\right)^2} - 1,$$
 (4.32a)

provided that 
$$4\left(\frac{C_1}{C_3}\right) > \left(\frac{C_2 - C_4}{C_3}\right)^2$$
 and  $\left(\frac{C_2 - C_4}{C_3}\right) < 0$ .

By using the symmetry condition (4.24) and the boundary condition (4.16), the solution  $\phi$  can be expressed in the form

$$\phi = A_1 \cosh \alpha \eta \cos \beta \eta + A_2 \sinh \alpha \eta \sin \beta \eta, \qquad (4.33)$$

where

$$A_1 = \frac{2(\alpha \cosh \alpha \rho \sin \beta \rho + \beta \sinh \alpha \rho \cos \beta \rho)}{\alpha \sin 2\beta \rho + \beta \sinh 2\alpha \rho}, \text{ and} (4.34a)$$

$$A_2 = \frac{2(\beta \cosh \alpha \rho \sin \beta \rho - \alpha \sinh \alpha \rho \cos \beta \rho)}{\alpha \sin 2\beta \rho + \beta \sinh 2\alpha \rho}.$$
 (4.34b)

In order to determine the stresses (4.13), it is necessary to calculate

$$\phi'(x) = \frac{1}{t_1} \frac{d \phi}{d \eta} = \frac{1}{t_1} \left[ (\alpha A_1 + \beta A_2) \sinh \alpha \eta \cos \beta \eta + (\alpha A_2 - \beta A_1) \cosh \alpha \eta \sin \beta \eta \right], \text{and} \quad (4.35a)$$

$$\phi''(x) = \frac{1}{t_1^2} \frac{d^{2\phi}}{d\eta^2} = \frac{1}{t_1^2} \Big[ \{ (\alpha^2 - \beta^2) A_1 + 2\alpha \beta A_2 \} \cosh \alpha \eta \cosh \eta + \{ (\alpha^2 - \beta^2) A_2 - 2\alpha \beta A_1 \} \sinh \alpha \eta \sin \beta \eta \Big].$$
 (4.35b)

Inserting equations (4.33)-(4.35) into equations (4.13), we can obtain all

perturbation stresses. Thus, the total stresses will be written as

$$\sigma_{x}^{(1)} = \sigma_{1} + \sigma_{x}^{p(1)},$$
 (4.36a)

$$\sigma_{xy}^{(1)} = \sigma_{xy}^{p(1)},$$
 (4.36b)

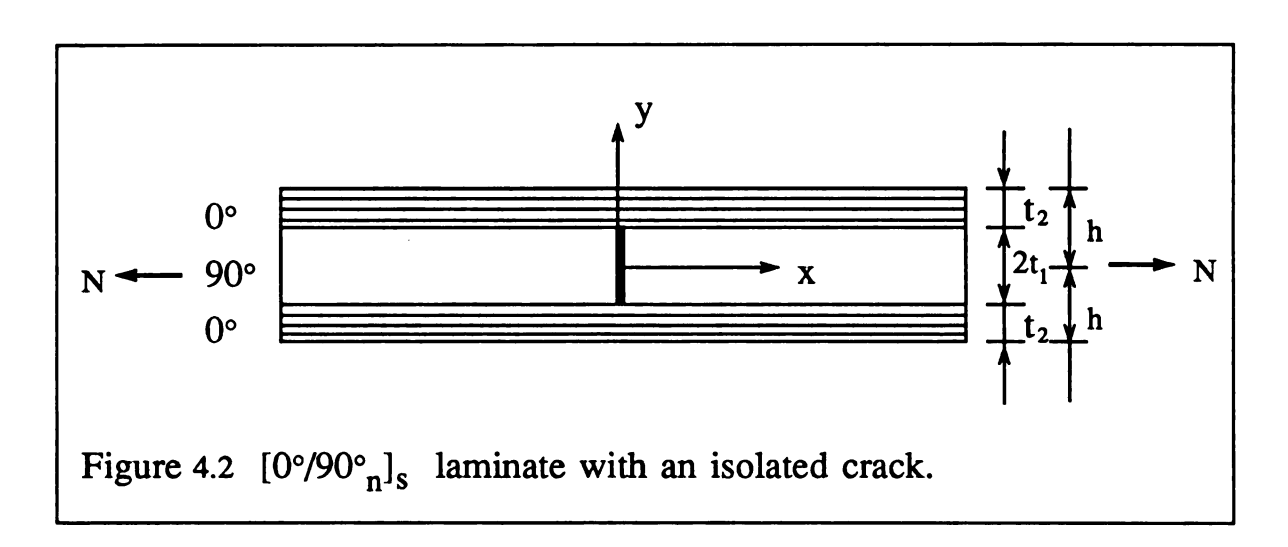
$$\sigma_{y}^{(1)} = \sigma_{y}^{p(1)},$$
 (4.36c)

$$\sigma_{\mathbf{x}}^{(2)} = \sigma_{2} + \sigma_{\mathbf{x}}^{p(2)},$$
 (4.36d)

$$\sigma_{xy}^{(2)} = \sigma_{xy}^{p(2)}$$
, and (4.36e)

$$\sigma_{y}^{(2)} = \sigma_{y}^{p(2)}$$
. (4.36f)

Now, it is interesting to consider a case when the cracks are far apart. Figure 4.2 shows a representative element when the cracks are remote from each other.



In this case, the boundary conditions will be expressed in the form

$$\phi(0) = 1$$
, and  $\phi'(0) = 0$ .  $0 \le |y| \le h$  (4.37)

The perturbation stresses will be written as

$$\phi = e^{-\alpha\eta}(\cos\beta\eta + \frac{\alpha}{\beta}\sin\beta\eta), \qquad (4.38a)$$

$$\phi'(x) = \frac{1}{t_1} \frac{d\phi}{d\eta} = -\frac{1}{t_1} \left(\frac{\alpha^2 + \beta^2}{\beta}\right) e^{-\alpha\eta} \sin\beta\eta, \text{ and}$$
 (4.38b)

$$\phi''(x) = \frac{1}{t_1^2} \frac{d^2 \phi}{d \eta^2} = \frac{1}{t_1^2} \left(\frac{\alpha^2 + \beta^2}{\beta}\right) e^{-\alpha \eta} (\alpha \sin \beta \eta - \beta \cos \beta \eta). \tag{4.38c}$$

Inserting equations (4.38) into equations (4.13), we have the total stresses from equations (4.36).

Prior to the calculation of perturbation stress components, it is necessary to calculate  $\sigma_1$  and  $\sigma_2$  by employing the classical lamination theory. Table 4.1 shows the ratio  $\sigma_1/\sigma_2$  and  $\sigma_1/\sigma$ , ( $\sigma = N/2h$ ), for  $[0^\circ/90^\circ]s$  and  $[0^\circ/90^\circ]s$  composite laminates with the material properties of glass/epoxy and graphite/epoxy in Table 2.2.

Table 4.1 Ratio  $\sigma_1/\sigma_2$  and  $\sigma_1/\sigma$  by the classical lamination theory.

	Glass/epoxy		Graphite/epoxy	
	[0°/90°] <sub>s</sub>	[0°/90°3]s	[0°/90°] <sub>s</sub>	[0°/90° <sub>3</sub> ] <sub>s</sub>
σ <sub>1</sub> /σ <sub>2</sub>	$ \begin{array}{r} 0.05720 \\ \hline 0.18911 \\ = 0.3025 \end{array} $	$ \begin{array}{r} 0.03919 \\ \hline 0.12874 \\ = 0.3044 \end{array} $	$   \begin{array}{r}     0.01693 \\     \hline     0.22938 \\     = 0.0738   \end{array} $	$   \begin{array}{r}     0.01491 \\     \hline     0.20157 \\     = 0.074   \end{array} $
σ <sub>1</sub> /σ	$   \begin{array}{r}     0.05720 \\     \hline     0.12316 \\     = 0.4645   \end{array} $	$   \begin{array}{r}     0.03919 \\     \hline     0.06158 \\     = 0.6364   \end{array} $	$   \begin{array}{r}     0.01693 \\     \hline     0.12316 \\     = 0.1375   \end{array} $	$   \begin{array}{r}     0.01491 \\     \hline     0.06158 \\     = 0.2421   \end{array} $

## 4.2 Analytical results and comparison with the finite element analysis results

The stress distributions from the principle of variational calculus using the theorem of minimum complementary potential energy, are presented in this section. Axial, shear, transverse stress distributions at the interface in 0° ply, and axial stress distributions at the interface and axial, transverse stress distributions at the midplane in 90° ply will be mainly discussed and compared to the results from the finite element analysis.

Prior to the discussion of stress distributions, it is useful to investigate variation of the complementary energy (U<sub>c</sub> '2) in equation (4.26a), with various power n in equations (4.13 d,e,f). Table 4.2 shows the variation of the complementary energy (U<sub>c</sub> '2). It is observed that as the power n increases, the complementary energy (U<sub>c</sub> '2) increases. This phenomenon can be predicted easily, since as the power n in equations (4.13 d,e,f) increases, the perturbation stress components become more intensified.

Table 4.2 Complementary energy (U<sub>c</sub> '2) variation with various power n in equations (4.13 d,e,f).

Power n	Complementary energy	
n = 0	1.0	
n = 5	1.072	
n = 10	1.255	
n = 15	1.44	
n = 20	1.619	

For the purpose of comparison between the finite element analysis results and the variational calculus results,  $[0^{\circ}/90^{\circ}]$ s glass/epoxy composite laminate with interacting cracks and  $[0^{\circ}/90^{\circ}]$ s glass/epoxy composite laminate with an isolated crack were investigated. (Note: x, y coordinates in the following figures are set up differently from those in Figures 4.1-4.2. The new x, y coordinates are shown in the following figures.)

Figures 4.3-4.8 show the variational calculus results and the finite element analysis results for  $[0^{\circ}/90^{\circ}]_{s}$  glass/epoxy composite laminate with interacting cracks (Type 2). In this case, the dimensions of the composite laminate in Figure 4.1 were taken as: a = h;  $t_1 : t_2 = 1 : 1$ . Figures 4.9-4.14 show the variational calculus results and the finite element analysis results for  $[0^{\circ}/90^{\circ}]_{s}$  glass/epoxy composite laminate with an isolated crack (Type 1). In this case, the dimensions of the composite laminate in Figure 4.2 were taken as: length in the positive x direction = 6  $t_1$ ;  $t_1 : t_2 = 1 : 1$ . In Figures 4.3-4.14, the case n = 0 stands for Hashin's primary results.

Figures 4.3 and 4.9 show the axial stress distributions at the interface in 0° ply. It is observed that, as the power n in equation (4.2c) increases, the axial stress concentration from variational calculus becomes stronger and gets closer to the value from the finite element analysis, as shown in Figures 4.3 and 4.9. But, some discrepancies can be observed between the variational calculus results and the finite element analysis results.

Figures 4.4 and 4.10 show the shear stress distributions at the interface in 0° ply. It is indicated that, as the power n in equation (4.2c) increases, the maximum compressive shear stress position moves closer to the crack locations, like the tendency in the finite element analysis results, as shown in Figures 4.4 and 4.10. But, there is a remarkable difference very near the crack locations between the variational calculus results and the finite element analysis results. As we mentioned earlier, the

tensile shear stress in the finite element analysis can be explained from the fact that a short crack transversing a few fibers in  $0^{\circ}$  ply can propagate in the vicinity of the crack tips, even though the tensile shear stress changes into compressive shear stress, rapidly. In order to explain the difference, one important investigation should be mentioned, here. The function  $f^{(m)}(y)$  in equations (4.4) (Note: it follows x, y coordinates in Figures 4.1-4.2), must be reconstructed separately, in the bulk and surface layer or interface region<sup>[24]</sup>. But, it is extremely difficult to set up the function  $f^{(m)}(y)$  in equations (4.4) (Note: it follows x, y coordinates in Figures 4.1-4.2) separately in the present problem. So, for the convenience of calculation, the function  $f^{(m)}(y)$  (Note: it follows x, y coordinates in Figures 4.1-4.2) was not separated in the present analysis. Thus, when the shortcoming in selecting the function  $f^{(m)}(y)$  (Note: it follows x, y coordinates in Figures 4.1-4.2) is taken into account, the finite element analysis result has reasonable agreement with the variational calculus result.

Figures 4.5 and 4.11 show transverse axial stress distributions at the interface in 0° ply. In Figures 4.5 and 4.11, it is noted that the transverse axial stress distributions from variational calculus have good agreement in the magnitude and the tendency with those from the finite element analysis, except for those very near the crack locations. However, as we mentioned before, the tensile transverse axial stress very near the crack locations from the finite element analysis can be explained from the point—that the tensile transverse axial stress before changing into compressive stress can break few fibers in the transverse direction.

Figures 4.6 and 4.12 show the axial stress distributions at the interface in 90° ply. It is observed that there are large amounts of discrepancies between the finite element analysis results and the variational calculus results, as shown in Figures 4.6 and 4.12. However, as in Figures 4.7 and 4.13 which show the axial stress

distributions at the midplane in 90° ply, it is indicated that in the region of midplane which belongs to the bulk area, the axial stress distribution from the finite element analysis has very good agreement with Hashin's primary result. And, it is noted that the maximum value of axial stress at the midplane in 90° ply is at the midpoint between two interacting cracks. This phenomenon can be observed from both the finite element analysis results and the variational calculus results. The maximum tensile axial stress at the midplane is responsible for new crack generation. Therefore, a new crack will be likely to occur midway between two existing cracks.

It would be useful to discuss several analytical models which have been proposed to predict the multiple transverse cracking in cross-ply composite laminates. It is noted that Bailey et al.<sup>[5]-[7]</sup> assumed that new cracks always occurred midway between any two consecutive cracks. Manders et al.[32] and Fukunaga et al.[33] used a statistical model. Manders et al.<sup>[32]</sup> proposed a simple statistical model which accurately fit the data and predicted a dependence of strength in 90° ply on size. It was shown that a model incorporating a Weibull distribution of strength in 90° ply was a good description of the crack spacings. Fukunaga et al. [33] investigated the failure characteristics of cross-ply laminates based upon the statistical strength analysis. The strength in 90° ply was assumed to obey a two-parameter Weibull cumulative distribution function. It was assumed that a new crack occurred midway between two existing cracks at 50% failure probability. Laws and Dyorak<sup>[17]</sup> supposed that a transverse crack would propagate when it was energetically favorable and that the location of this transverse crack was associated with a probability density function. Based on simple statistical fracture mechanics they suggested a choice for the required probability density, namely that it was proportional to the stress in the transverse ply.

From the above discussion, it is observed that a statistical model is better for prediction the multiple transverse cracking in cross-ply composite laminates.

However, a new crack will still be likely to occur midway between two existing cracks.

Figures 4.8 and 4.14 show transverse axial stress distributions at the midplane in 90° ply. Hashin's primary transverse axial stress distribution shows that the maximum stress occurs at the midpoint between two interacting cracks, as shown in Figure 4.8. But, as the power n in equation (4.2c) increases, the maximum transverse axial stress positions are moving closer to each interacting crack. From the finite element analysis, it can be expected that each maximum stress may influence the other, so the value between two maximum stress positions reaches the maximum stress, too. Therefore, as in the result from the finite element analysis, the maximum stress value may spread into wider region. And, in Figure 4.14, it is observed that as the power n in equation (4.2c) increases, the maximum tensile transverse axial stress position moves near to the crack location, like the tendency in stress distribution from the finite element analysis. In Figures 4.8 and 4.14, it is indicated that the transverse axial stress distributions from the finite element analysis have more similar magnitude and tendency to those from the variational calculus, in the region of midplane which belongs to the bulk area, than in the region of interface.

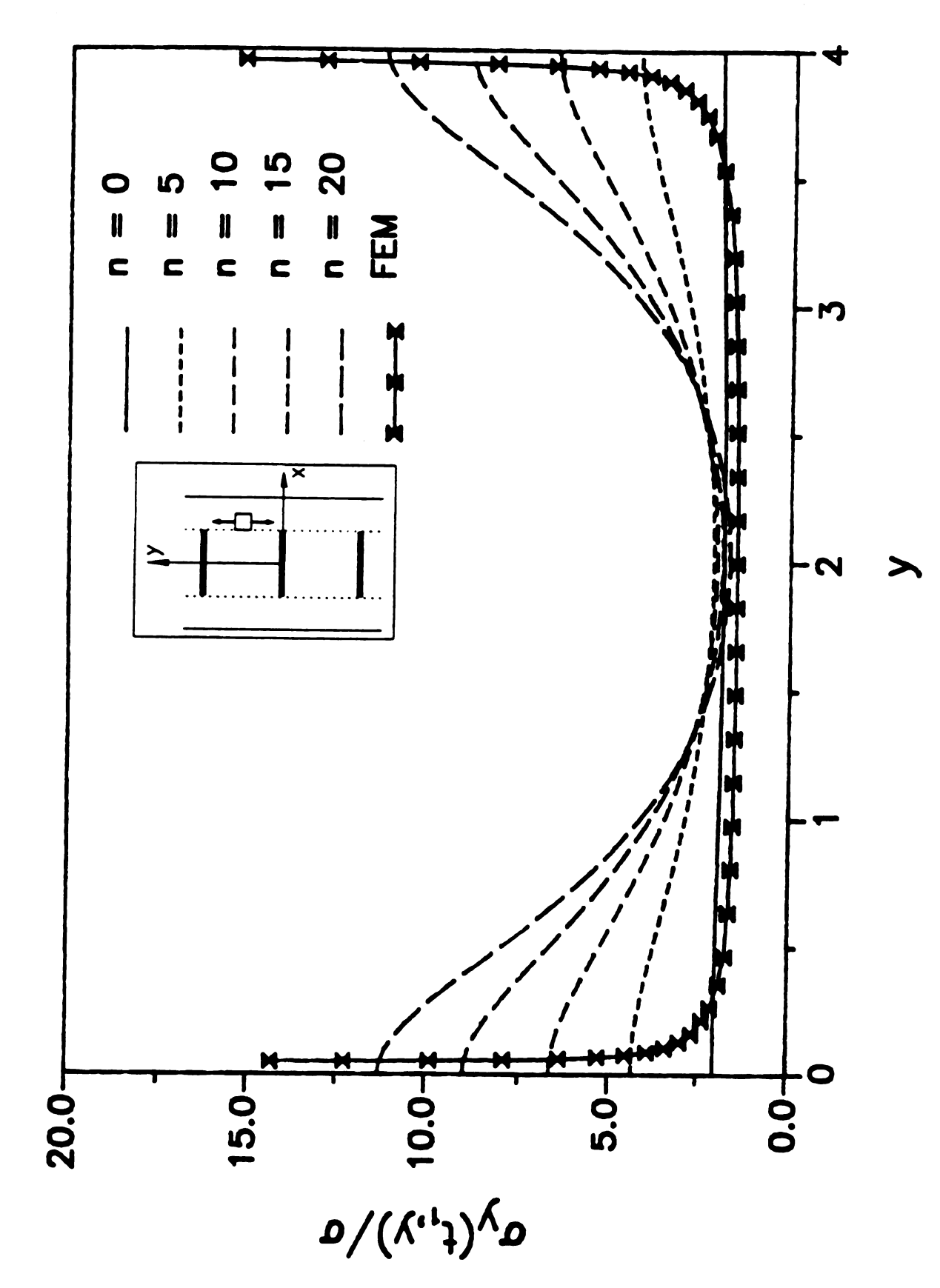


Figure 4.3 Stress component  $\sigma_y$  at the interface in 0° ply. [0°/90°]<sub>s</sub> glass/epoxy laminate (Type 2).

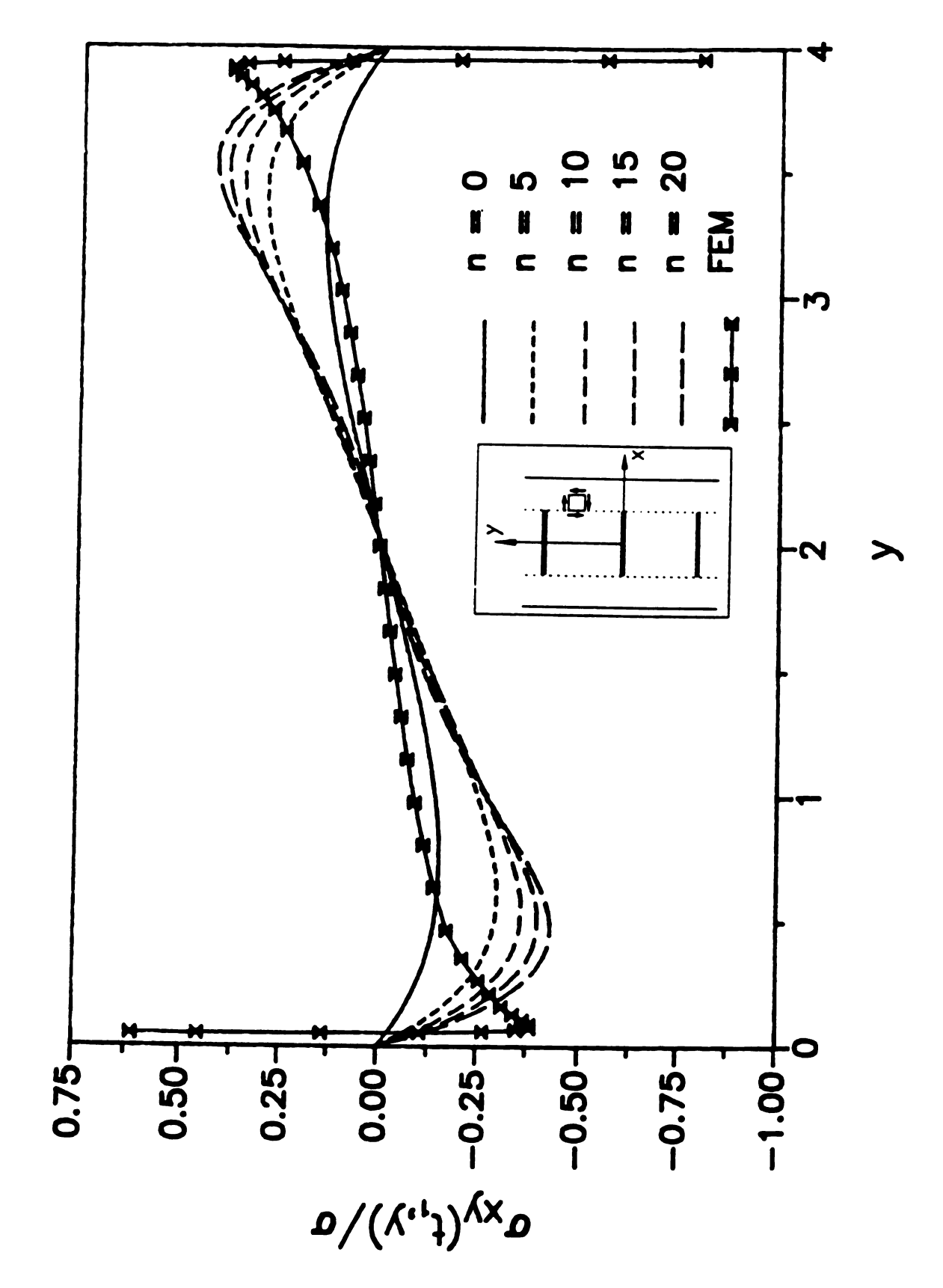


Figure 4.4 Stress component  $\sigma_{xy}$  at the interface in 0° ply.  $\{0^{\circ}/90^{\circ}\}_{s}$  glass/epoxy laminate (Type 2).

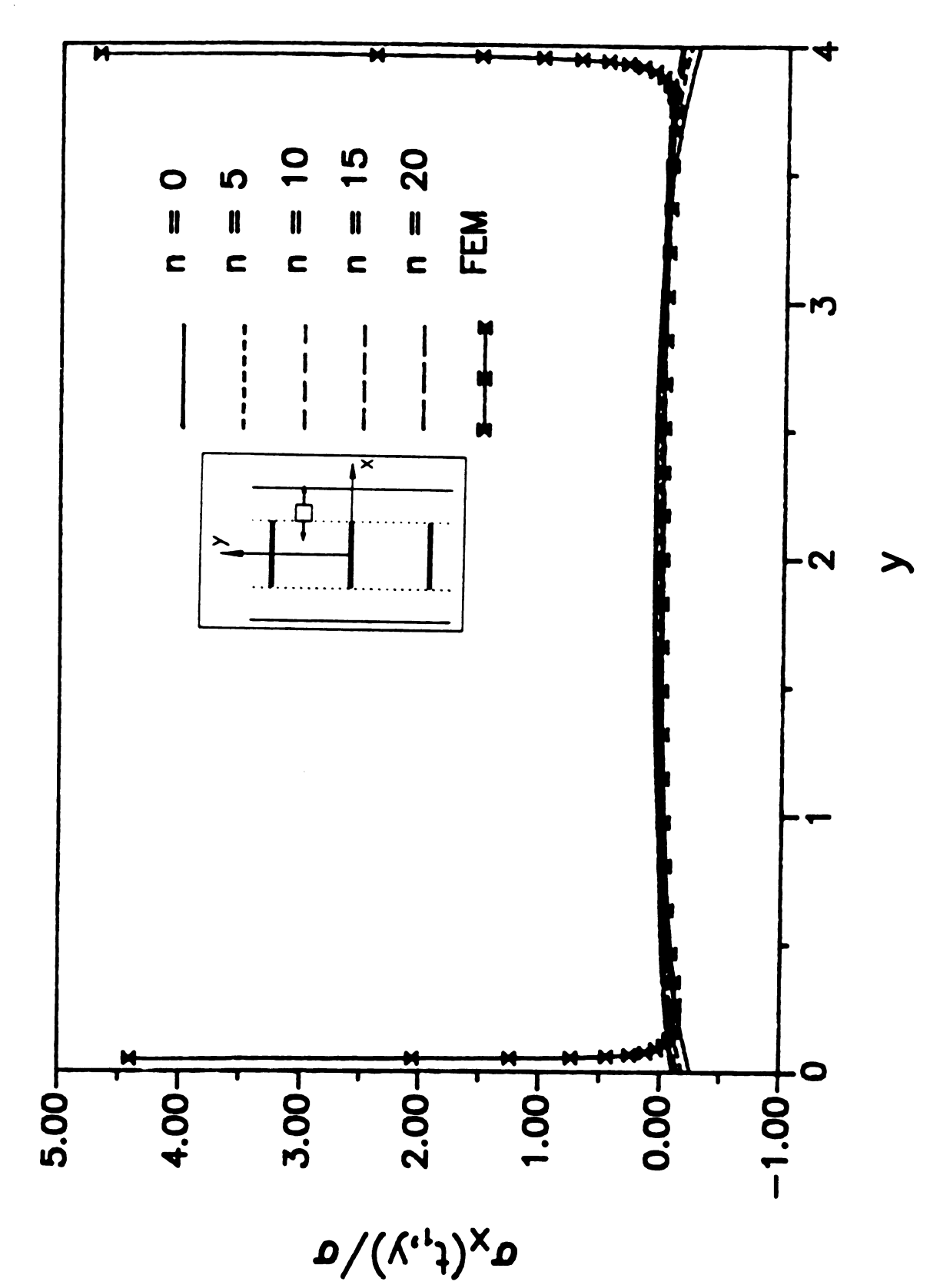


Figure 4.5 Stress component  $\sigma_x$  at the interface in 0° ply.  $[0^{\circ}/90^{\circ}]_s$  glass/epoxy laminate (Type 2).

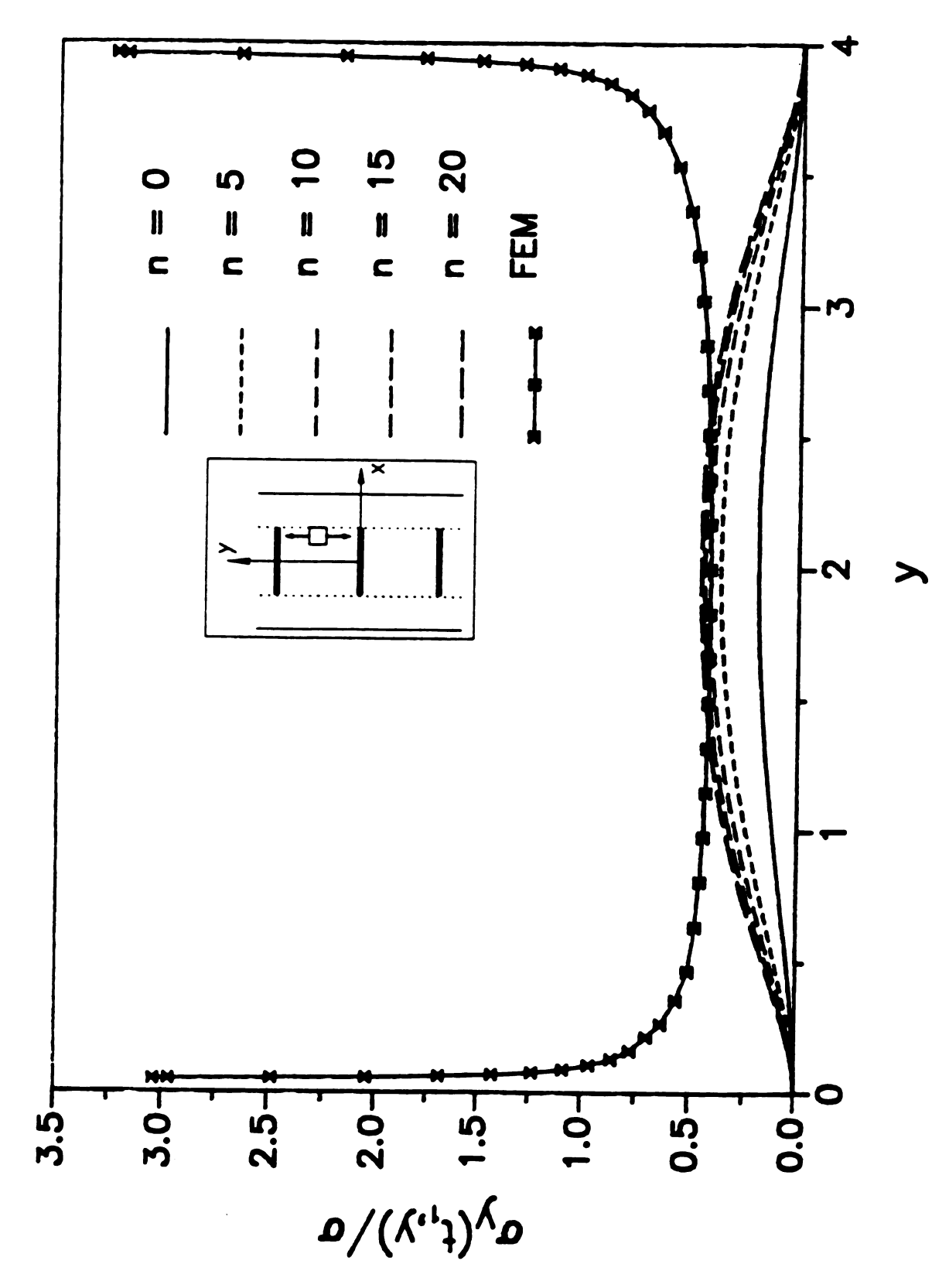


Figure 4.6 Stress component  $\sigma_y$  at the interface in 90° ply.  $[0^{\circ}/90^{\circ}]_s$  glass/epoxy laminate (Type 2).

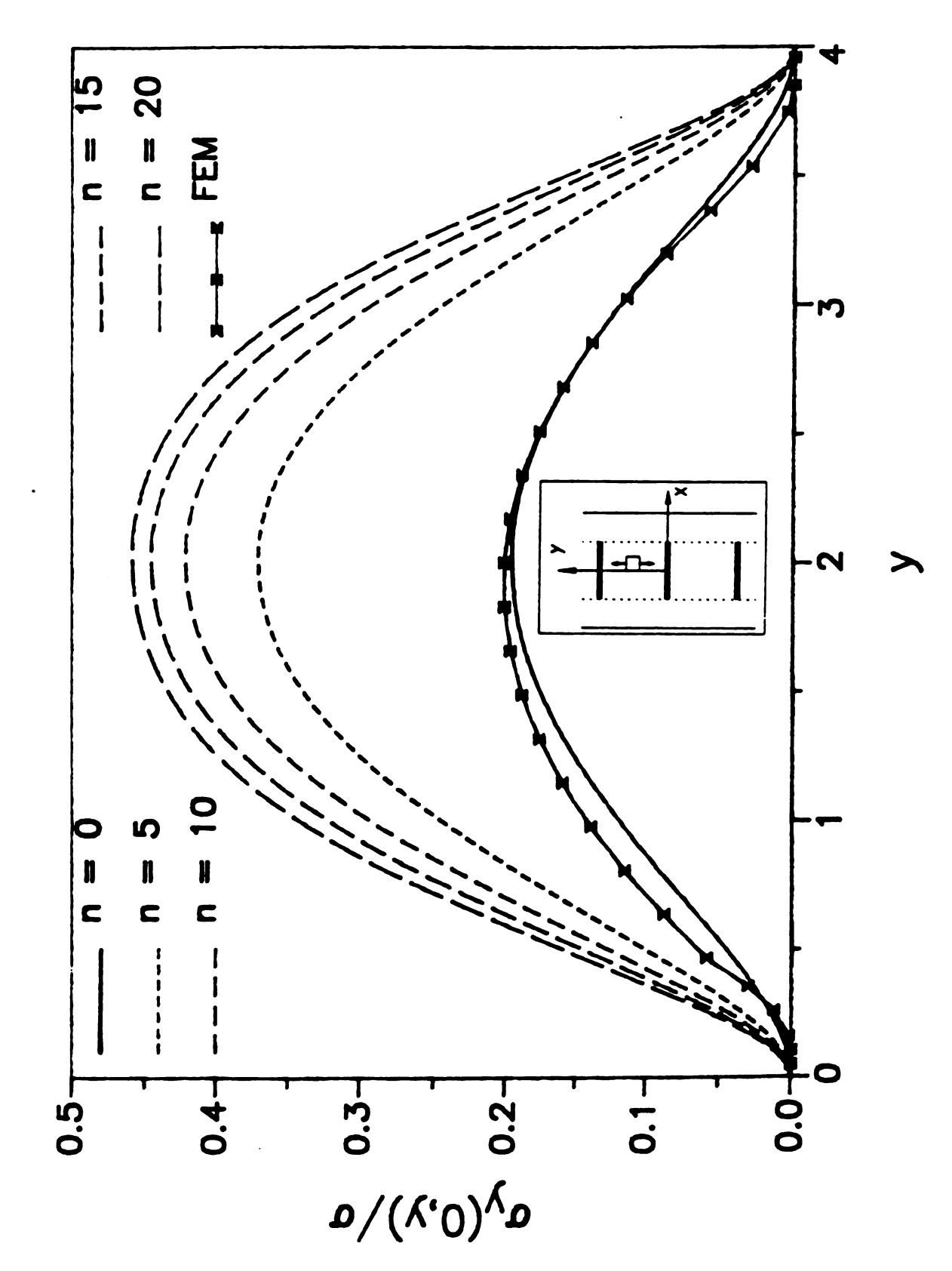


Figure 4.7 Stress component  $\sigma_y$  at the midplane in 90° ply.  $[0^{\circ}/90^{\circ}]_s$  glass/epoxy laminate (Type 2).

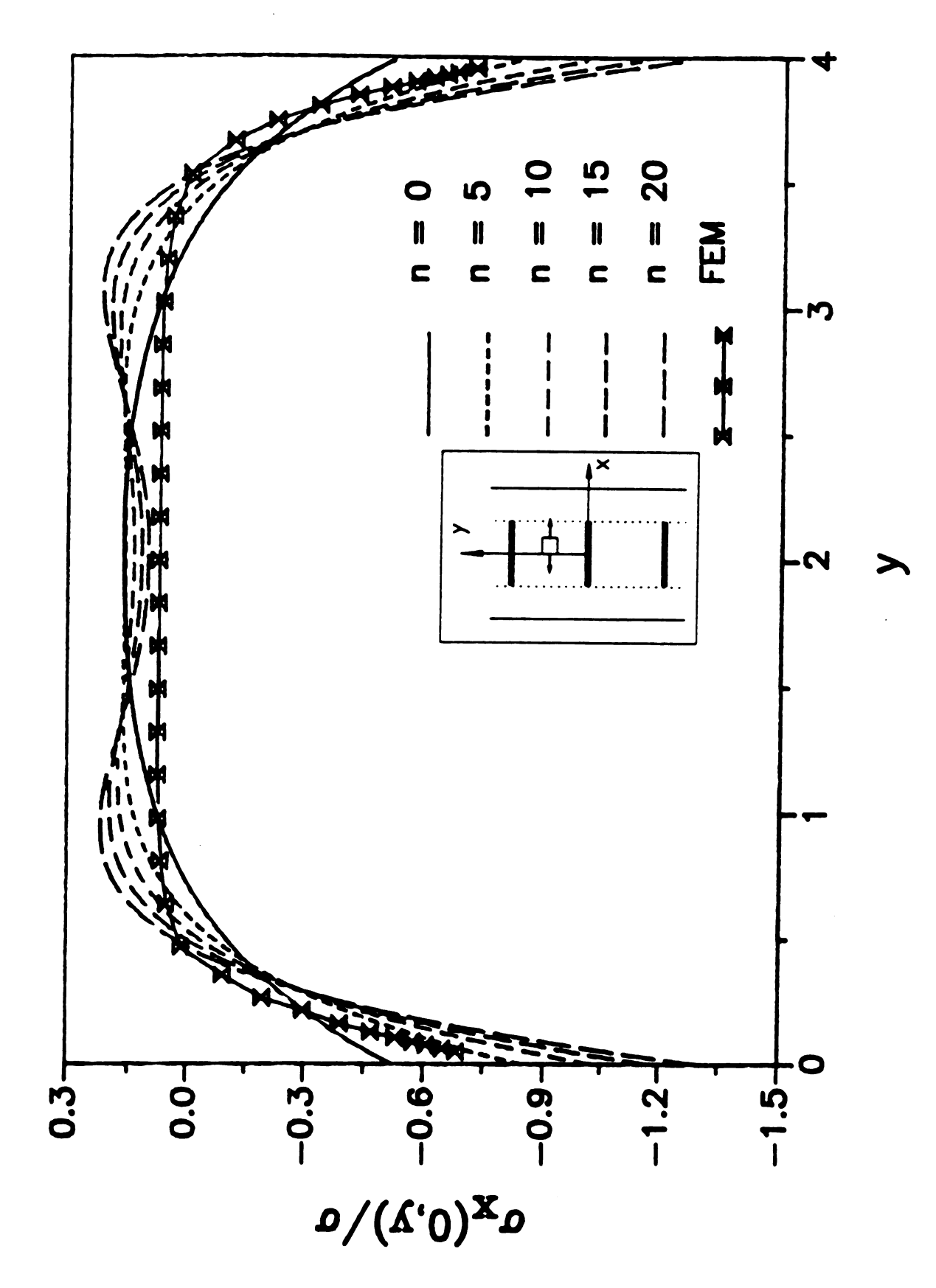


Figure 4.8 Stress component  $\sigma_x$  at the midplane in 90° ply.  $[0^{\circ}/90^{\circ}]_s$  glass/epoxy laminate (Type 2).

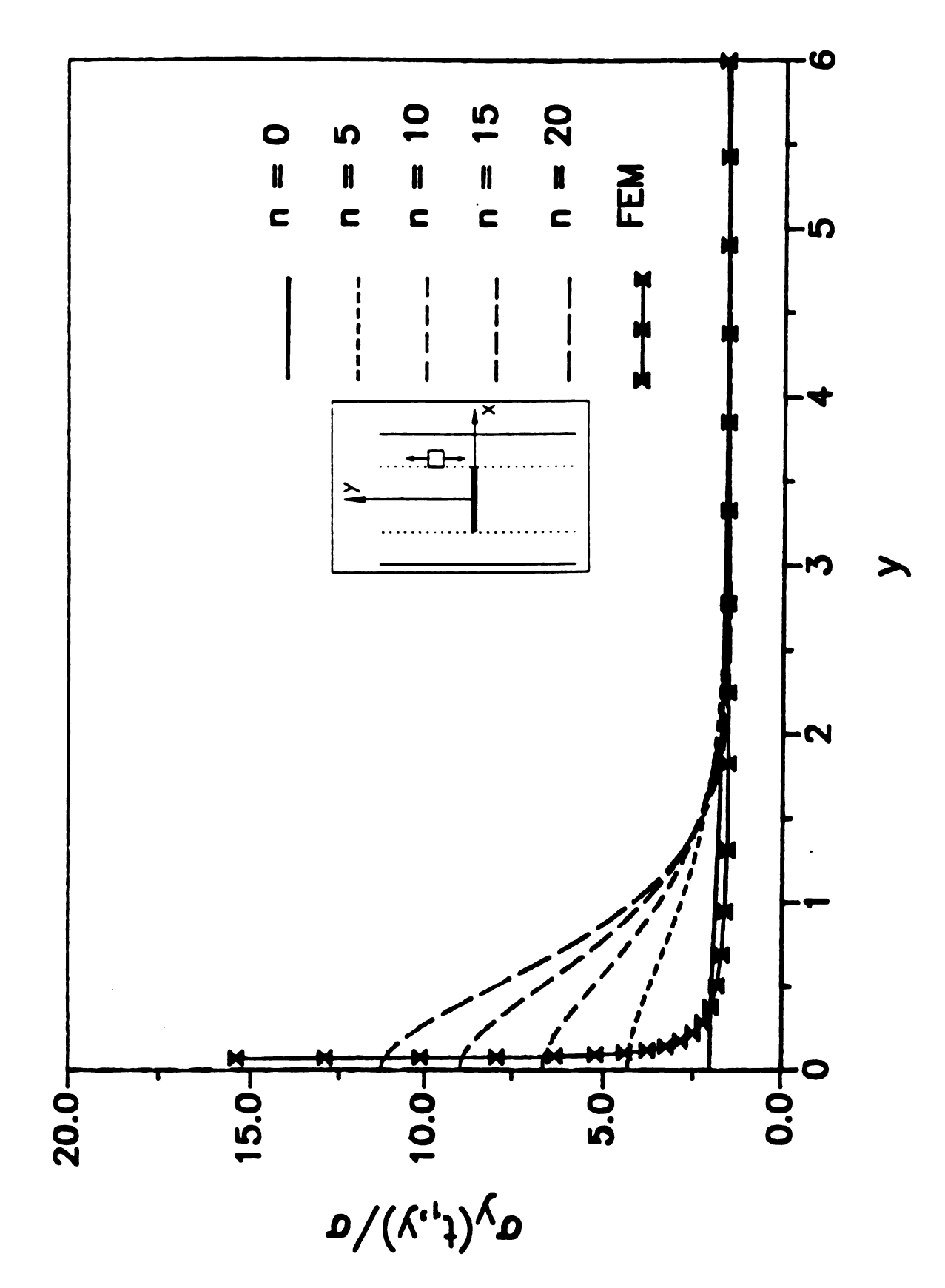


Figure 4.9 Stress component  $\sigma_y$  at the interface in 0° ply.  $[0^{\circ}/90^{\circ}]_s$  glass/epoxy laminate (Type 1).

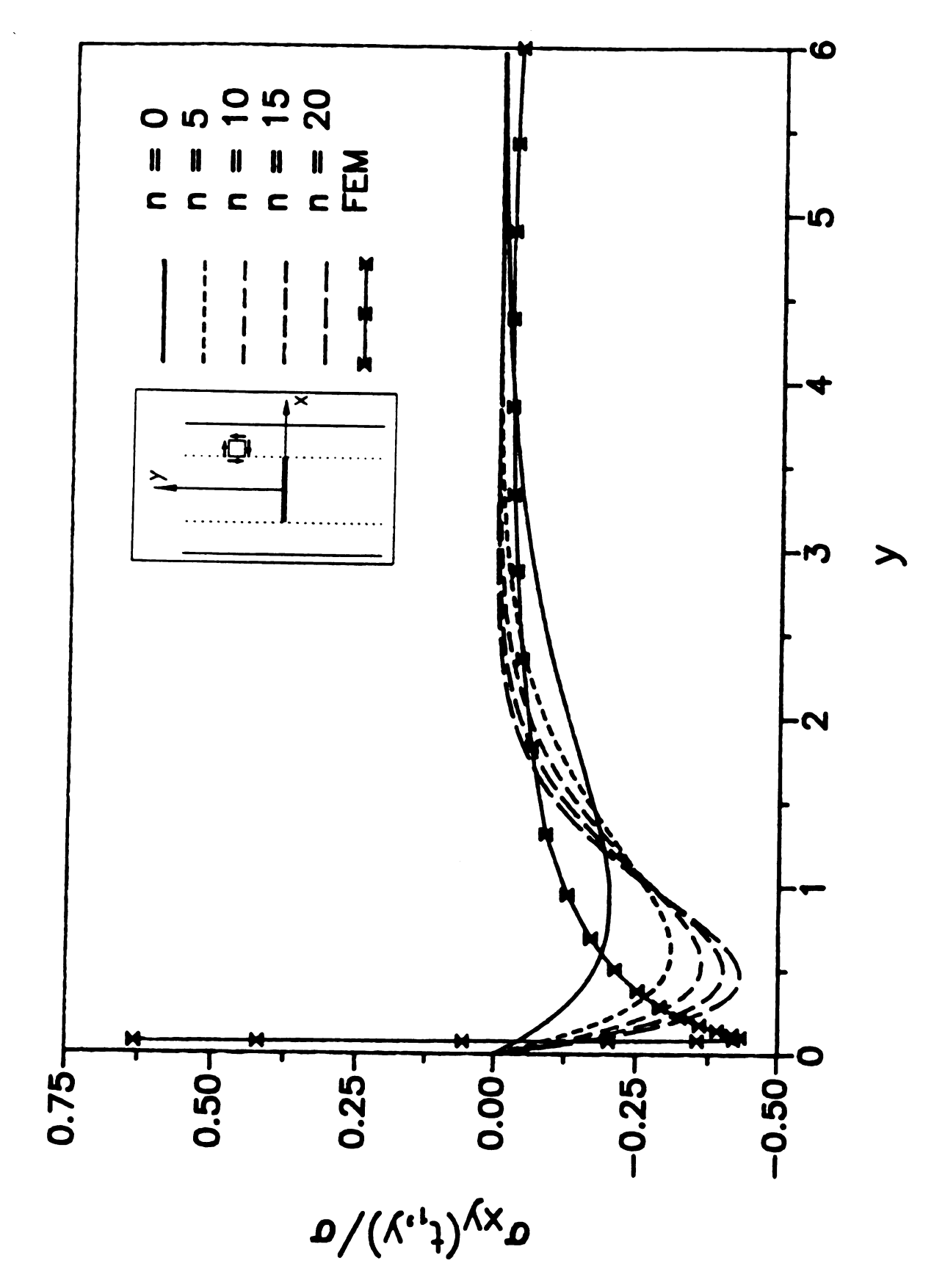


Figure 4.10 Stress component  $\sigma_{xy}$  at the interface in 0° ply.  $[0^{\circ}/90^{\circ}]_{s}$  glass/epoxy laminate (Type 1).

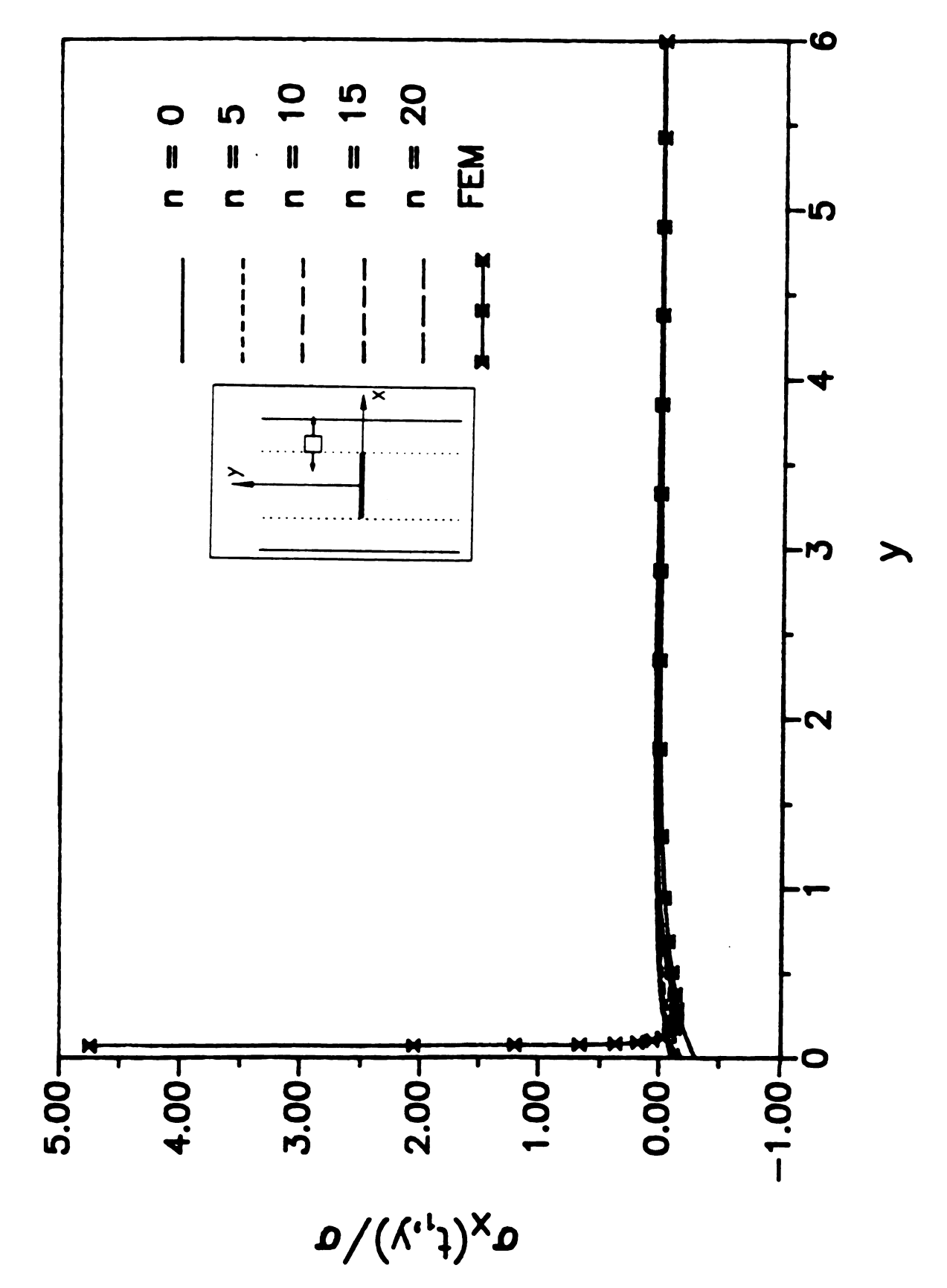


Figure 4.11 Stress component  $\sigma_x$  at the interface in 0° ply.  $[0^{\circ}/90^{\circ}]_s$  glass/epoxy laminate (Type 1).

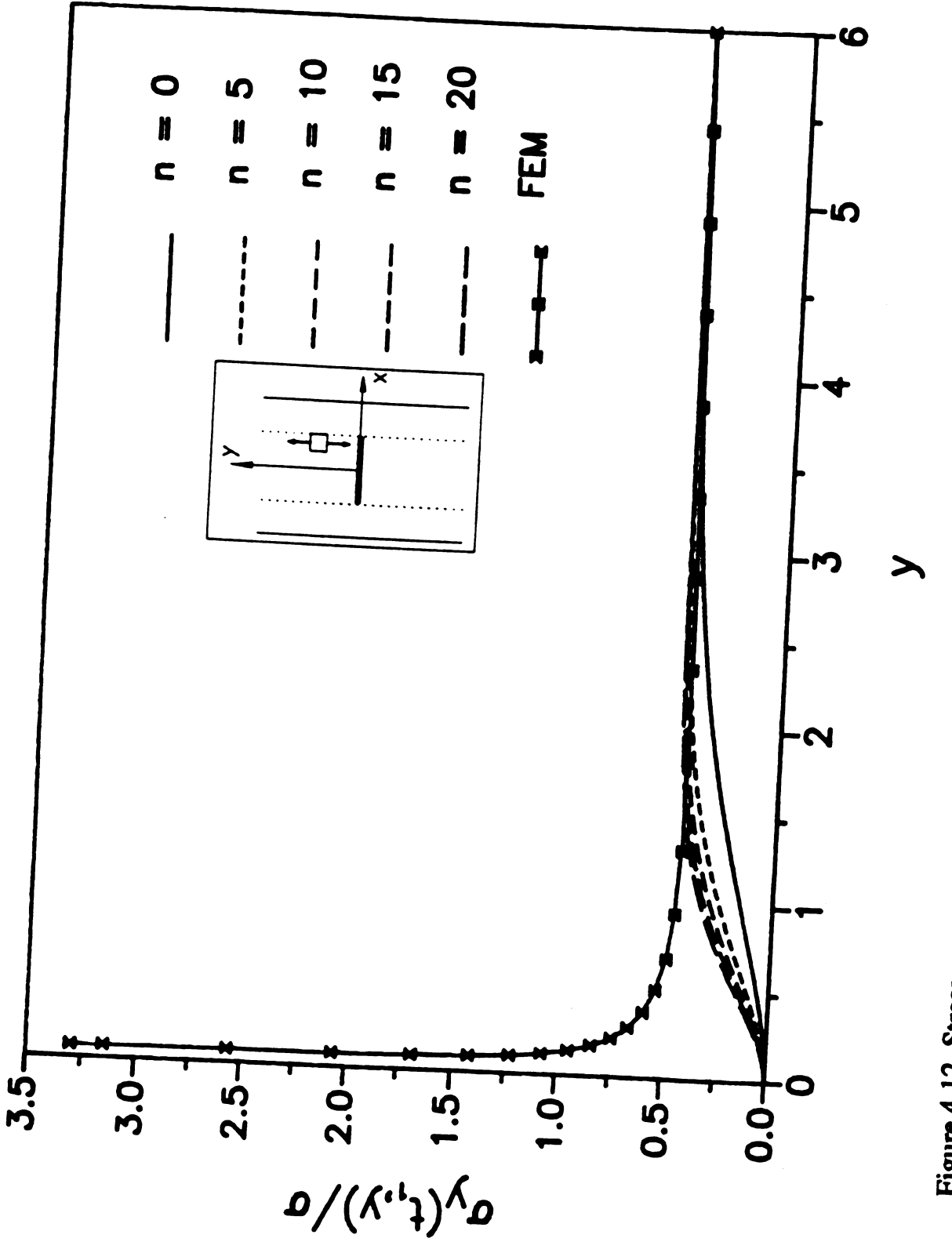


Figure 4.12 Stress component  $\sigma_y$  at the interface in 90° ply.  $[0^{\circ}/90^{\circ}]_s$  glass/epoxy laminate (Type 1).

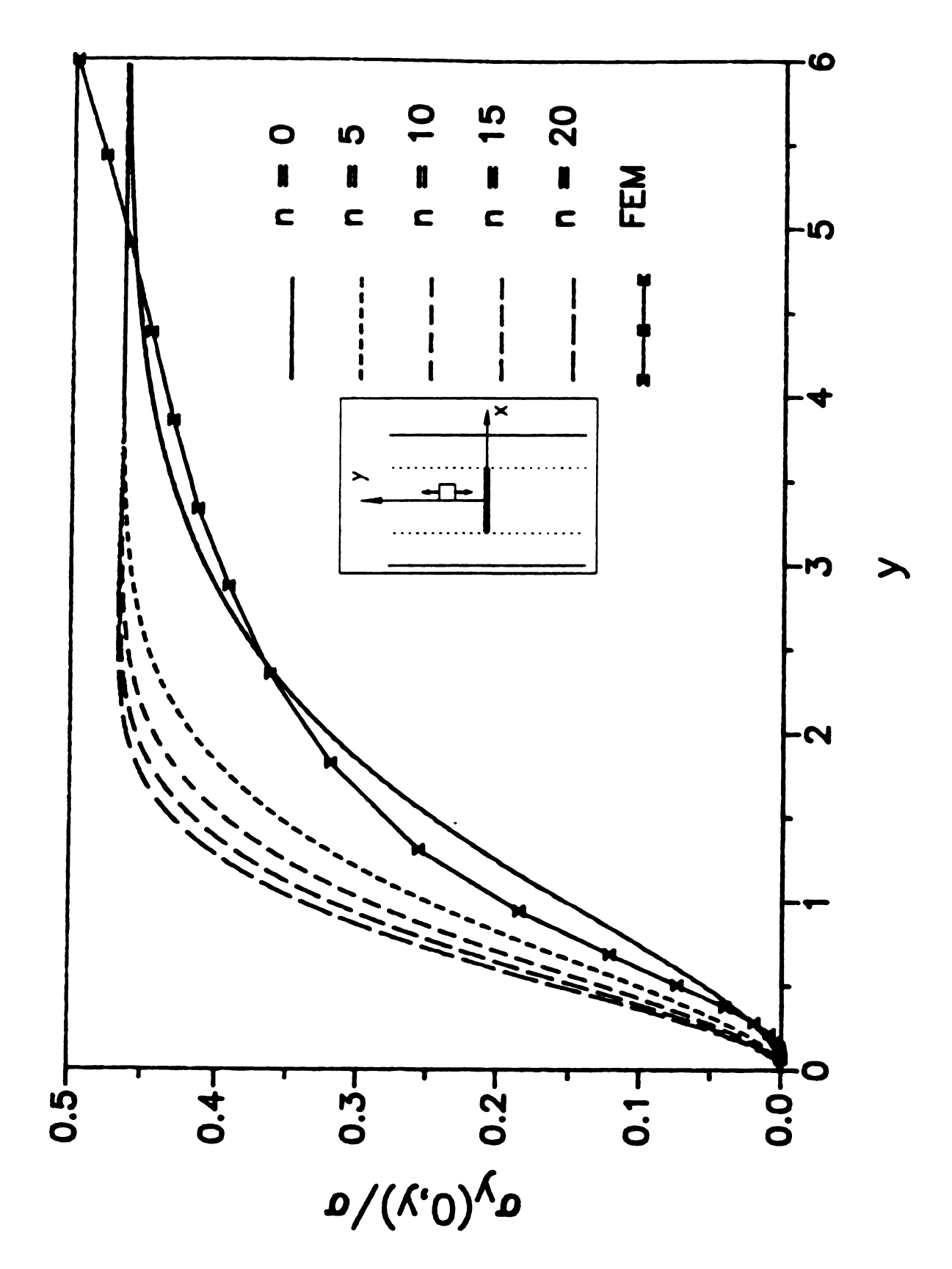


Figure 4.13 Stress component  $\sigma_y$  at the midplane in 90° ply. [0°/90°]<sub>s</sub> glass/epoxy laminate (Type 1).

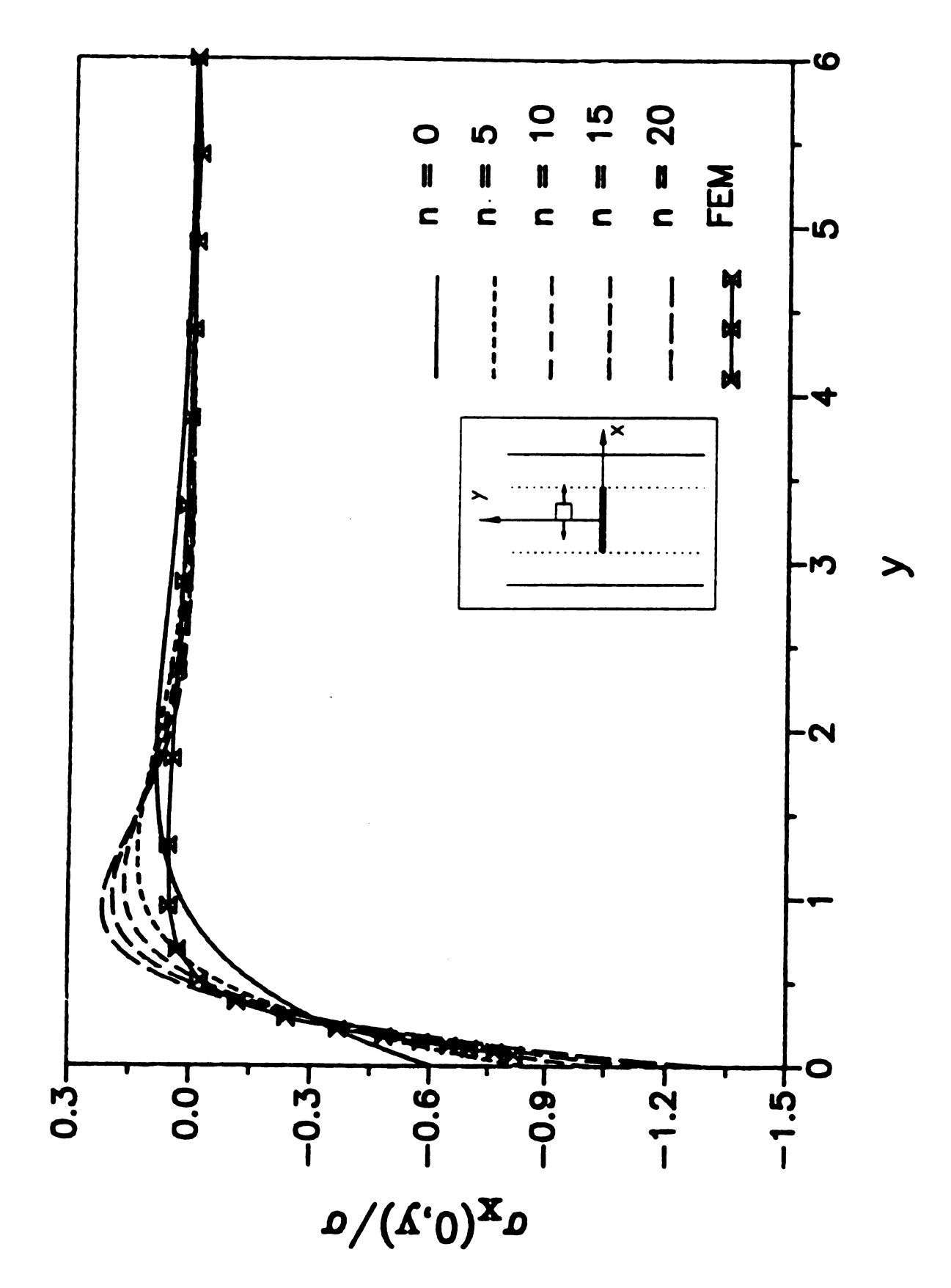


Figure 4.14 Stress component  $\sigma_x$  at the midplane in 90° ply.  $[0^{\circ}/90^{\circ}]_s$  glass/epoxy laminate (Type 1).

## CHAPTER 5

## CONCLUDING REMARKS

The finite element analysis has been presented to analyze the stress distributions in symmetric cross-ply laminates damaged by transverse matrix cracks. Four types of problems for glass/epoxy and graphite/epoxy laminates were considered: (1)  $[0^{\circ}/90^{\circ}]_{s}$  laminate with an isolated crack; (2)  $[0^{\circ}/90^{\circ}]_{s}$  laminate with interacting cracks; (3)  $[0^{\circ}/90^{\circ}]_{s}$  laminate with an isolated crack; (4)  $[0^{\circ}/90^{\circ}]_{s}$  laminate with interacting cracks.

The finite element analysis yielded the following important results: (1) Strong axial stress concentrations occurred at the crack tips in 0° ply. This phenomenon explains that the transverse matrix crack can be considered a likely site for the nucleation of longitudinal cracks and/or delamination cracking. The axial stress concentration in glass/epoxy laminates is stronger than that in graphite/epoxy laminates. Axial stress concentrations in  $[0^{\circ}/90^{\circ}_{3}]_{s}$  laminates with an isolated crack or interacting cracks become stronger than those in  $[0^{\circ}/90^{\circ}]_{s}$  laminates with an isolated crack or interacting cracks; (2) Axial stress concentrations occurred at the crack tips in 90° ply. But, the axial stress concentrations were not so strong as those in 0° ply; (3) Near the crack tips, the transverse stresses and shear stresses are tensile, and changed into compressive, rapidly. These tensile stresses play an important role in damage development in cracked laminates; (4) At the midplane of the laminates, a sort of compressive transverse stress concentration occurred, especially for the  $[0^{\circ}/90^{\circ}]_{s}$  laminate with an isolated crack and  $[0^{\circ}/90^{\circ}]_{s}$  laminate with interacting cracks; (5)

Axial stress at the midplane in 90° ply reaches the maximum tensile stress at the midpoint between two consecutive cracks. This phenomenon explains that a new crack will be likely to occur midway between any two adjacent cracks.

Furthermore, the finite element analysis results for [0°/90°]s glass/epoxy composite laminate with interacting cracks and [0°/90°]s glass/epoxy composite laminate with an isolated crack, were compared to variational calculus results using the minimum complementary energy theorem. These variational calculus results which included the stress concentration effects at the crack tips in 0° ply, were obtained by employing a more generalized test function according to more generalized perturbation stress functions, than that used by Hashin. Although it should be separated into the bulk area and surface layer or interface region in order to obtain more exact stress distributions in variational calculus, the perturbation stress function in variational calculus was not separated in this analysis. Thus, some discrepancies between the finite element analysis results and the variational calculus results can be found.

However, as mentioned earlier, it will be extremely difficult to separate the perturbation stress function according to the specifically interesting areas. Hence, taking into account the shortcoming in selecting the perturbation stress function, we can see reasonable agreement between the finite element analysis results and the more generalized variational calculus results.

Generally speaking, as the power n in more generalized perturbation stress function in variational calculus increases, the stress distributions from the finite element analysis and the variational calculus become closer to each other, except for the axial stress distribution at the midplane in 90° ply. In the axial stress distribution at the midplane in 90° ply, result from the finite element analysis has very good agreement with Hashin's primary stress distribution.



## LIST OF REFERENCES

- [1] K.L. Reifsnider, E.G. Henneke, W.W. Stinchcomb and J.C. Duke, Mechanics of Composite Materials, Recent Advances, Editors Z. Hashin and C.T. Herakovich, Pergamon, New York, 1983, pp. 399-420.
- [2] R. Talreja, Damage Mechanics of Composite Materials, Department of Solid Mechanics, The Technical University of Denmark, Lyngby, Denmark, Report S 32, May, 1986.
- [3] R.D. Jamison, K. Schulte, K.L. Reifsnider and W.W. Stinchcomb, Characterization and Analysis of Damage Mechanisms in Tension -Tension Fatigue of Graphite/Epoxy Laminates, Effects of Defects in Composite Materials, ASTM STP 836, American Society for Testing and Materials, 1984, pp. 21-55.
- [4] A.L. Highsmith and K.L. Reifsnider, Stiffness-Reduction Mechanisms in Composite Laminates, Damage in Composite Materials, ASTM STP 775, K.L. Reifsnider, Ed., American Society for Testing and Materials, 1982, pp. 103-117.
- [5] K.W. Garrett and J.E. Bailey, Multiple Transverse Fracture in 90° Cross-Ply Laminates of a Glass Fibre-Reinforced Polyester, J. Mater. Sci., 12, 1977, pp. 157-168.
- [6] A. Parvizi, K.W. Garrett and J.E. Bailey, Constrained Cracking in Glass Fibre-Reinforced Epoxy Cross-Ply Laminates, J. Mater. Sci., 13, 1978, pp. 195-201.
- [7] A. Parvizi and J.E. Bailey, On Multiple Transverse Cracking in Glass Fibre Epoxy Cross-Ply Laminates, J. Mater. Sci., 13, 1978, pp. 2131-2136.
- [8] R. M. Christensen, Mechanics of Composite Materials, Wiley, New York, 1979, pp. 59-61.
- [9] A. V. Hershey, The Elasticity of an Isotropic Aggregate of Anisotropic Cubic Crystals, J. Appl. Mech., 21, 1954, pp. 236-240.
- [10] E. Kröner, Berechnung der Elastischen Konstanten des Vielkristalls aus den Konstanten des Einkristalls, Zeitschrift für Physik, 151, 1958, pp. 504-518.

- [11] R. Hill, A Self-Consistent Mechanics of Composite Materials, J. Mech. Phys. Solids, 13, 1965, pp. 213-222.
- [12] B. Budianski, On the Elastic Moduli of Some Heterogeneous Materials, J. Mech. Phys. Solids, 13, 1965, pp. 223-227.
- [13] B. Budianski and R. T. O'Connell, Elastic Moduli of a Cracked Solid, Int. J. Solids Structures, 12, 1976, pp. 81-97.
- [14] N. Laws, G.J. Dvorak and M. Hejazi, Stiffness Changes in Unidirectional Composites Caused by Crack Systems, Mechanics of Materials, 2, 1983, pp. 123-137.
- [15] G.J. Dvorak, N. Laws and M. Hejazi, Analysis of Progressive Matrix Cracking in Composite Laminates I: Thermoelastic Properties of a Ply with Cracks, J. Composite Materials, 19, 1985, pp. 216-234.
- [16] G.J. Dvorak and M. Hejazi, Analysis of Progressive Matrix Cracking in Composite Laminates II: First Ply Failure, J. Composite Materials, 21, 1987, pp. 309-329.
- [17] N. Laws and G..J. Dvorak, Progressive Transverse Cracking in Composite Laminates, J. Composite Materials, 22, 1988, pp. 900-916.
- [18] R. Talreja, Estimation of Weibull Parameters for Composite Material Strength and Fatigue Life Data, Fatigue of Fibrous Composite Materials, ASTM STP 723, American Society for Testing and Materials, 1981, pp. 291-311.
- [19] R. Talreja, in H. Lilholt and R. Talreja, Eds., Damage Models for Fatigue of Composite Materials, Proceedings of the 3rd Riso International Symposium on Metallurgy and Materials Science, 1982, pp. 137-153.
- [20] R. Talreja, Fatigue of Composite Materials: Damage Mechanisms and Fatigue-Life Diagrams, Proc. R. Soc. Lond. A378, 1981, pp. 461-475.
- [21] R. Talreja, A Continuum Mechanics Characterization of Damage in Composite Materials, Proc. R. Soc. Lond. A399, 1985, pp. 195-216.
- [22] R. Talreja, Transverse Cracking and Stiffness Reduction in Composite Laminates, J. Composite Materials, 1985, pp. 355-375.
- [23] R. Talreja, Stiffness Properties of Composite Laminates with Matrix Cracking and Interior Delamination, Engineering Fracture Mechanics, 25, 1986, pp. 751-762.
- [24] E.P. Chen and G.C. Sih, Stress Intensity Factor for a Three-Layered Plate with a Crack in the Center Layer, Engineering Fracture Mechanics, 14, 1980, pp. 195-214.

- [25] Z. Hashin, Analysis of Cracked Laminates: A Variational Approach, Mechanics of Materials, 4, 1985, pp. 121-136.
- [26] Z. Hashin, Analysis of Stiffness Reduction of Cracked Cross-Ply Laminates, Engineering Fracture Mechanics, 25, 1986, pp. 771-778.
- [27] Swanson Analysis Systems, Inc., ANSYS Engineering Analysis System User's Manual, Vol. 1-2, June 1985.
- [28] J.J. Guydish and J.F. Fleming, Optimization of the Finite Element Mesh for the Solution of Fracture Problems, Engineering Fracture Mechanics, 10, 1978, pp. 31-42.
- [29] A. Tezuka and O. Okuda, An Adaptive Mesh Refinement for the Finite Element Method (Trial by  $\gamma$ -method), JSME Int. J., 31, 1988, pp. 50-55.
- [30] C. O. Horgan, Saint-Venant End Effects In Composites, J. Composite Materials, 16, 1982, pp. 411-422.
- [31] I. S. Sokolnikoff, Mathematical Theory of Elasticity, McGraw-Hill, New York, 1978, pp. 387-390.
- [32] P. W. Manders, T. W. Chou, F. R. Jones, and J. W. Rock, Statistical Analysis of Multiple Fracture in 0°/90°/0° Glass Fibre/Epoxy Resin Laminates, J. Mater. Sci., 18, 1983, pp. 2876-2889.
- [33] H. Fukunaga, T. W. Chou, P. W. M. Peters and K. Schulte, Probabilistic Failure Strength Analysis of Graphite/Epoxy Cross-Ply Laminates, J. Composite Materials, 18, 1984, pp. 339-356.

